The present is the key to the past ….

… The past is the key to the future

Some thoughts on paleoceanography

Hanno Kinkel 12/2022

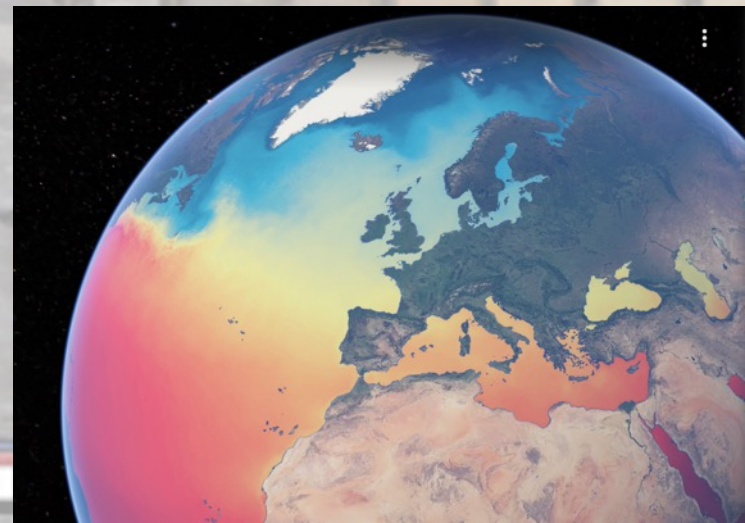

What do we know about ocean circulation

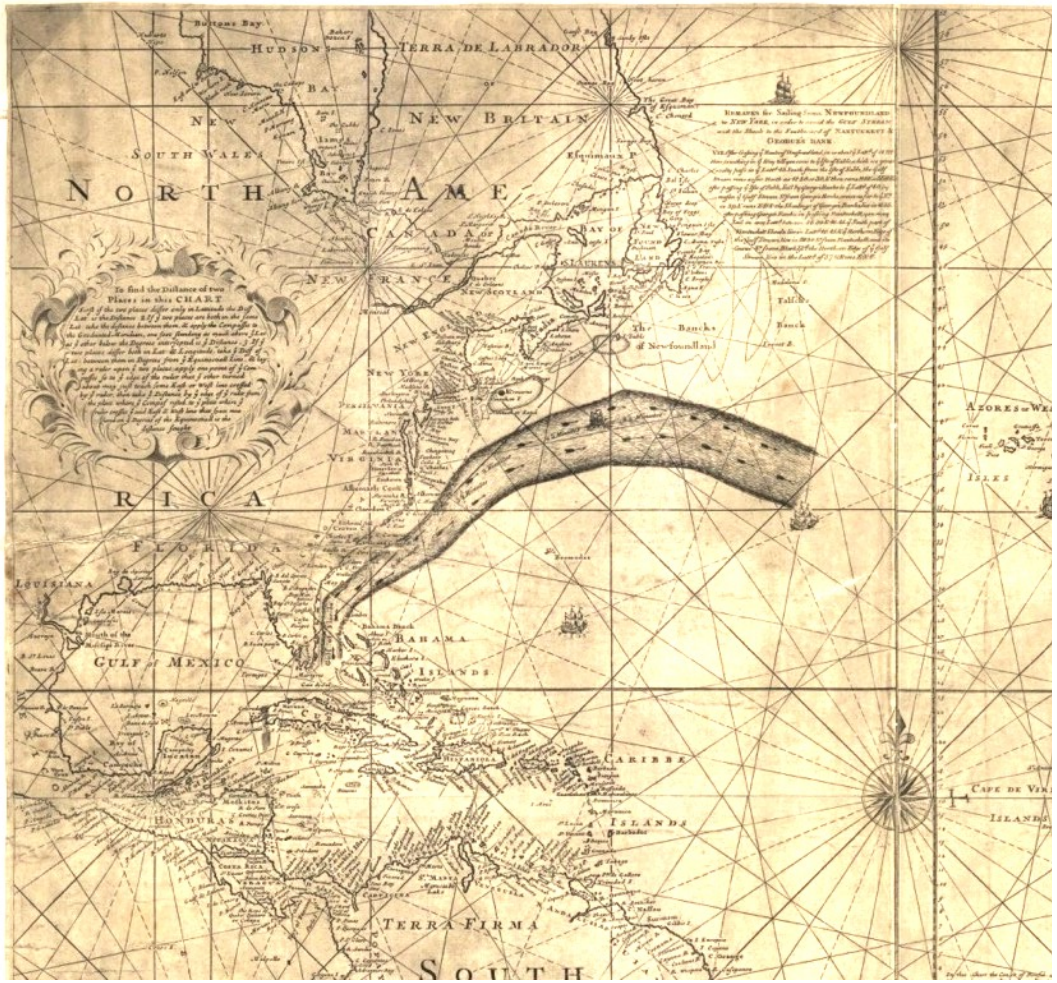

[Franklin-Folger chart of the Gulf Stream]. 1768. Geography and Map Division, Library of Congress.

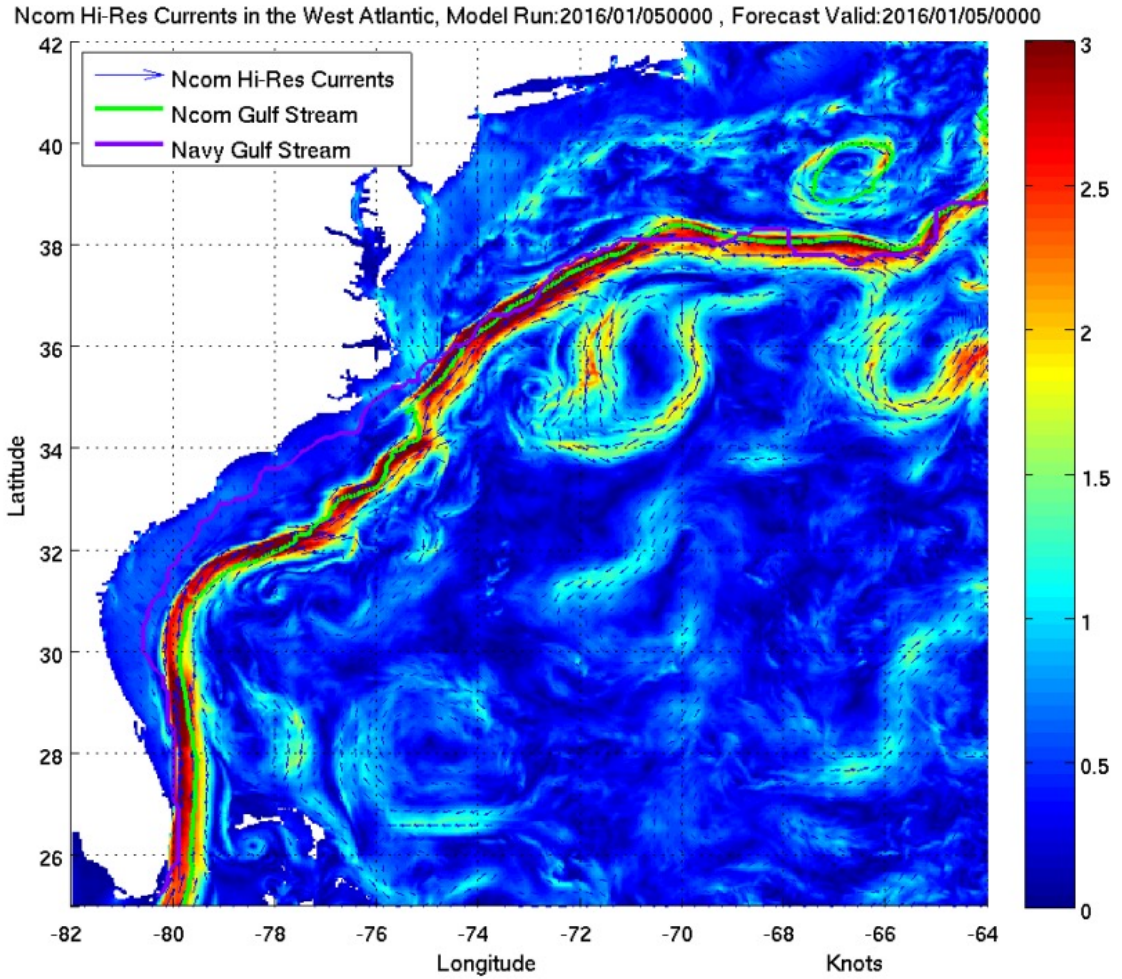

The Gulf Stream location in the Global Real Time Ocean Forecast System model (RTOFS). Courtesy of NOAA.

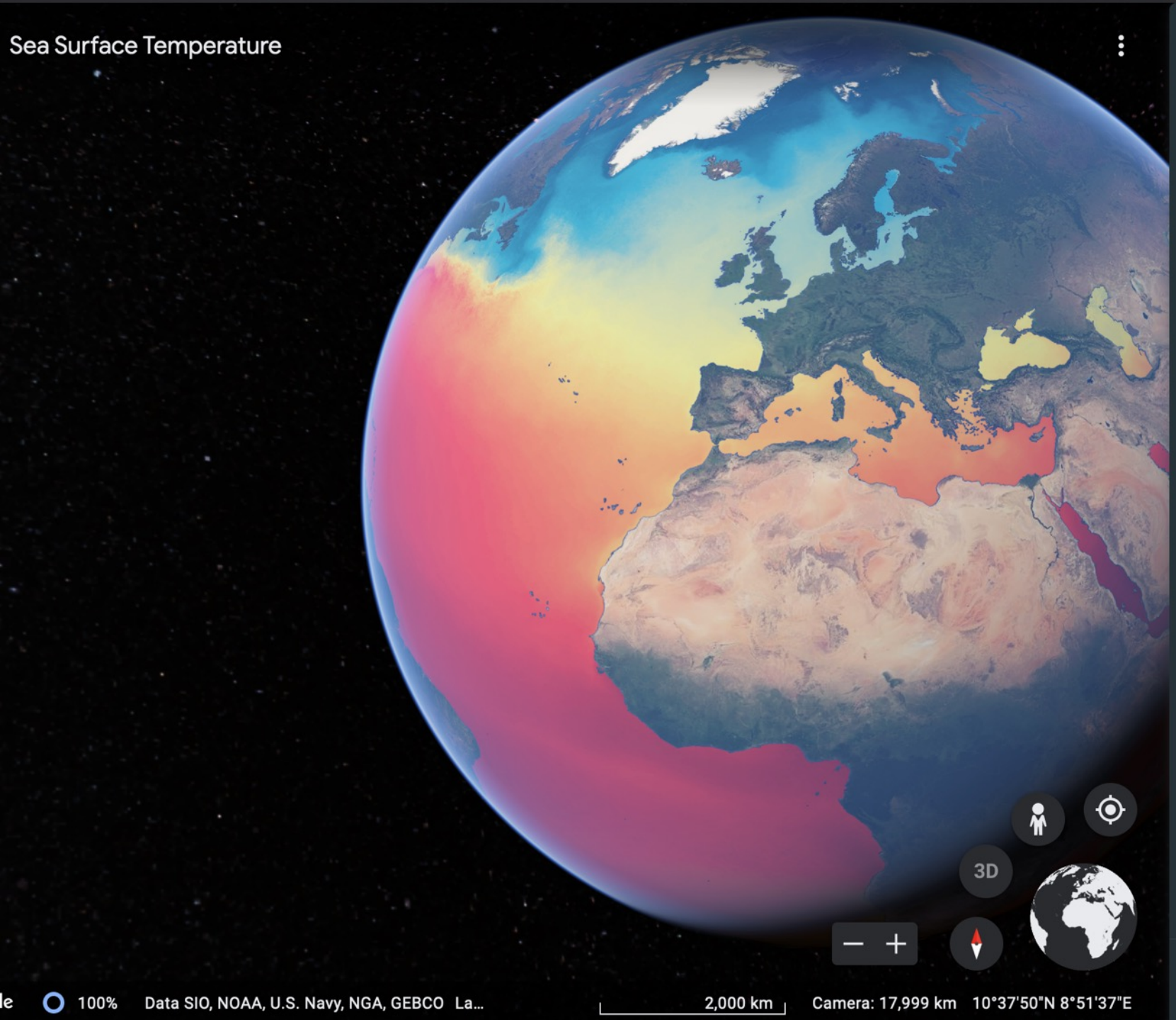

Sea Surface Temperature

Data from: 2009

National Oceanographic Data Center, NOAA

Celsius

-2 7 16 24 33

SWITCH TO FAHRENHEIT

Scientists monitor sea surface temperature because of its impact on weather, climate and the health of marine life. This visualization shows sea surface temperatures averaged over nearly a quarter century of data collected by the Pathfinder Earth observation program. These day-night combined monthly and yearly mean averages were produced from cloud-screened day-night monthly full resolution data from 1985–2009, among the most comprehensive and accurate sea surface temperature climate datasets available.

Credit: Baker-Yeboah, Sheekela; Saha, Korak; Zhang, Dexin; Casey, Kenneth S.; Kilpatrick, Katherine A.; Evans, Robert H.; Ryan, Thomas (2016). AVHRR Pathfinder version 5.3 level 3 collated (L3C) global 4km sea surface temperature for 1981-2014. NOAA National Centers for Environmental Information. Dataset.doi:10.7289/V52J68XX [Date accessed: May 7, 2018]

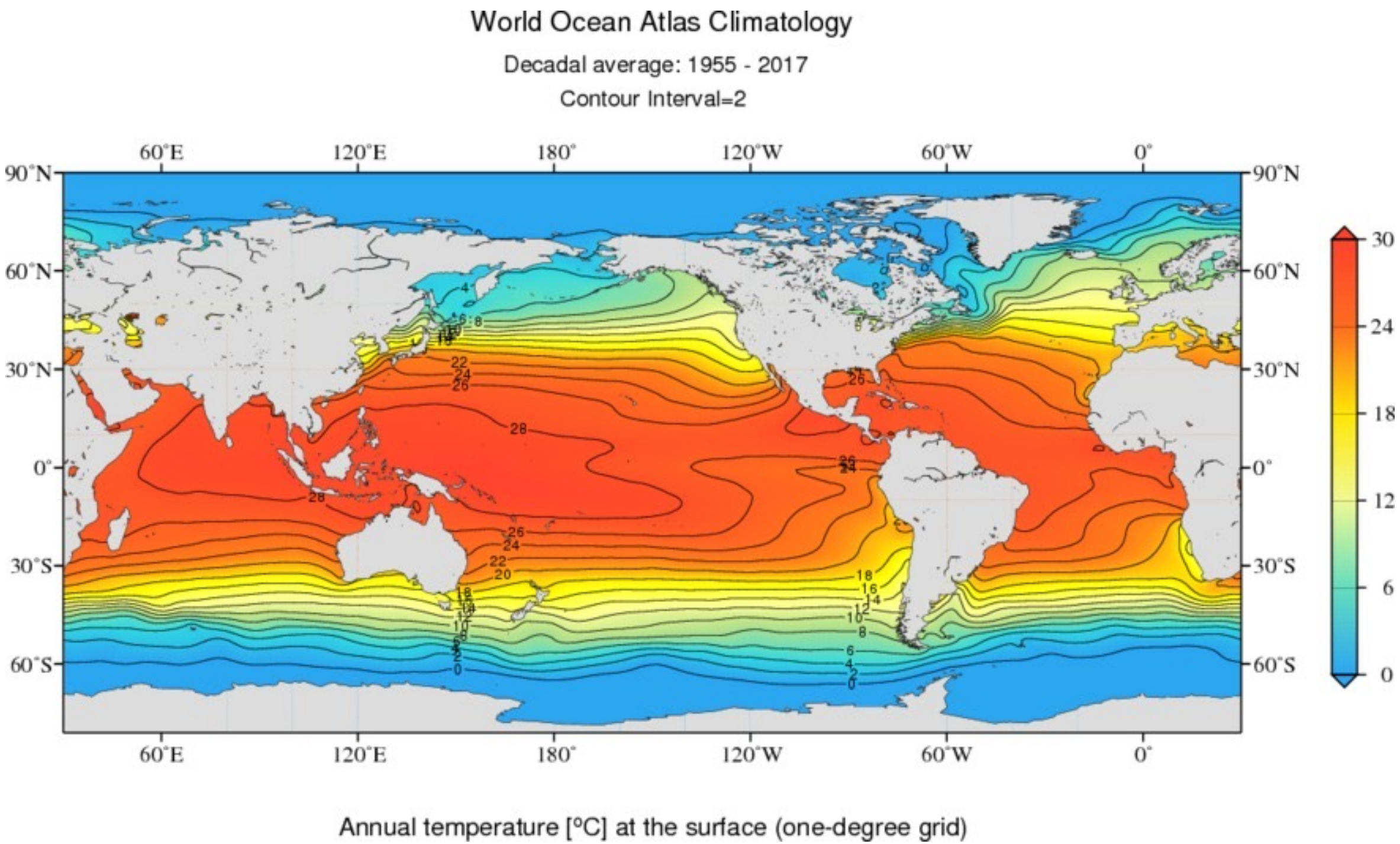

Annual temperature [°C] at the surface (one-degree grid)

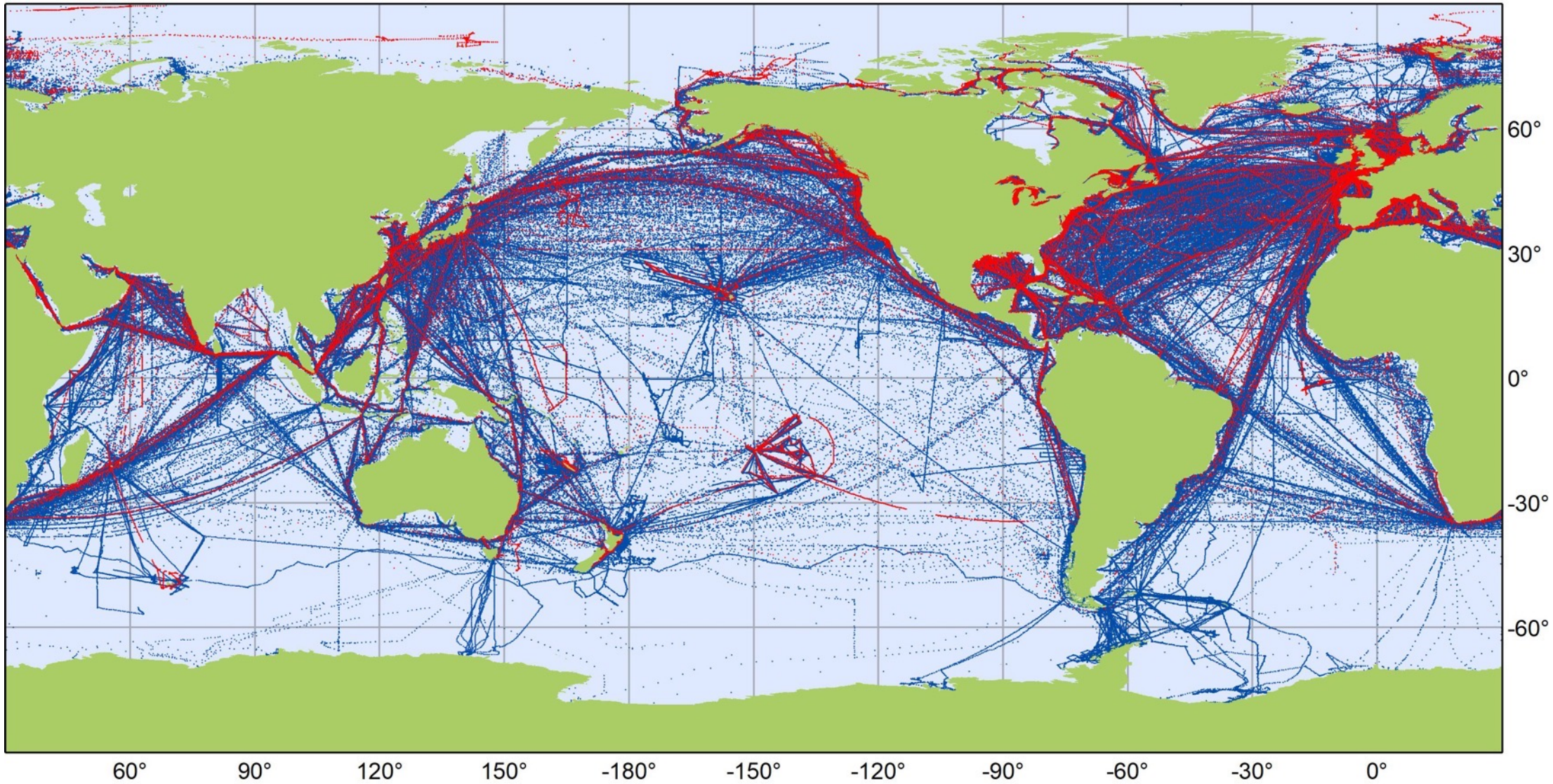

Ship Observations Team

VOS: Yearly (2017) and monthly (September 2018) Coverage

- **Yearly**
- **Monthly**

Generated by www.jcommops.org

Climate Change 2022: Impacts, Adaptation and Vulnerability

Global and regional risks for increasing levels of global warming

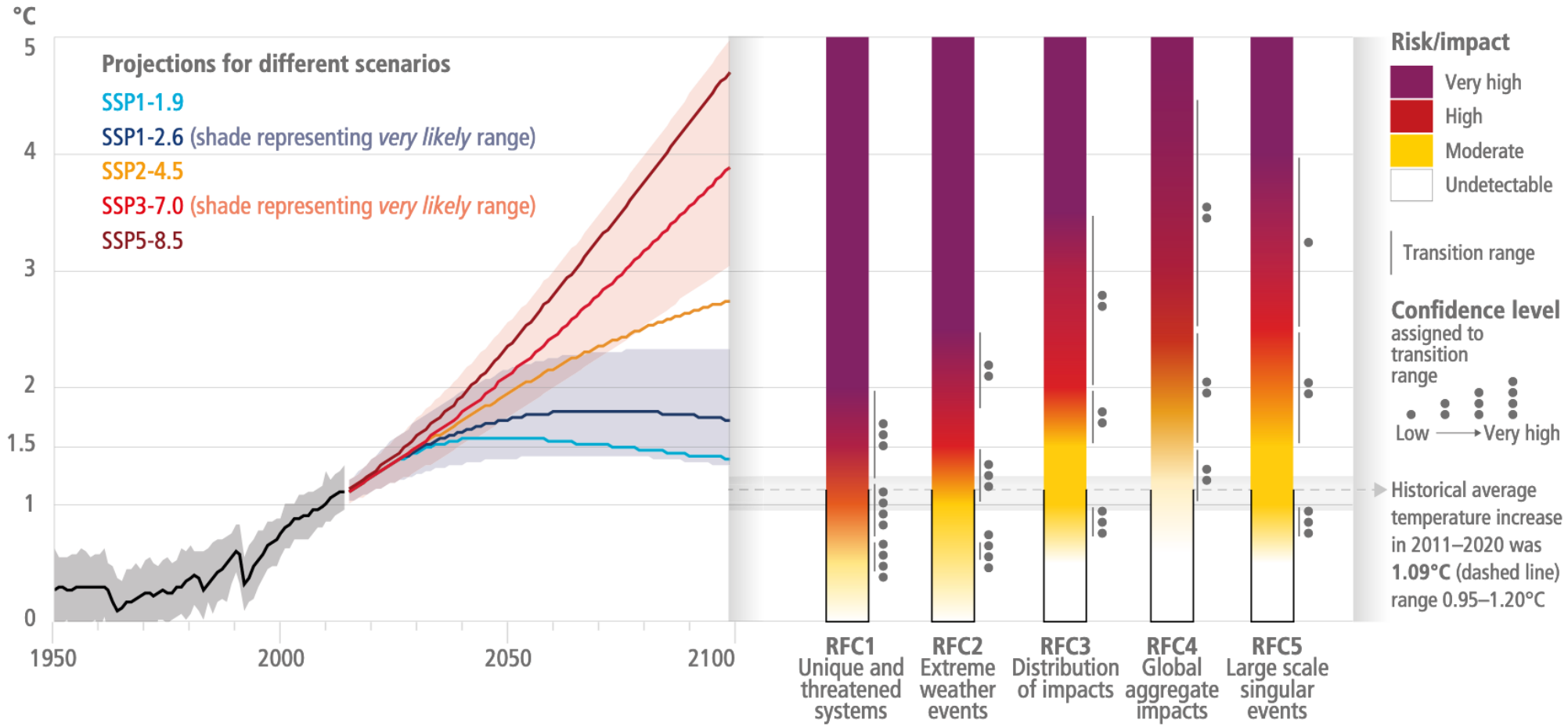

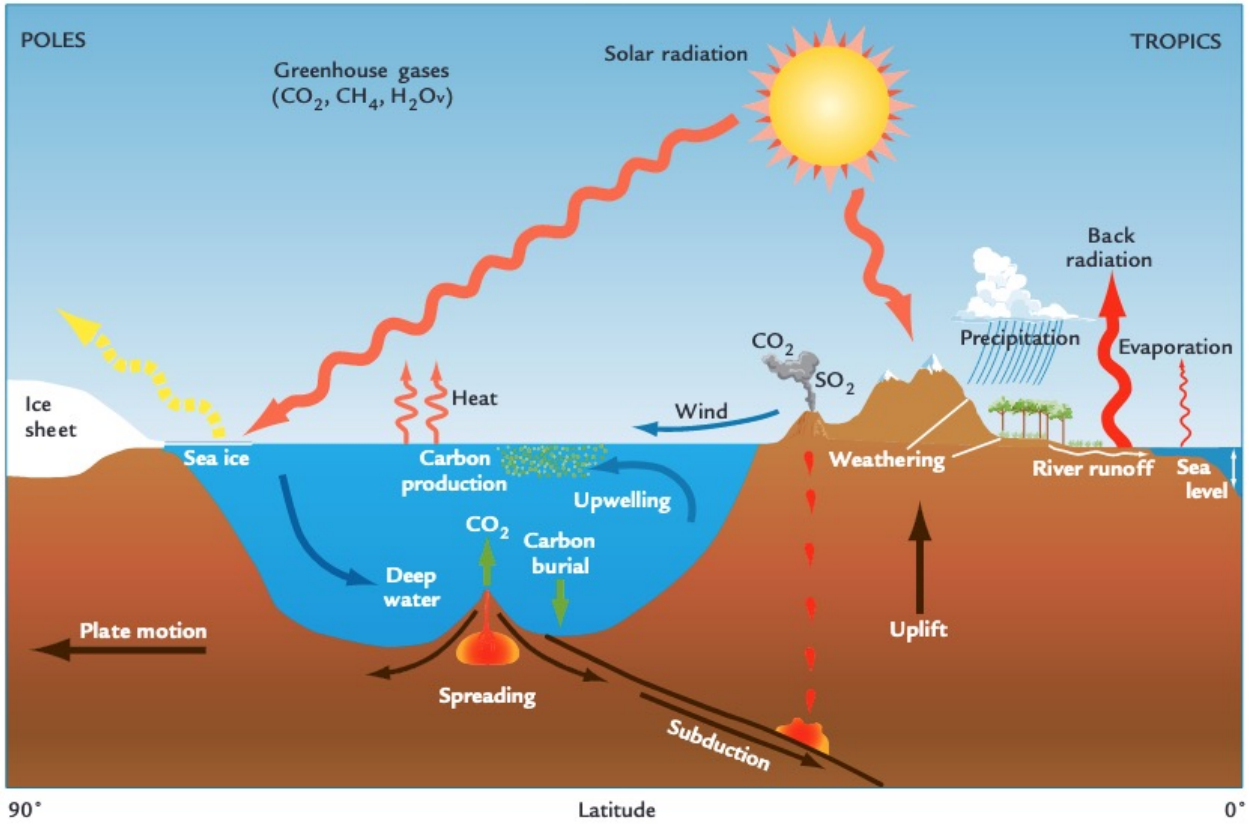

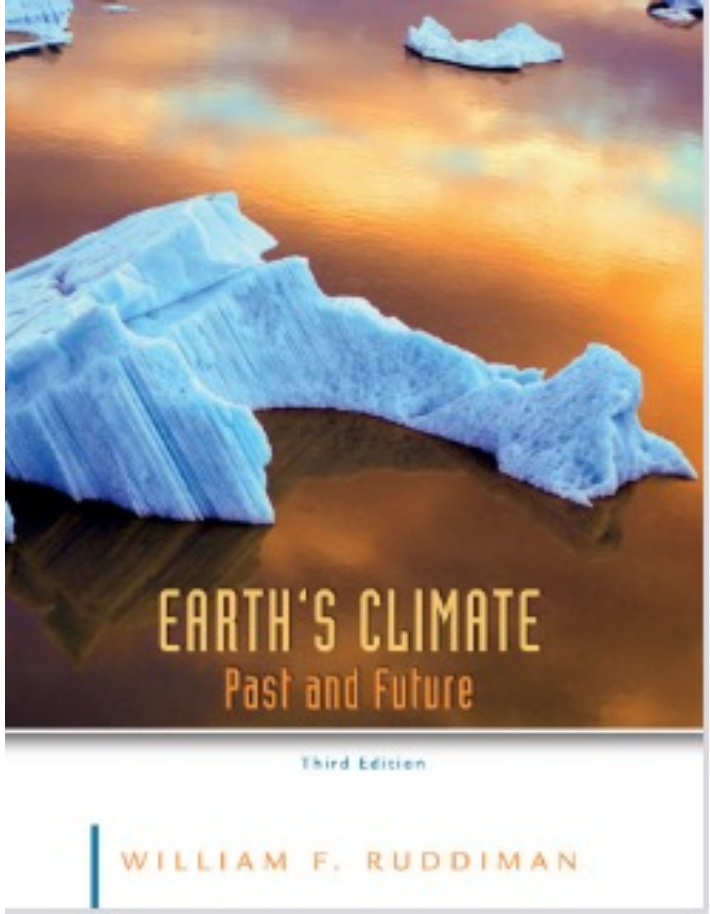

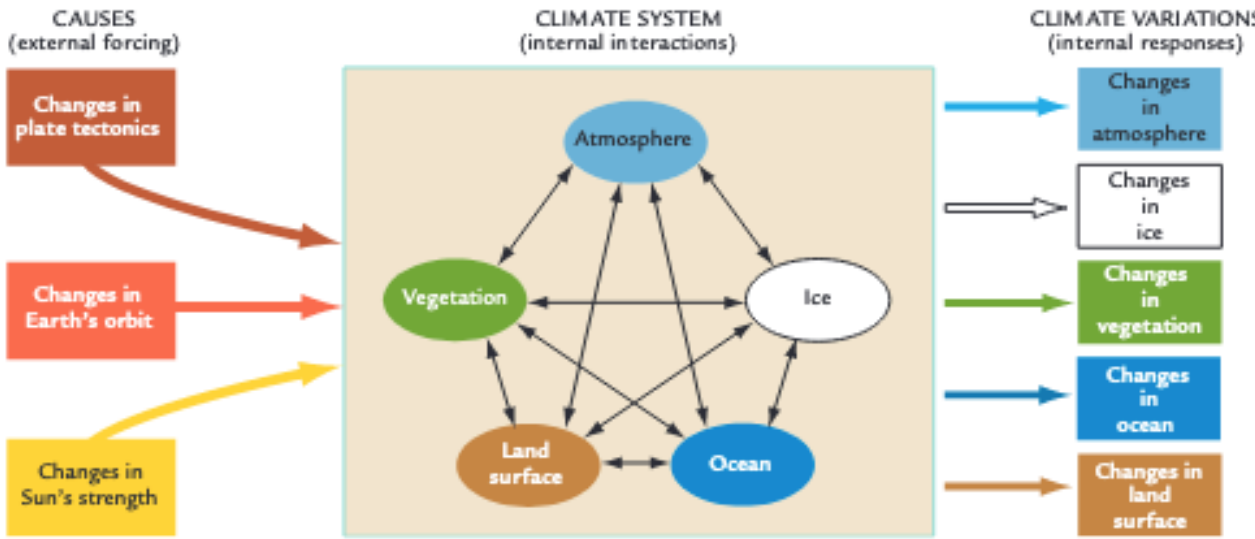

FIGURE 1-5

Earth's climate system and interactions of its components

Studies of Earth's climate cover a wide range of processes, indicated at the top. Climate scientists organize and simplify this complexity, as shown at the bottom. A small number of factors drive, or force, climate change. These factors cause interactions among the internal components of the climate system (air, water, ice, land surfaces, and vegetation). The results are the measurable variations known as climate responses.

HOW TO RECONSTRUCT THE OCEANS PAST

Paleoceanographic Proxies

Biological:

Foraminifera
Diatoms
Coccolithophores
Dinoflagellates
Ostracodes
Pteropods
Biomarker

Physical:

Grain Size
Colour
Density
Magnetics

Chemical:

Elemental ratios
Isotopes
Biomarker

and many more …

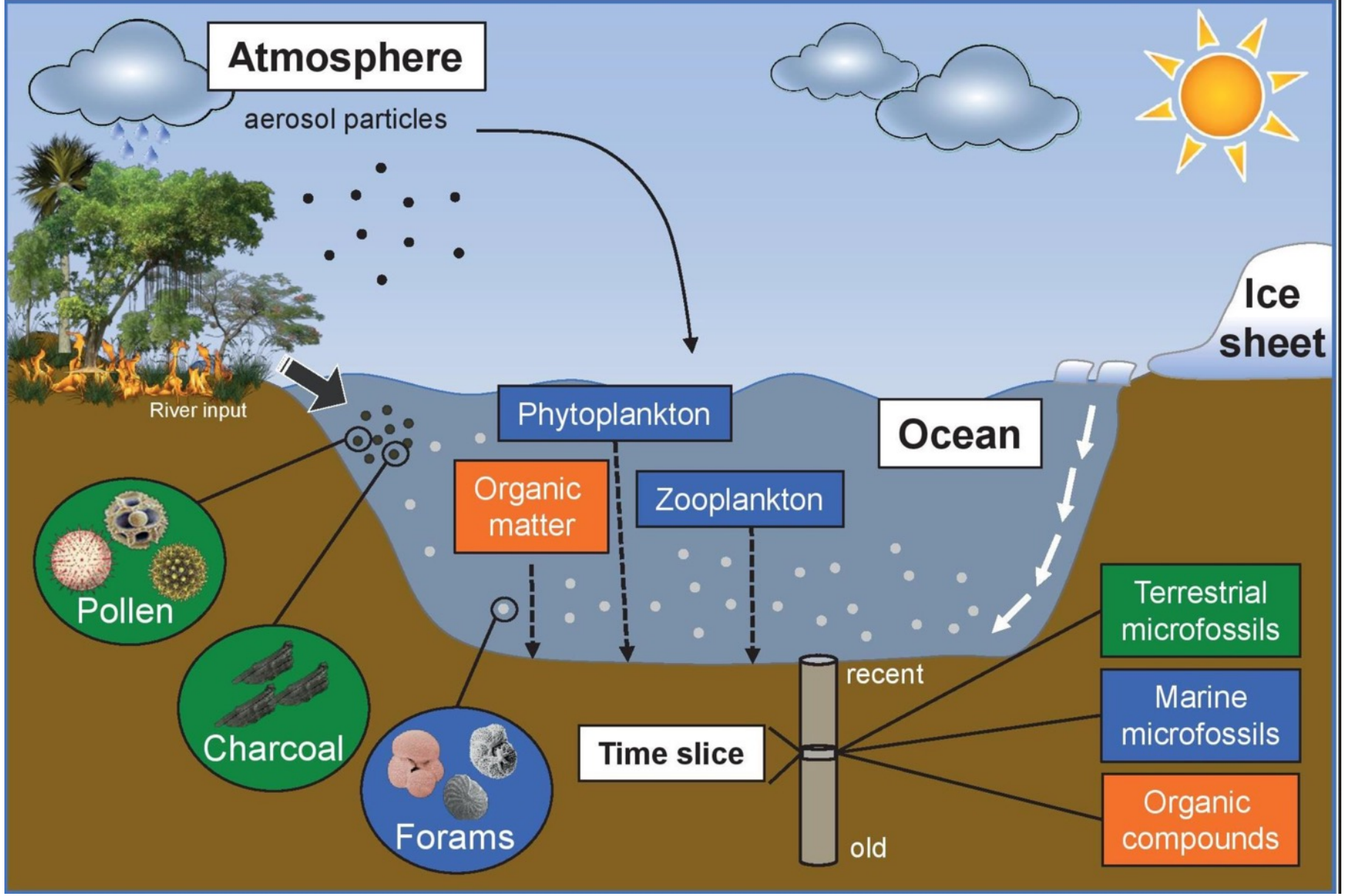

Figure 5. Integrated approach using marine sedimentary sequences to unravel terrestrial and oceanic changes during abrupt climate events and pathways of terrestrial and marine microfossil deposition. Forams: foraminifera. Modified from Center for Advanced Marine Core Research, Kochi University. (2020) https://www.kochi-u.ac.jp/marine-core/research/.

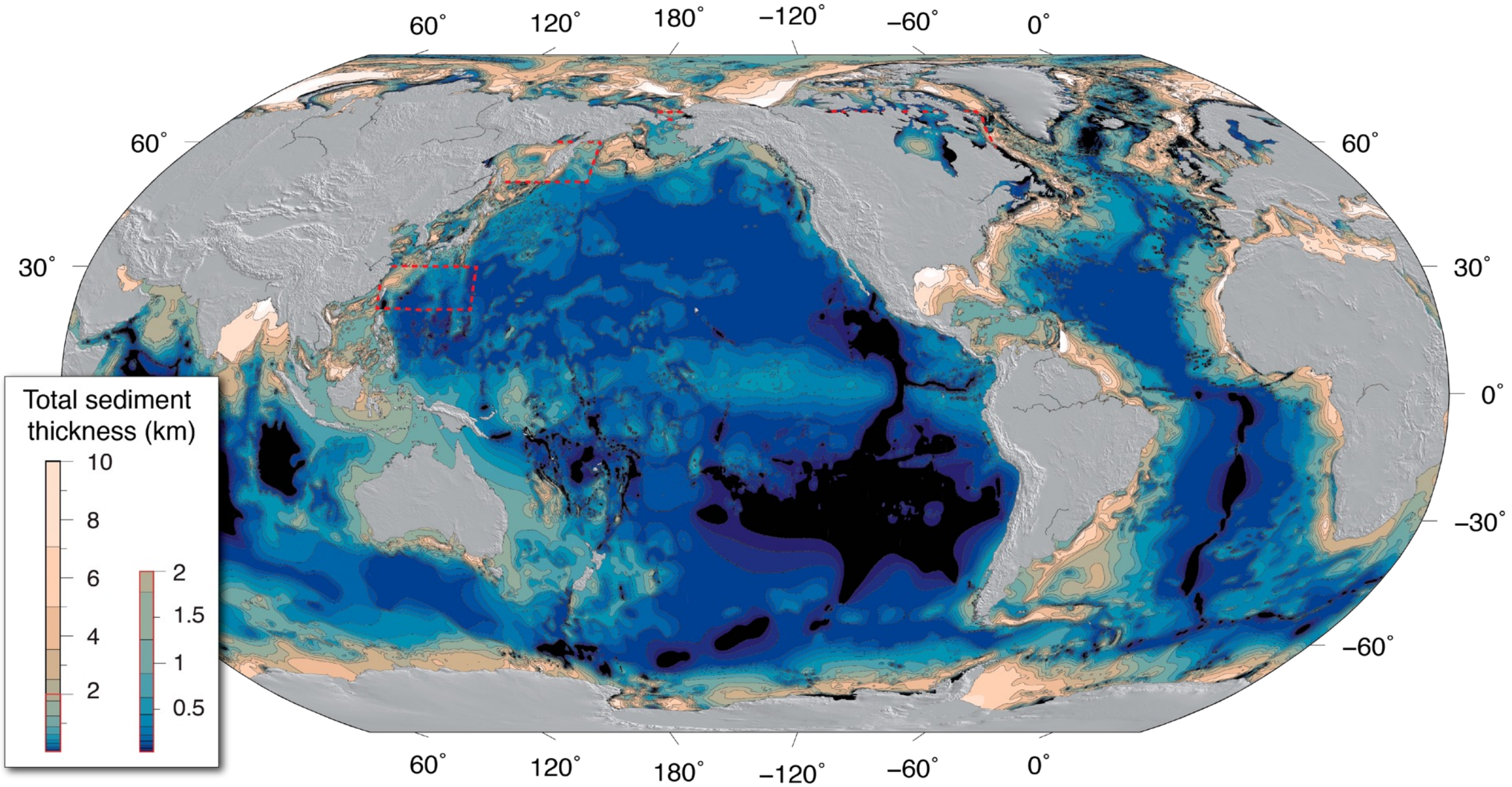

Straume, E.O., Gaina, C., Medvedev, S., Hochmuth, K., Gohl, K., Whittaker, J. M., et al. (2019). GlobSed: Updated total sediment thickness in the world's oceans. Geochemistry, Geophysics, Geosystems, 20. [DOI: 10.1029/2018GC008115](https://doi.org/10.1029/2018GC008115)

Temperatures of Pacific Bottom Waters and Polar Superficial Waters during the Tertiary

CESARE EMILIANI Authors Info & Affiliations

SCIENCE • 18 Jun 1954 • Vol 119, Issue 3103 • pp. 853-855 • DOI: 10.1126/science.119.3103.853

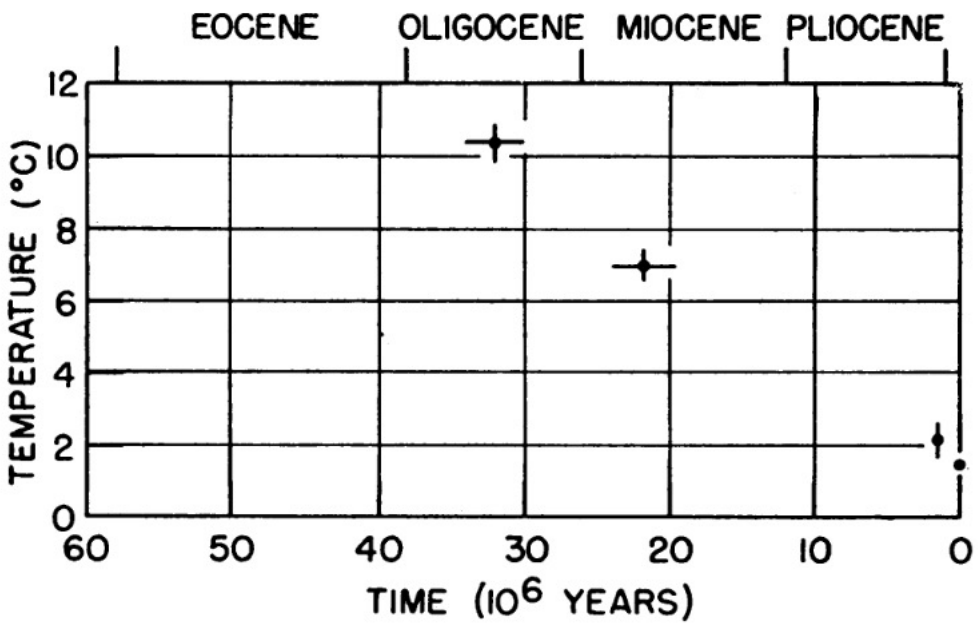

Fig. 1. Temperature change of Pacific abyssal waters during the Tertiary.

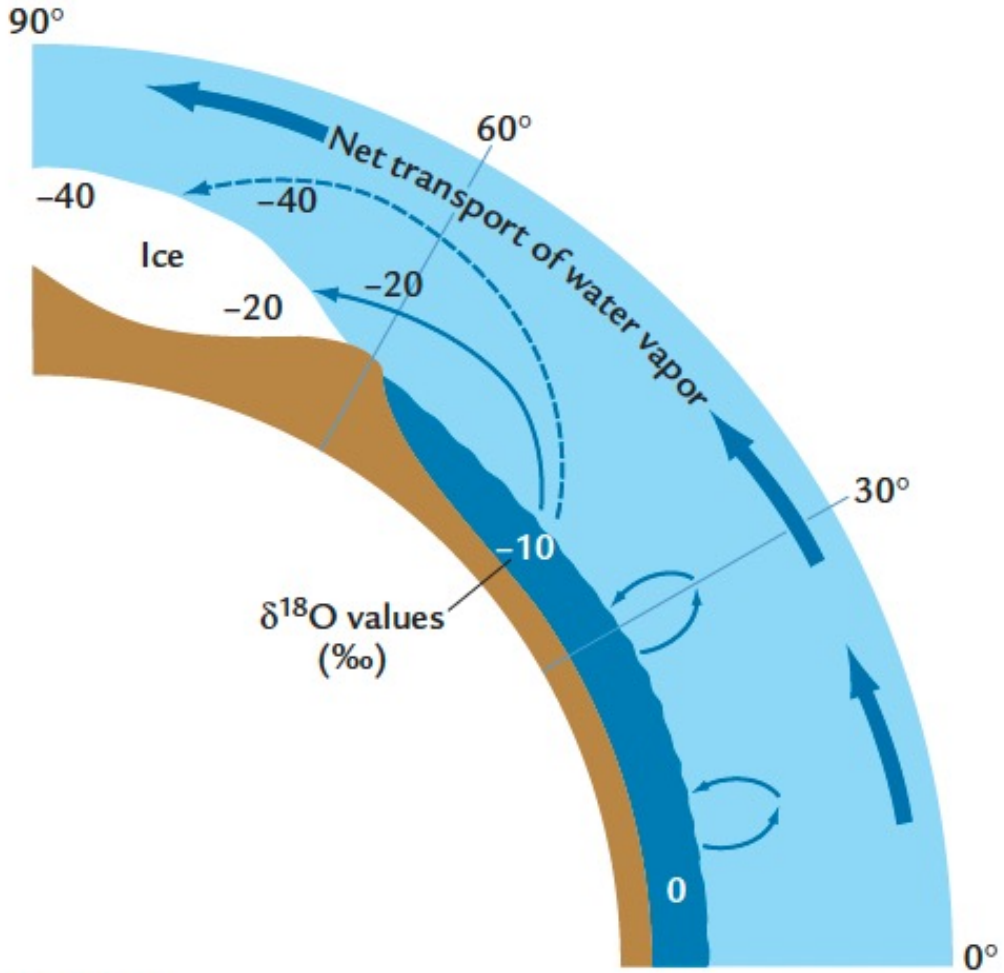

FIGURE-2

Isotope fractionation

As water vapor moves from the tropics toward the poles, it is enriched in the ^{16}O isotope during each step of evaporation and condensation. This fractionation process makes the $\delta^{18}O$ values of snow falling on (and stored in) ice sheets more negative (^{16}O-rich).

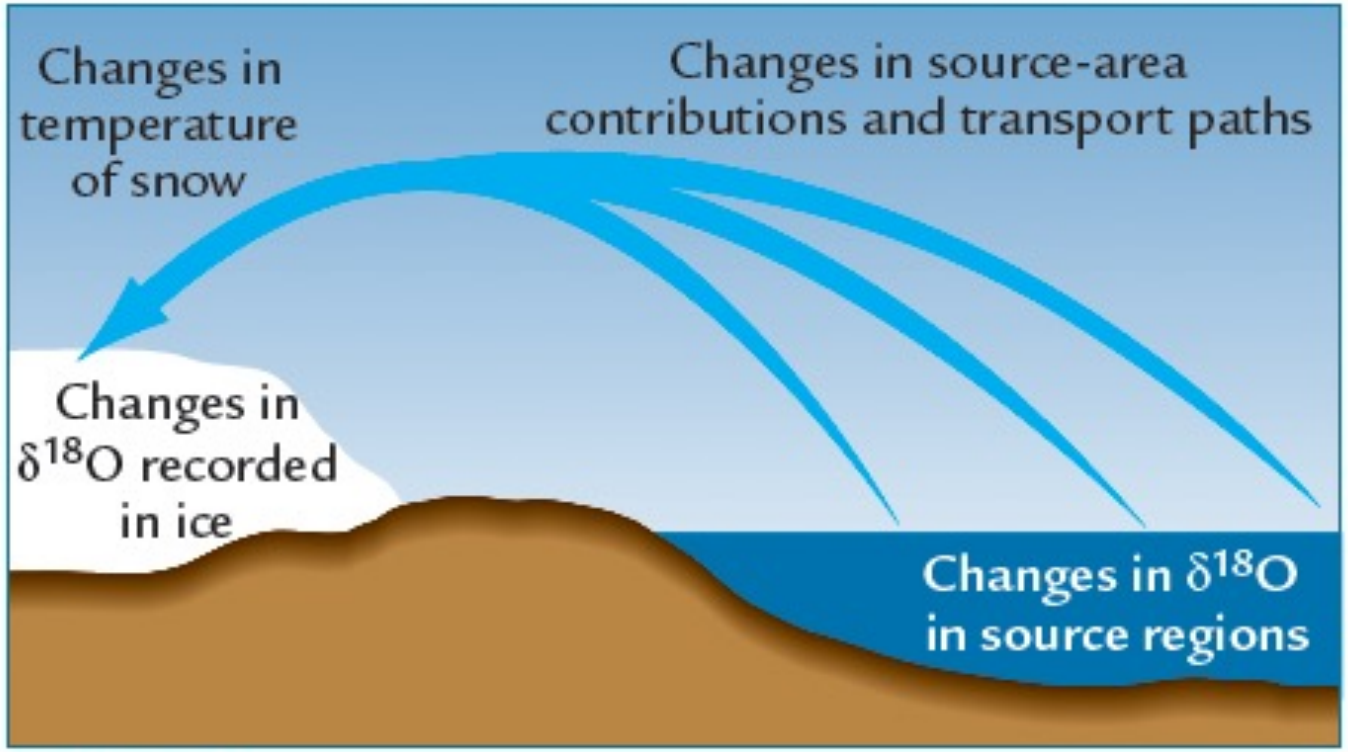

FIGURE-3

Controls on variations in ice-core $\delta^{18}O$

The $\delta^{18}O$ values recorded in ice cores vary with changes in the local temperature of the snow that falls on the ice, changes in the relative contributions among the source areas of water vapor, and $\delta^{18}O$ changes within the source regions.

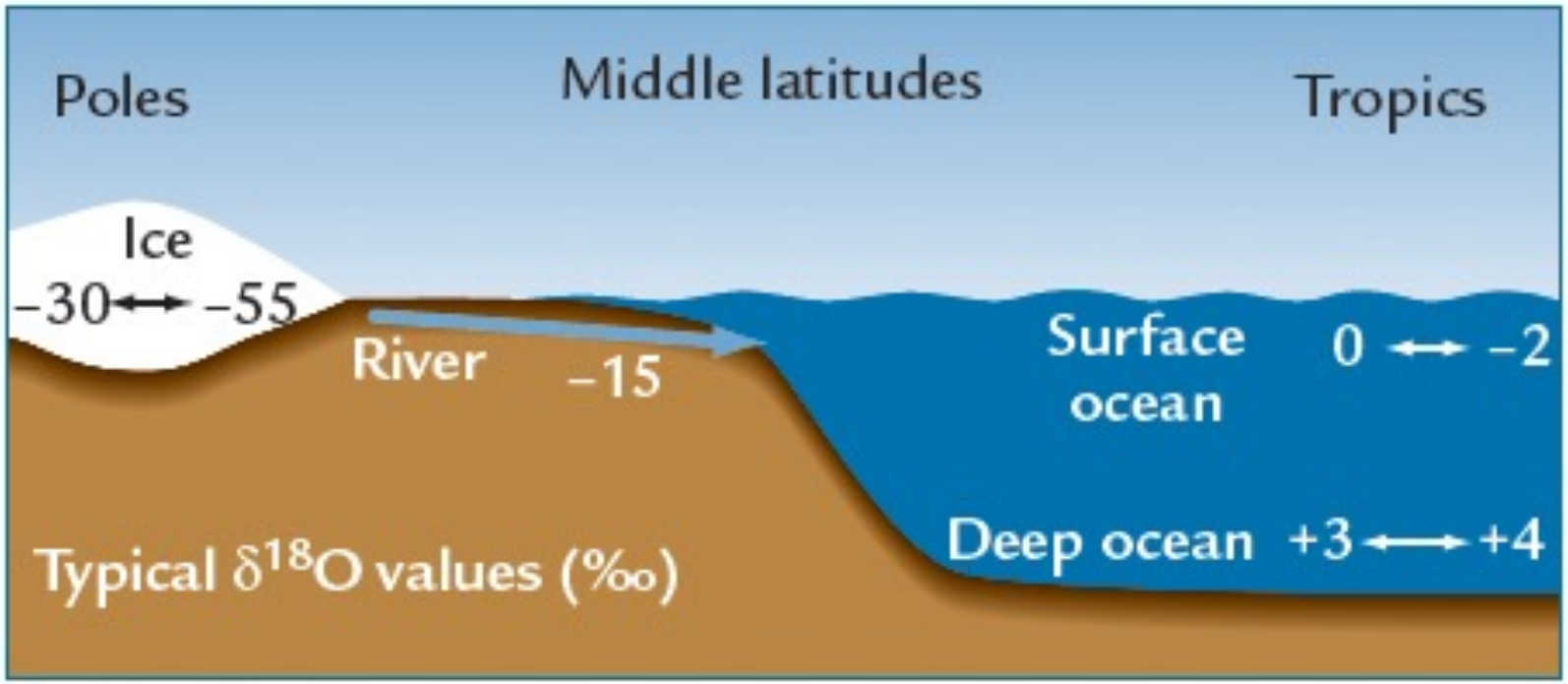

$$\delta^{18}O\ (\text{in }‰) = \frac{(^{18}O/^{16}O)_{\text{sample}} - (^{18}O/^{16}O)_{\text{standard}}}{(^{18}O/^{16}O)_{\text{standard}}} \times 1{,}000$$

FIGURE-1

$\delta^{18}O$ values in the modern world

In the modern ocean, $\delta^{18}O$ values vary from 0 to $-2‰$ in warm tropical surface waters to as much as $+3$ to $+4‰$ in cold deep-ocean waters. In present ice sheets, typical $\delta^{18}O$ values reach $-30‰$ in Greenland and $-55‰$ in Antarctica.

$$\delta^{13}C\ (\text{in } ‰) = \frac{(^{13}C/^{12}C)_{sample} - (^{13}C/^{12}C)_{standard}}{(^{13}C/^{12}C)_{standard}} \times 1{,}000$$

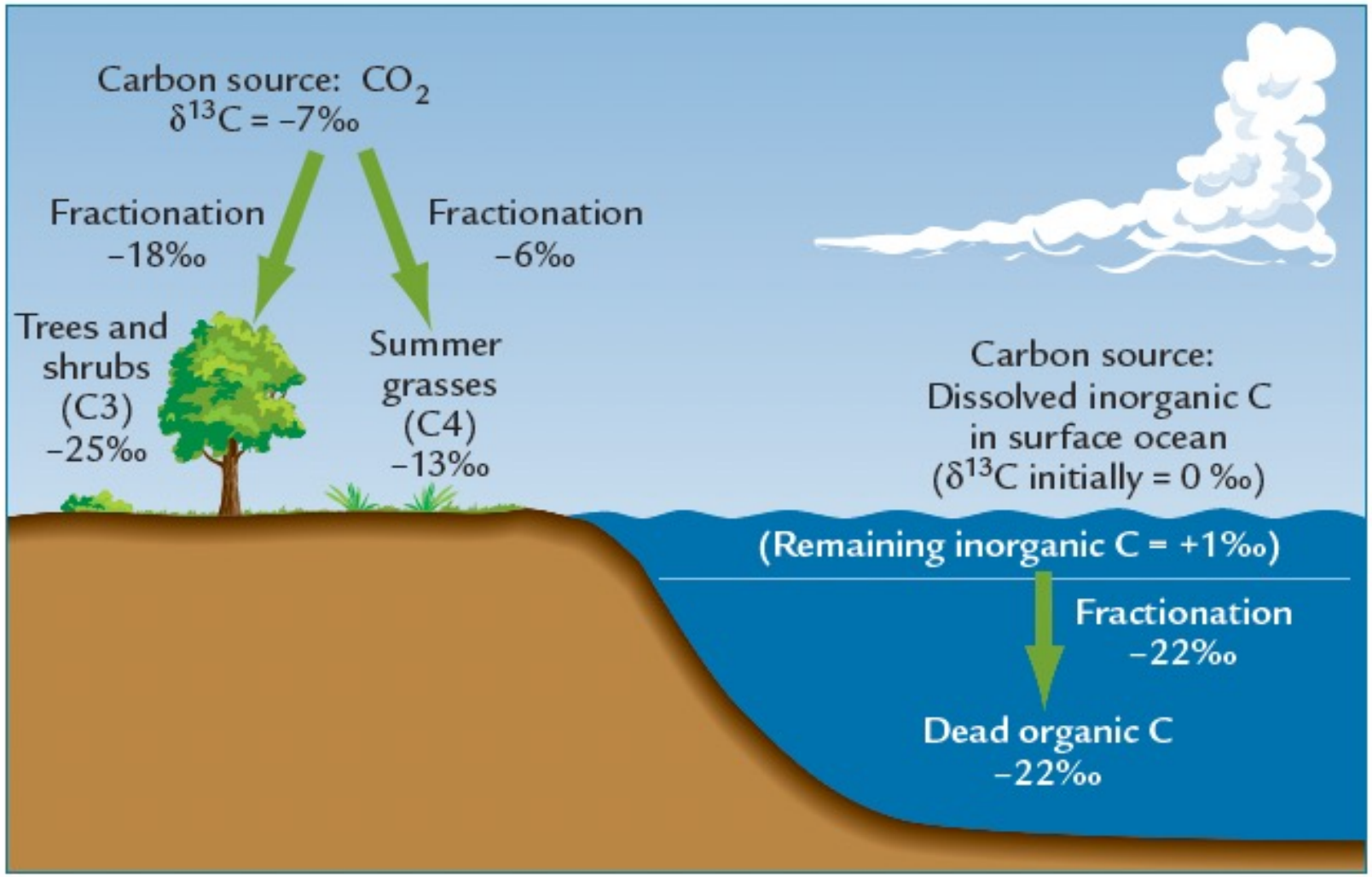

FIGURE-1

Photosynthesis and carbon isotope fractionation

Photosynthesis on land and in the surface ocean converts inorganic carbon to organic form and causes large negative shifts in $\delta^{13}C$ values of the organic carbon produced.

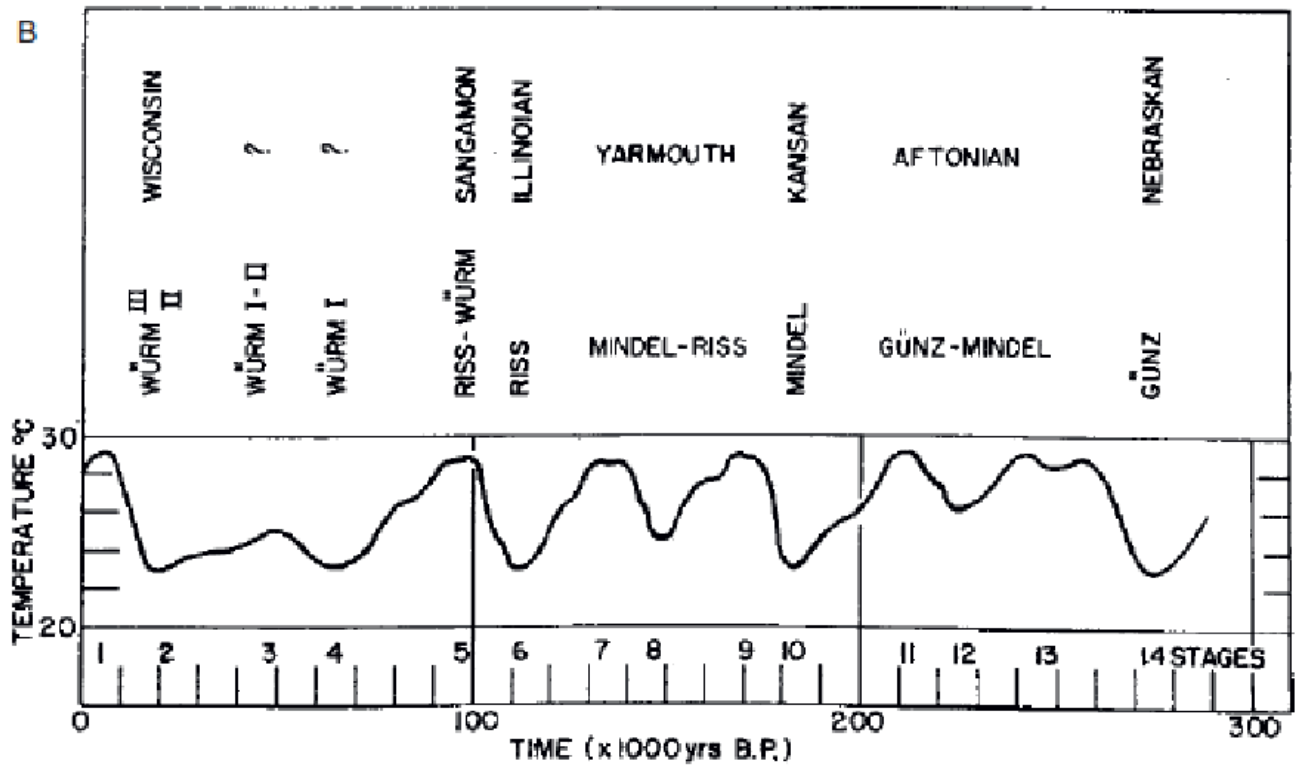
B
WISCONSIN
?
?
SANGAMON
ILLINOIAN
YARMOUTH
KANSAN
AFTONIAN
NEBRASKAN
WÜRM III
WÜRM II
WÜRM I-II
WÜRM I
RISS-WÜRM
RISS
MINDEL-RISS
MINDEL
GÜNZ-MINDEL
GÜNZ
TEMPERATURE °C
30
20
1
2
3
4
5
6
7
8
9
10
11
12
13
14 STAGES
0
100
200
300
TIME (x 1000 yrs B.P.)

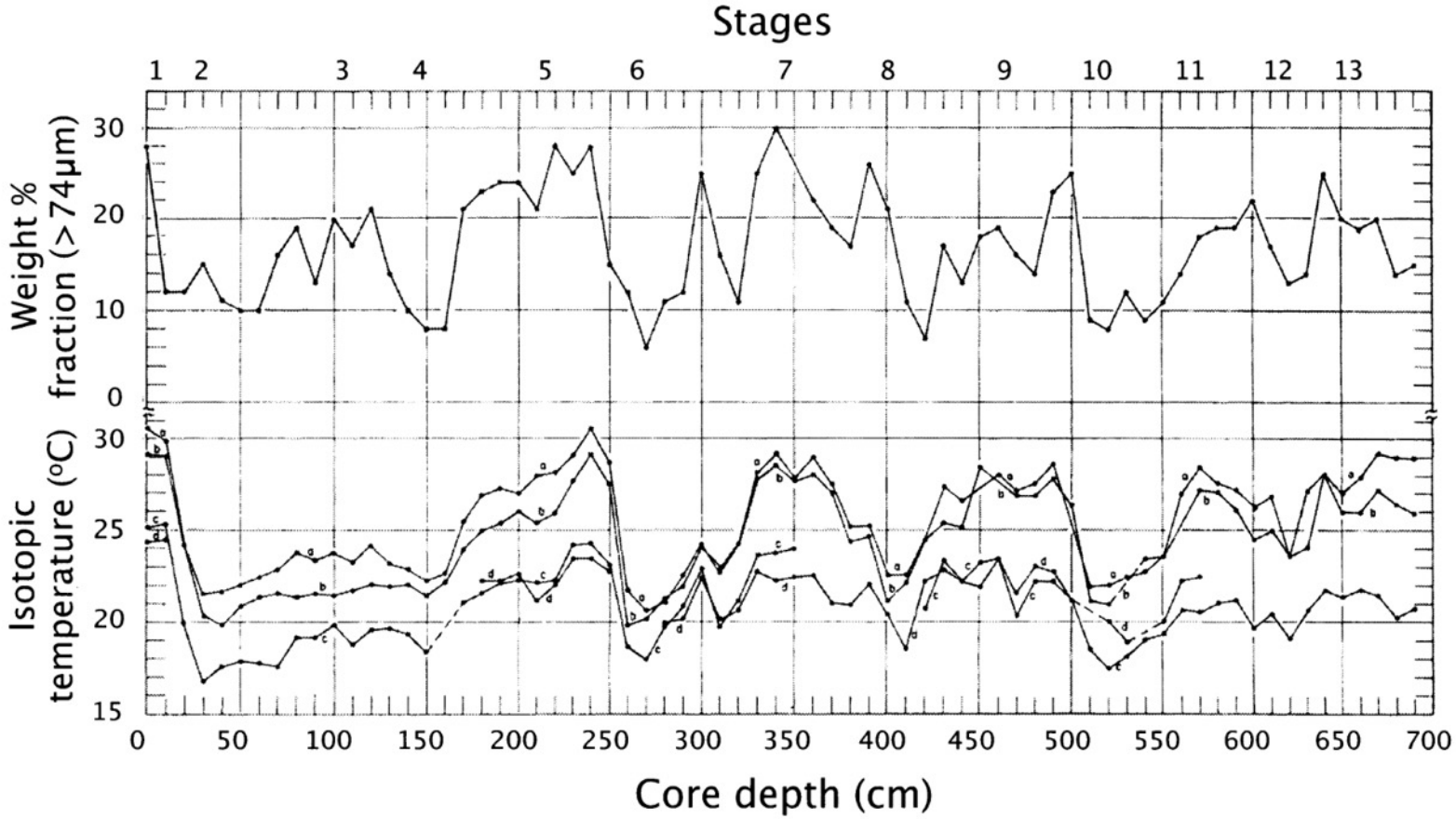

FIGURE *3*.—First view of the glacial cycles from oxygen isotopes: coarse sediment fraction (top panel) and planktonic foraminiferal oxygen-isotope paleotemperature estimates (bottom panel) from Piston Core A-1794 (Caribbean, Lamont Geological Observatory). Isotope 'stages' are labeled at the top. Temperature offsets between the planktonic foraminifer species are mainly related to depth habitat (and hence temperature) of calcification. This record is now considered to span ~400 kyr. (compare with Figure 12). Small letters represent different species. Modified from Emiliani, 1955.

Pearson, Paul N. (2012). *Oxygen Isotopes in Foraminifera: Overview and Historical Review. The Paleontological Society Papers, 18(), 1–38.* doi:10.1017/S1089332600002539

Figure 2. Schematic representation of the potential of planktonic foraminifera to provide insights in zooplankton ...

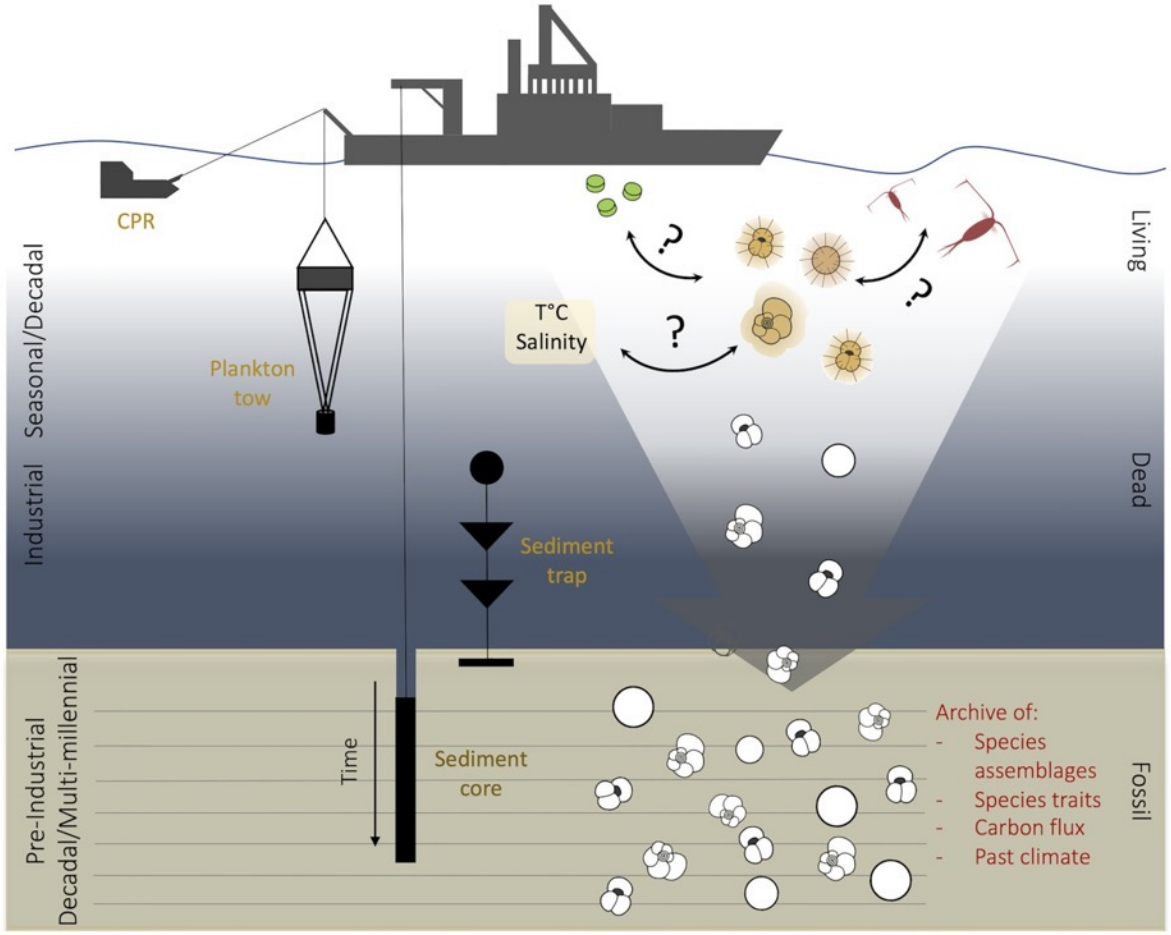

ICES J Mar Sci, Volume 79, Issue 3, April 2022, Pages 917–924, https://doi.org/10.1093/icesjms/fsab123

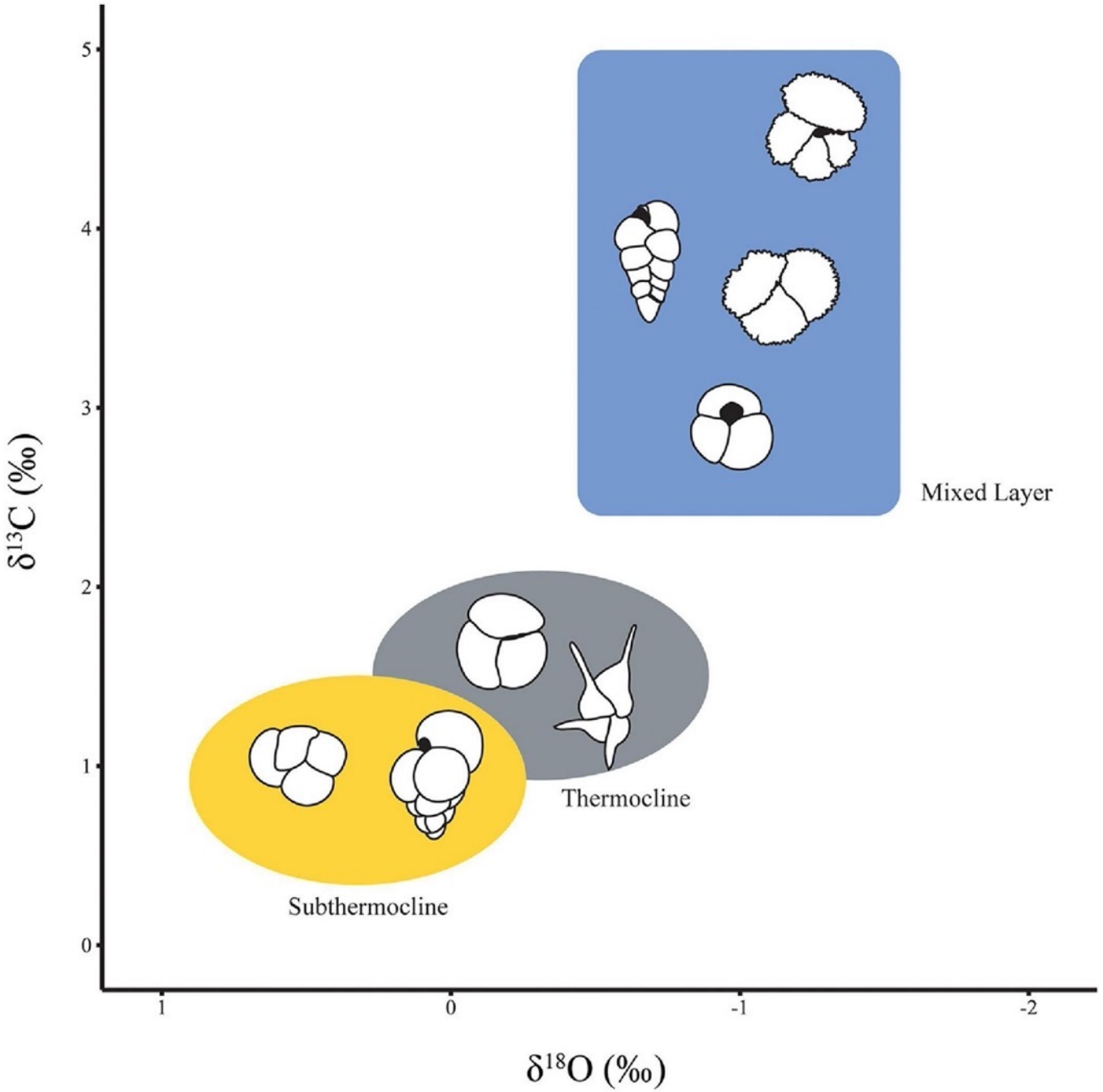

Figure 1. Schematic figure showing the three main eco groups as defined in Aze et al. (2011) based on stable isotope measurements. This figure is illustrative and does not represent absolute values for each ecogroup. Top to bottom the mixed layer is represented by schematic outlines of *Acaranina* spp., *Chiloguembelina* spp., *Morozovelloides* spp. *and Globigerinatheka* spp. Left to right the thermocline is represented by *Subbotina* spp. and *Hantkenina* spp. and the subthermocline represented by *Catapsydrax* spp. and *Jenkinsina* spp. Note the reversed scale on the *x*-axis. Modified from Pearson (1998).

Figure 1. Living and fossil planktonic foraminifera. Panel (a) shows living specimens of planktonic foraminifera ...

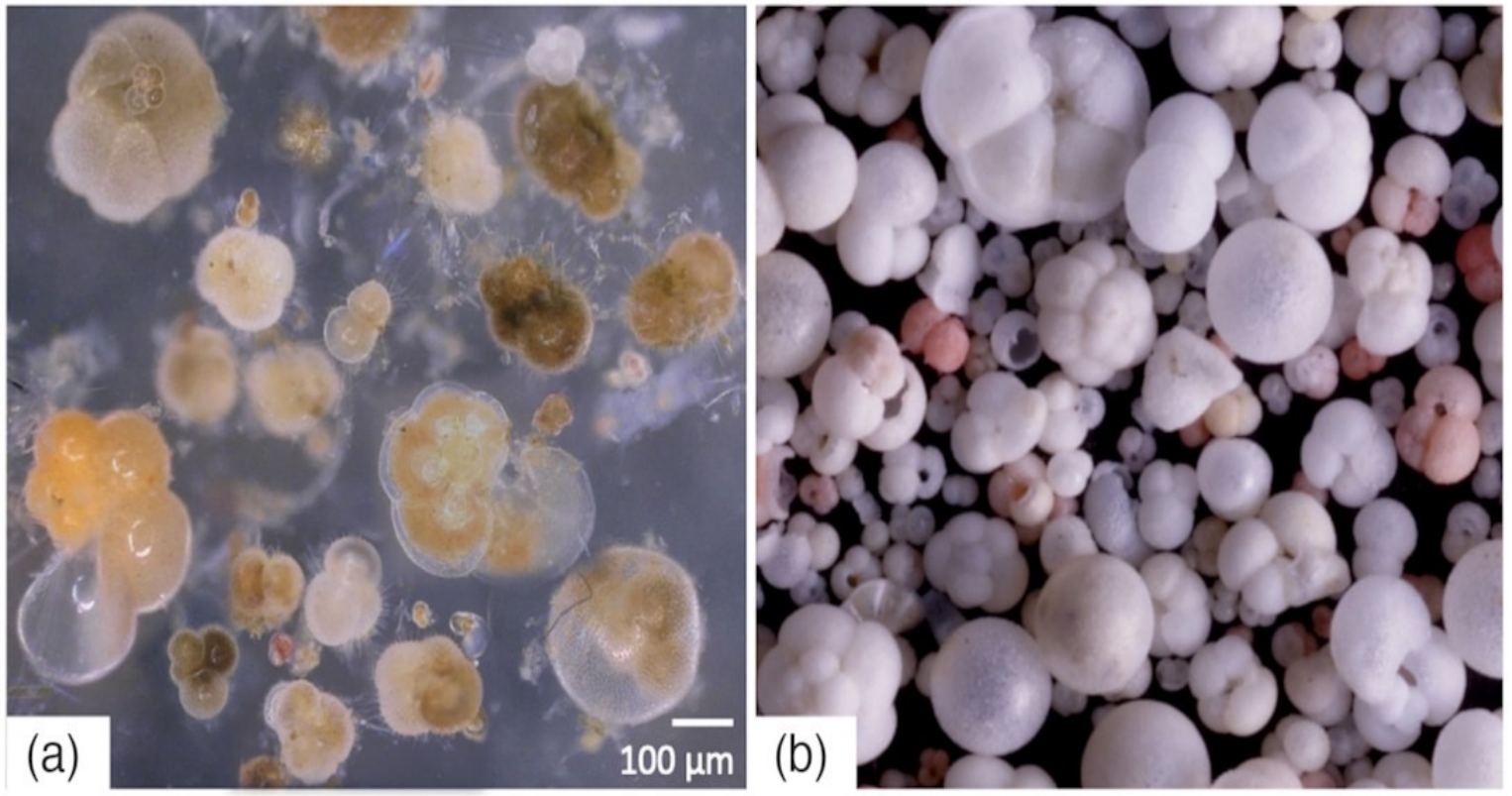

ICES J Mar Sci, Volume 79, Issue 3, April 2022, Pages 917–924, https://doi.org/10.1093/icesjms/fsab123

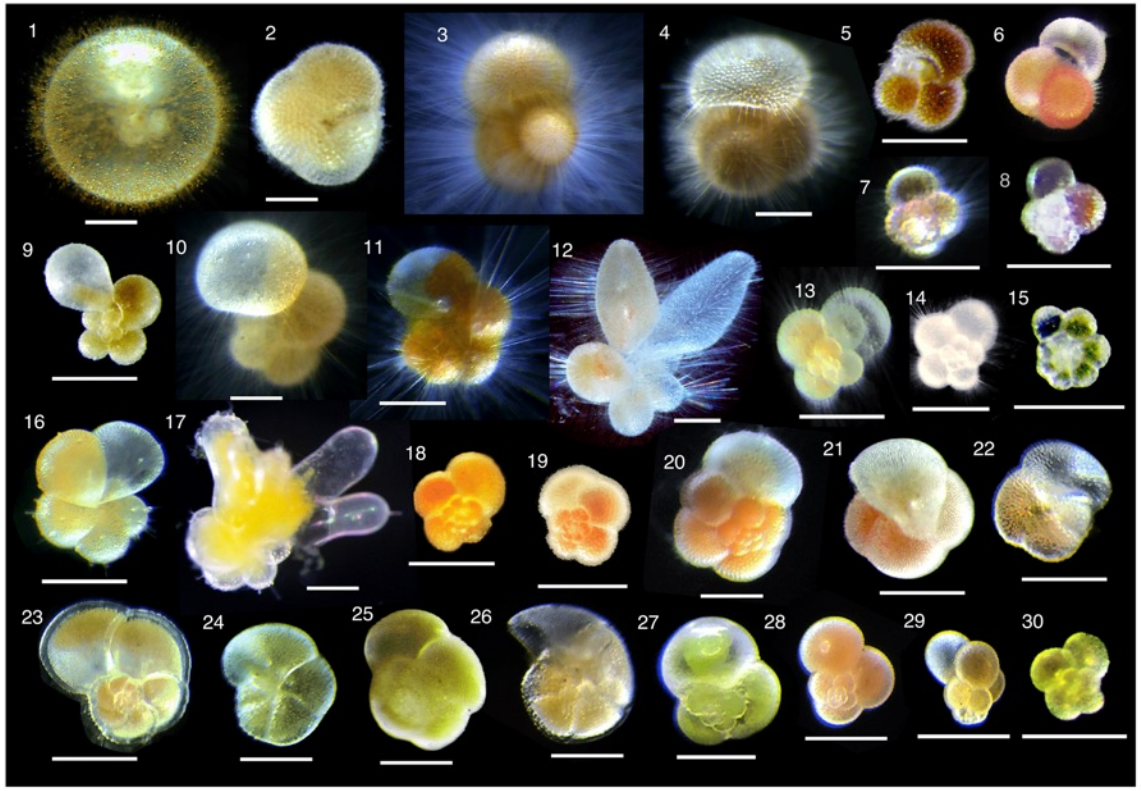

Planktonic foraminifera assemblage from Caribbean sediments.
Source: Michal Kucera

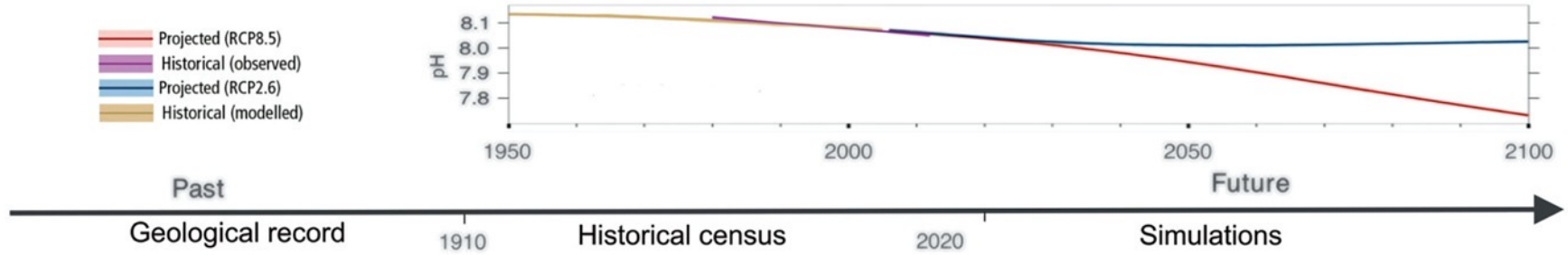

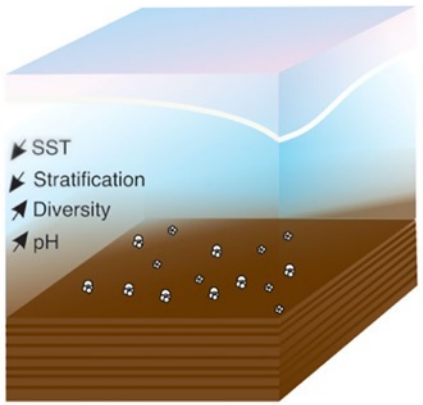

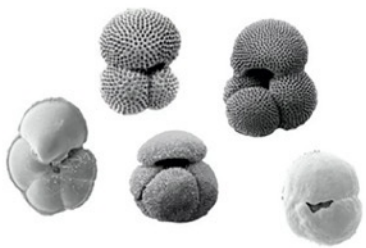

Planktonic foraminifera

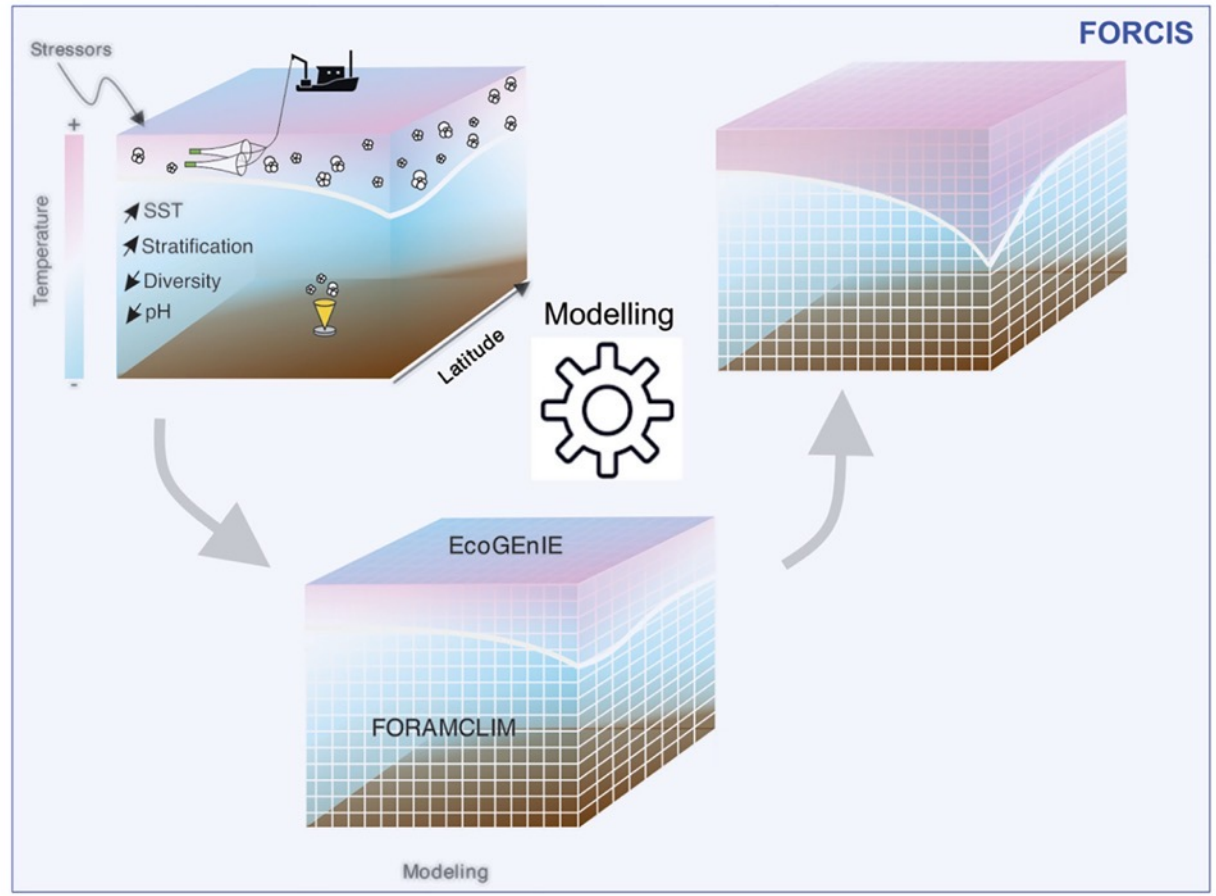

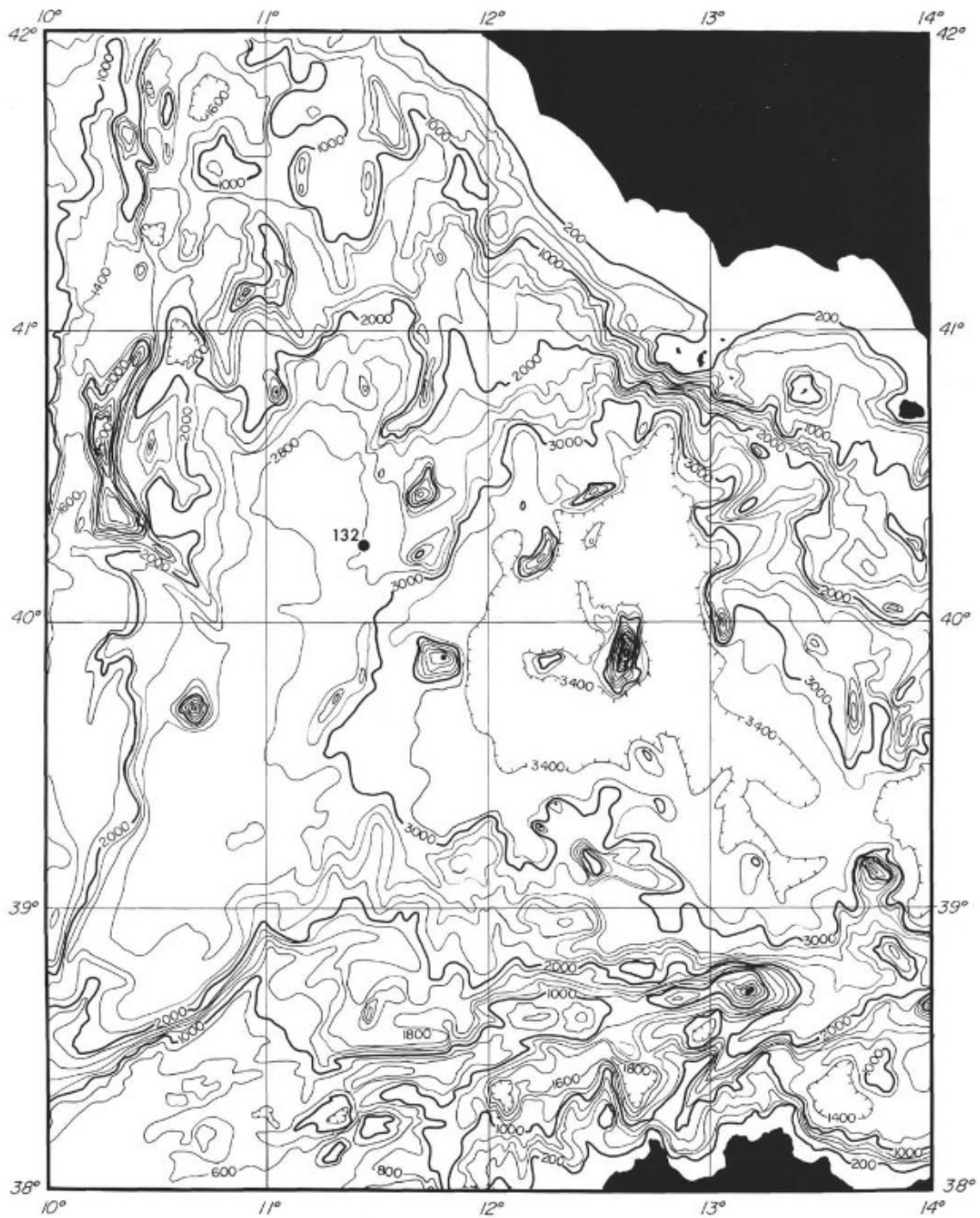
10°
11°
12°
13°
14°
42°
41°
40°
39°
38°
132
200
600
800
1000
1400
1600
1800
2000
2400
3000
3400

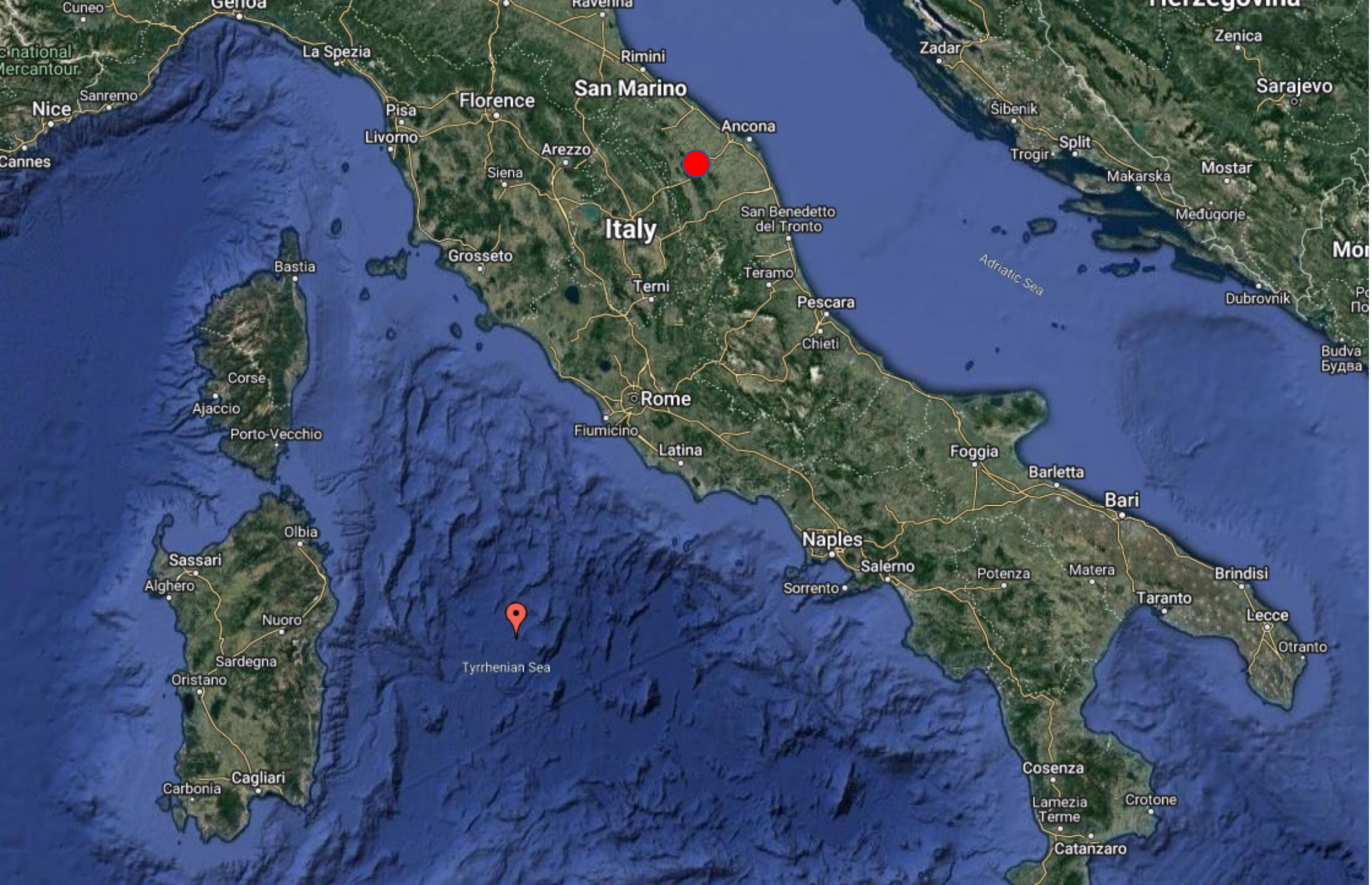
Cuneo
Genoa
La Spezia
Rimini
Ravenna
Zadar
Zenica
Sarajevo
Sanremo
Nice
Cannes
Pisa
Florence
San Marino
Livorno
Ancona
Arezzo
Siena
Šibenik
Split
Trogir
Mostar
Makarska
Međugorje
Italy
San Benedetto del Tronto
Grosseto
Adriatic Sea
Bastia
Terni
Teramo
Pescara
Dubrovnik
Chieti
Budva
Corse
Ajaccio
Rome
Porto-Vecchio
Fiumicino
Latina
Foggia
Barletta
Bari
Olbia
Naples
Sassari
Salerno
Potenza
Matera
Brindisi
Alghero
Sorrento
Taranto
Nuoro
Lecce
Otranto
Sardegna
Tyrrhenian Sea
Oristano
Cosenza
Cagliari
Carbonia
Lamezia Terme
Crotone
Catanzaro

46. THE QUATERNARY RECORD IN THE TYRRHENIAN AND IONIAN BASINS OF THE MEDITERRANEAN SEA

M. B. Cita, Institute of Paleontology, University of Milano, Milan, Italy
M. A. Chierici, AGIP Mineraria, San Donato Milanese, Milan, Italy
G. Ciampo, Institute of Paleontology, University of Naples, Naples, Italy
M. Moncharmont Zei, Institute of Paleontology, University of Naples, Naples, Italy
S. d'Onofrio, Institute of Geology, University of Bologna, Bologna, Italy
W. B. F. Ryan, Lamont-Doherty Geological Observatory of Columbia University, Palisades, New York
and
R. Scorziello, Institute of Paleontology, University of Naples, Naples, Italy

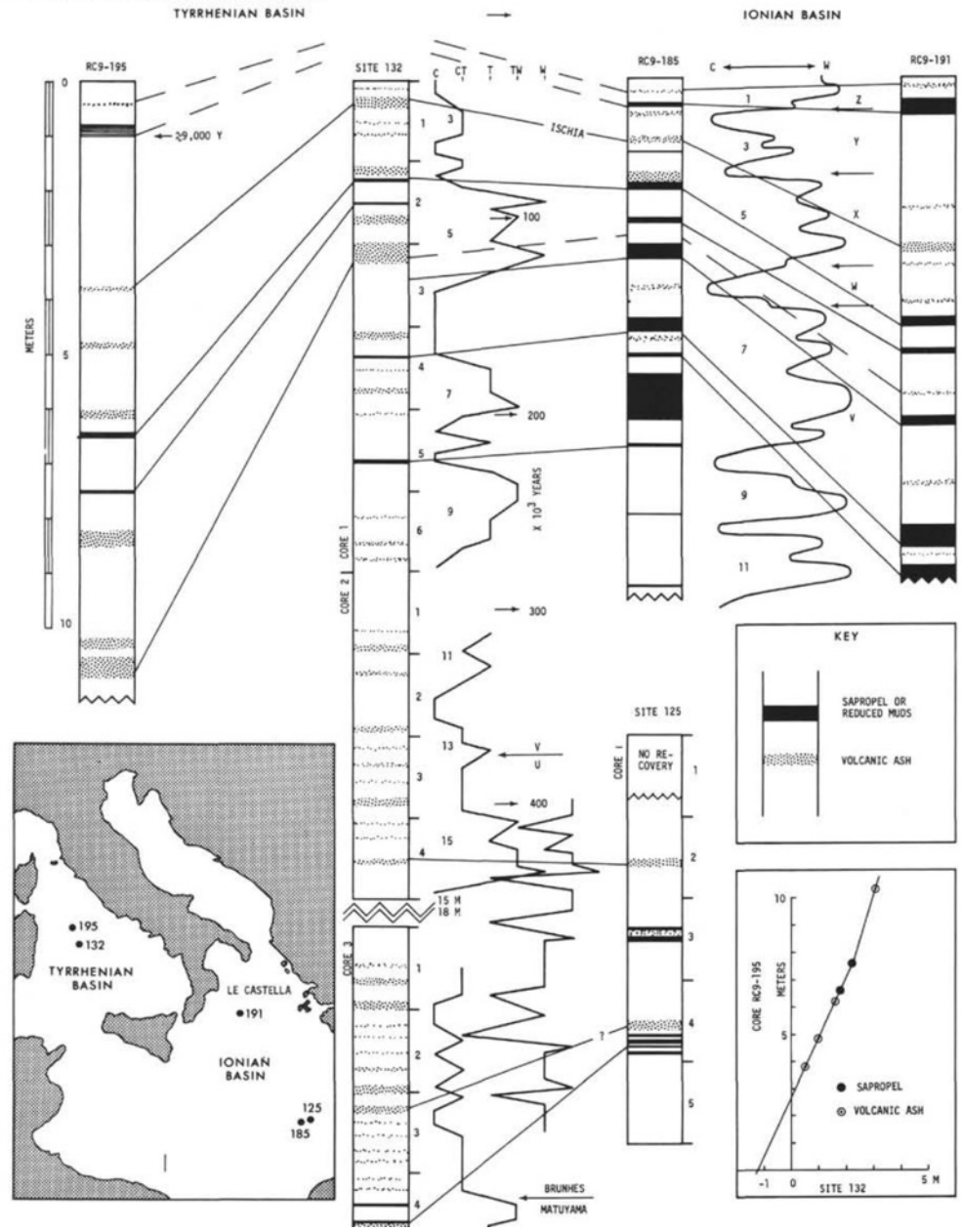

REPORT

Oxygen and Carbon Isotopes from Calcareous Nannofossils as Paleoceanographic Indicators

STANLEY V. MARGOLIS, PETER M. KROOPNICK, DAVID E. GOODNEY, WALTER C. DUDLEY, AND , MAUREEN E. MAHONEY Authors Info & Affiliations

SCIENCE · 15 Aug 1975 · Vol 189, Issue 4202 · pp. 555-557 · DOI: 10.1126/science.189.4202.555

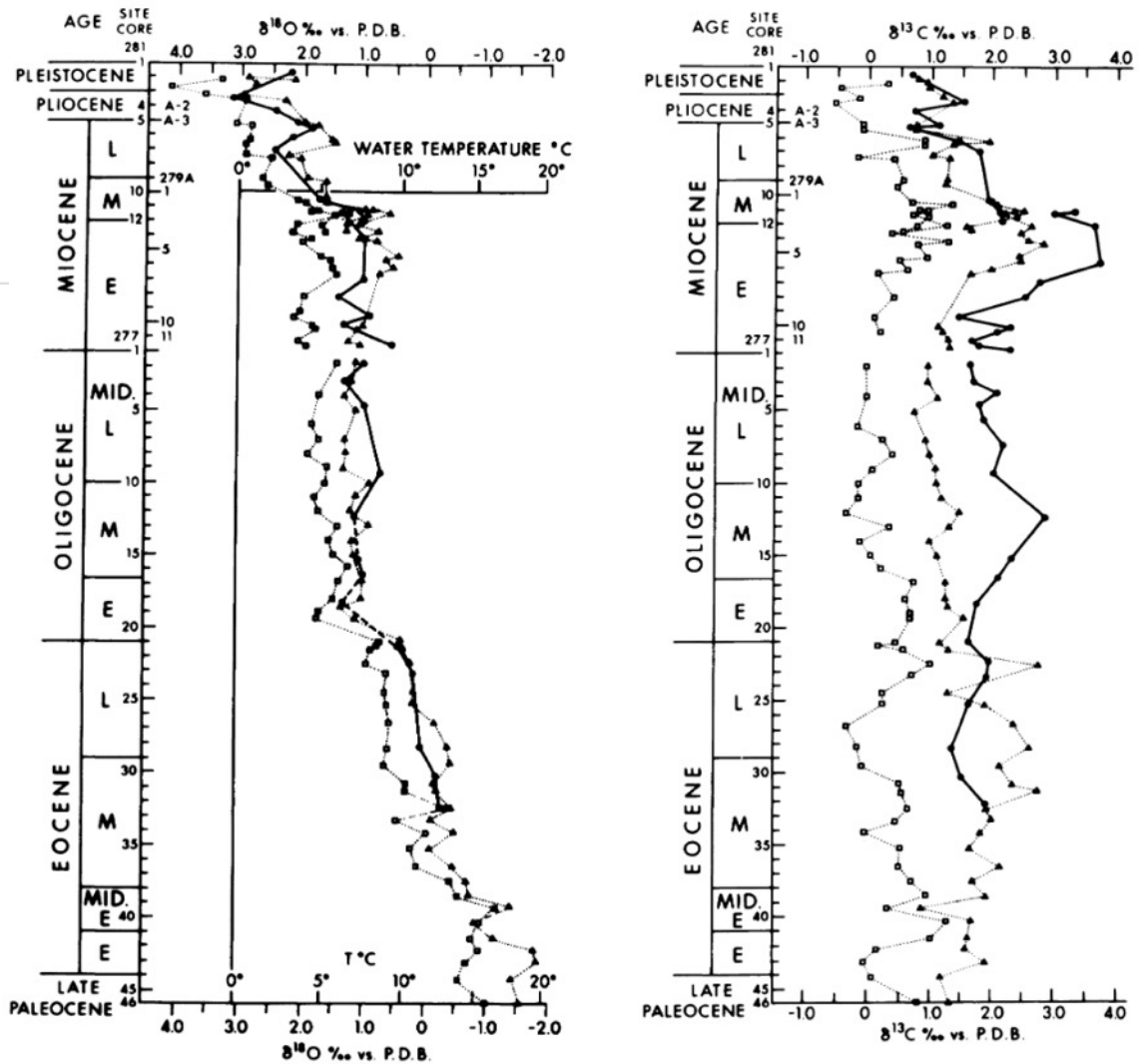

Fig. 1 (left). Oxygen isotope data from DSDP Leg 29, sites 277, 279, and 281, showing the per mil deviation from PDB for planktonic (▲) and benthic (□) foraminifera (*5*) and calcareous nannofossils (●) (this study). Note the close correspondence between nannofossil and planktonic foraminifera curves. Stratigraphic plots (*6*) are not based on thickness or age differences between samples, but represent relative positions in each cored interval. Water temperature values (*5*) are valid from base of sequence to middle Miocene only. Above core 10 at site 281 water temperature estimations are complicated by seawater isotopic changes (*5*). Calcareous nannofossils are assumed to be equilibrating with surface waters during growth. Nannofossil values that are higher than planktonic foraminifera values represent possible isotope exchange with deeper waters. Fig. 2 (right). Carbon isotope data from sites 277, 279, and 281 showing per mil deviation from PDB for planktonic (▲) and benthic (□) foraminifera (*5*) and calcareous nannofossils (●) (this study). Nannofossil $\delta^{13}C$ trends parallel those for foraminifera, but are higher than planktonic foraminifera values in Oligocene to middle Miocene samples. Nannofossil $\delta^{13}C$ values significantly lower than those for associated planktonic foraminifera represent possible isotope exchange with deeper waters. Stratigraphic plots are not based on thickness or age differences between samples, but represent relative positions in each cored interval.

19 March 1976, Volume 191, Number 4232 SCIENCE

The Surface of the Ice-Age Earth

Quantitative geologic evidence is used to reconstruct boundary conditions for the climate 18,000 years ago.

CLIMAP Project Members

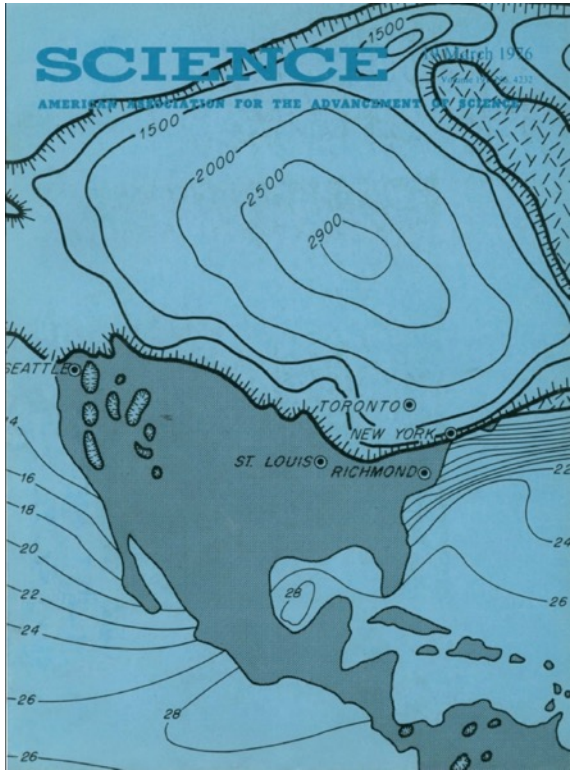

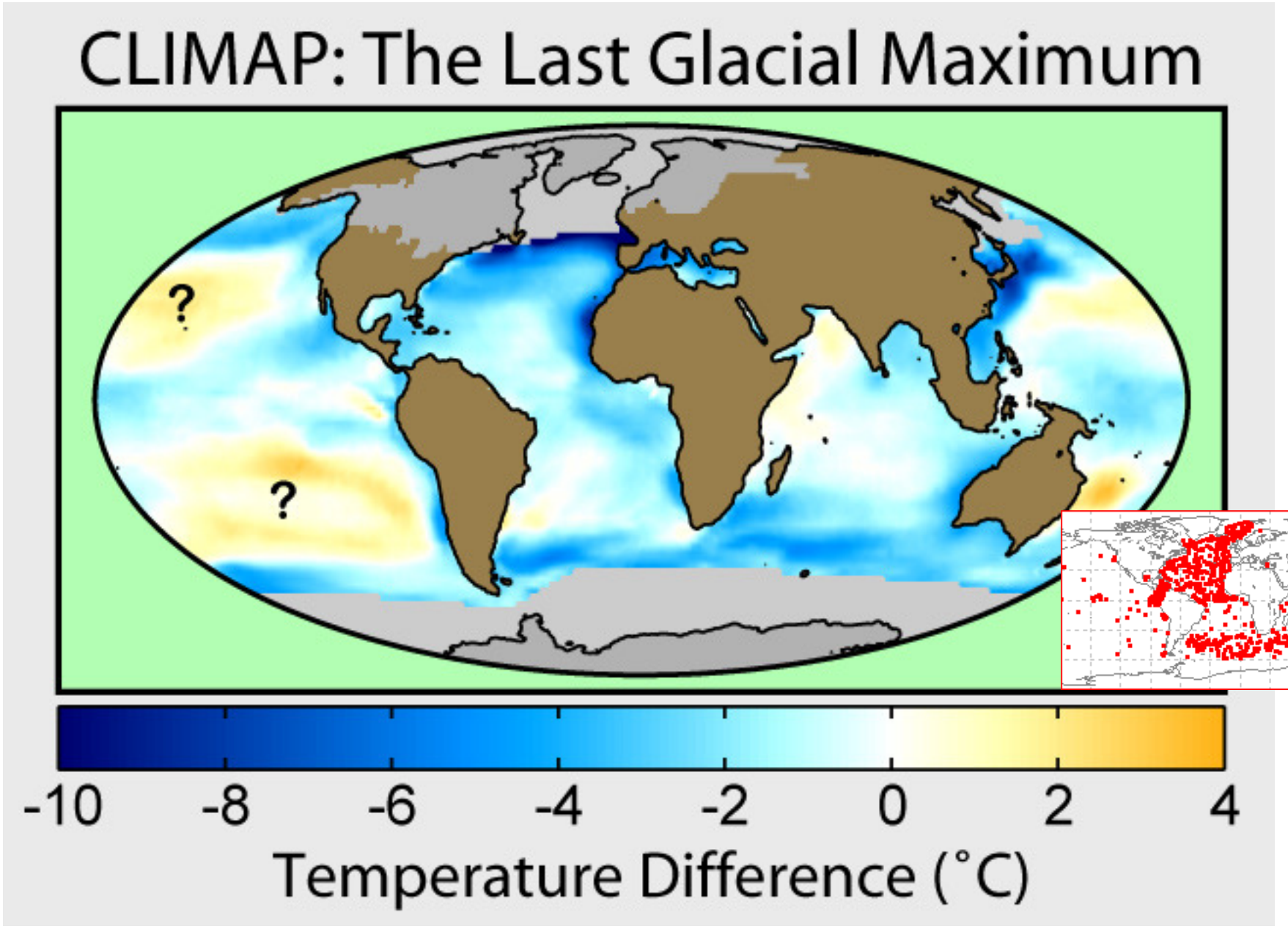

CLIMAP Project Members (1976): CLIMAP sea surface temperature anomaly (LGM-modern).

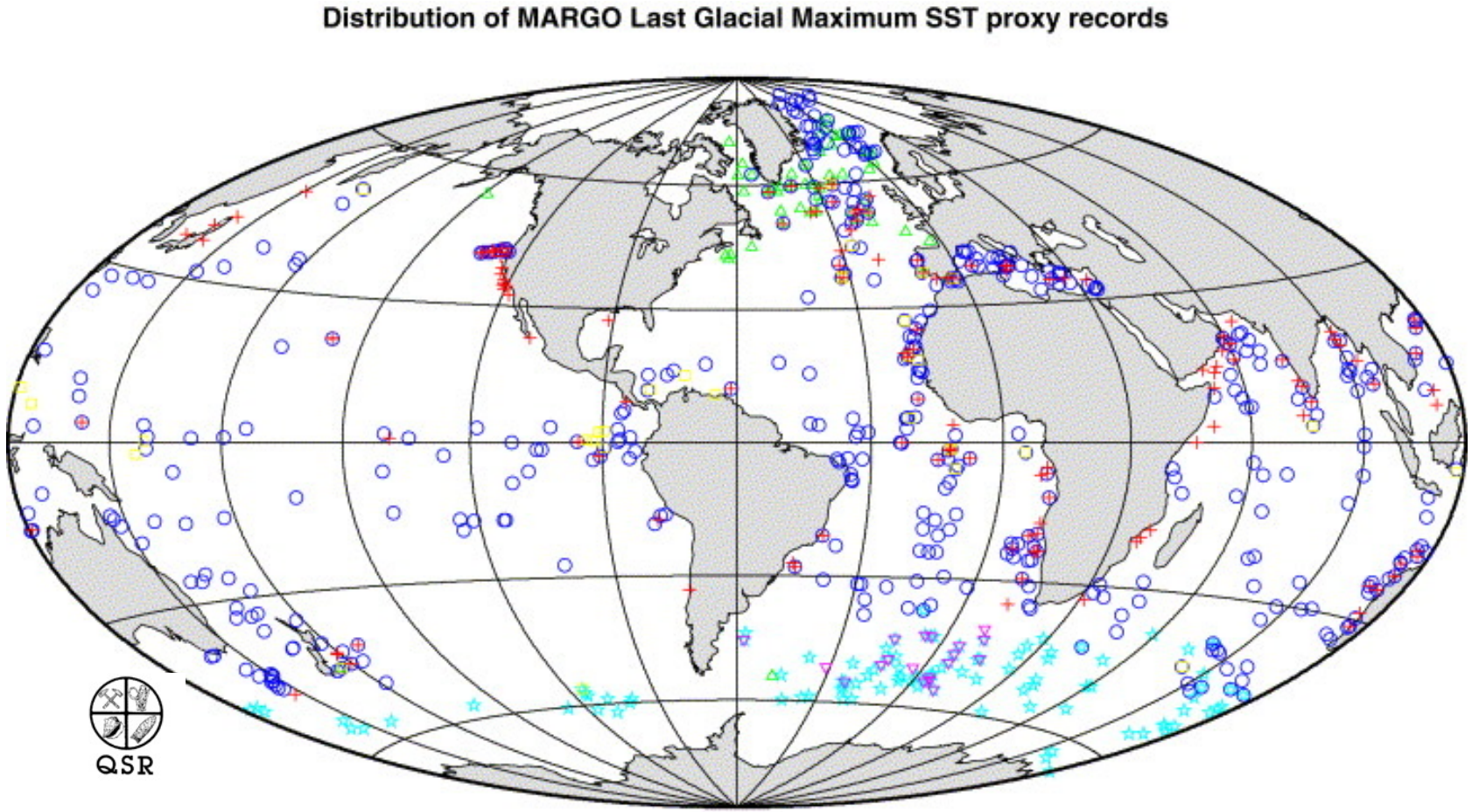

ELSEVIER

Quaternary Science Reviews 24 (2005) 813–819

QSR

margo

Multiproxy approach for the reconstruction of the glacial ocean surface (MARGO)

Michal Kucera[a,*], Antoni Rosell-Melé[b], Ralph Schneider[c], Claire Waelbroeck[d], Mara Weinelt[e]

ELSEVIER
Quaternary Science Reviews 24 (2005) 813–819
QSR

margo

Multiproxy approach for the reconstruction of the glacial ocean surface (MARGO)

Michal Kucera[a,*], Antoni Rosell-Melé[b], Ralph Schneider[c], Claire Waelbroeck[d], Mara Weinelt[e]

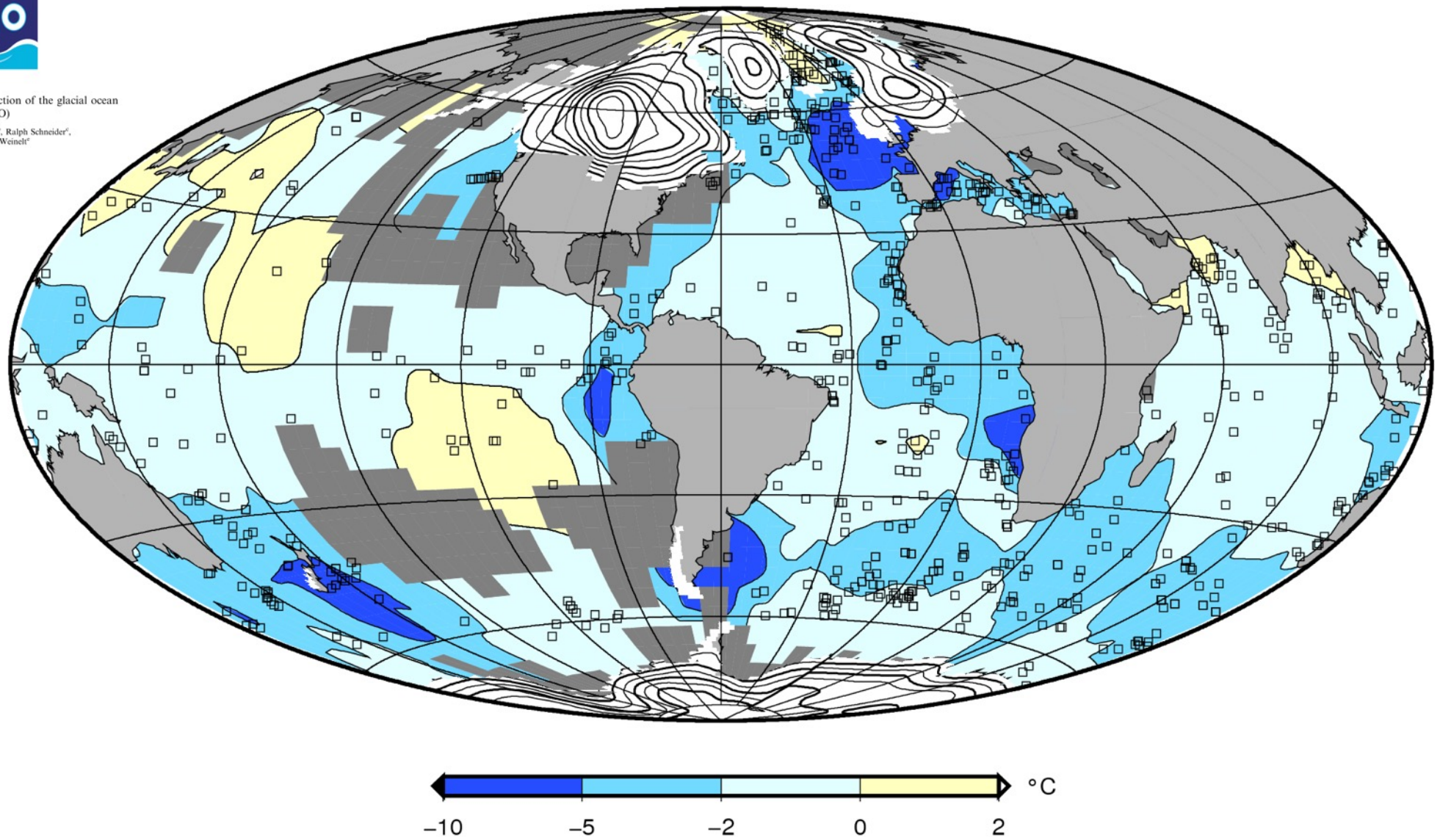

This map shows the reconstructed LGM sea-surface temperature anomaly, computed as the difference between the Last Glacial Maximum (LGM, between 19,000 and 23,000 years before present) and present day, in units of °C for the Northern Hemisphere winter season (January-February-March).

Open Access | Published: 22 August 2017

ForCenS, a curated database of planktonic foraminifera census counts in marine surface sediment samples

Michael Siccha ✉ & Michal Kucera

Scientific Data **4**, Article number: 170109 (2017) | Cite this article

From: ForCenS, a curated database of planktonic foraminifera census counts in marine surface sediment samples

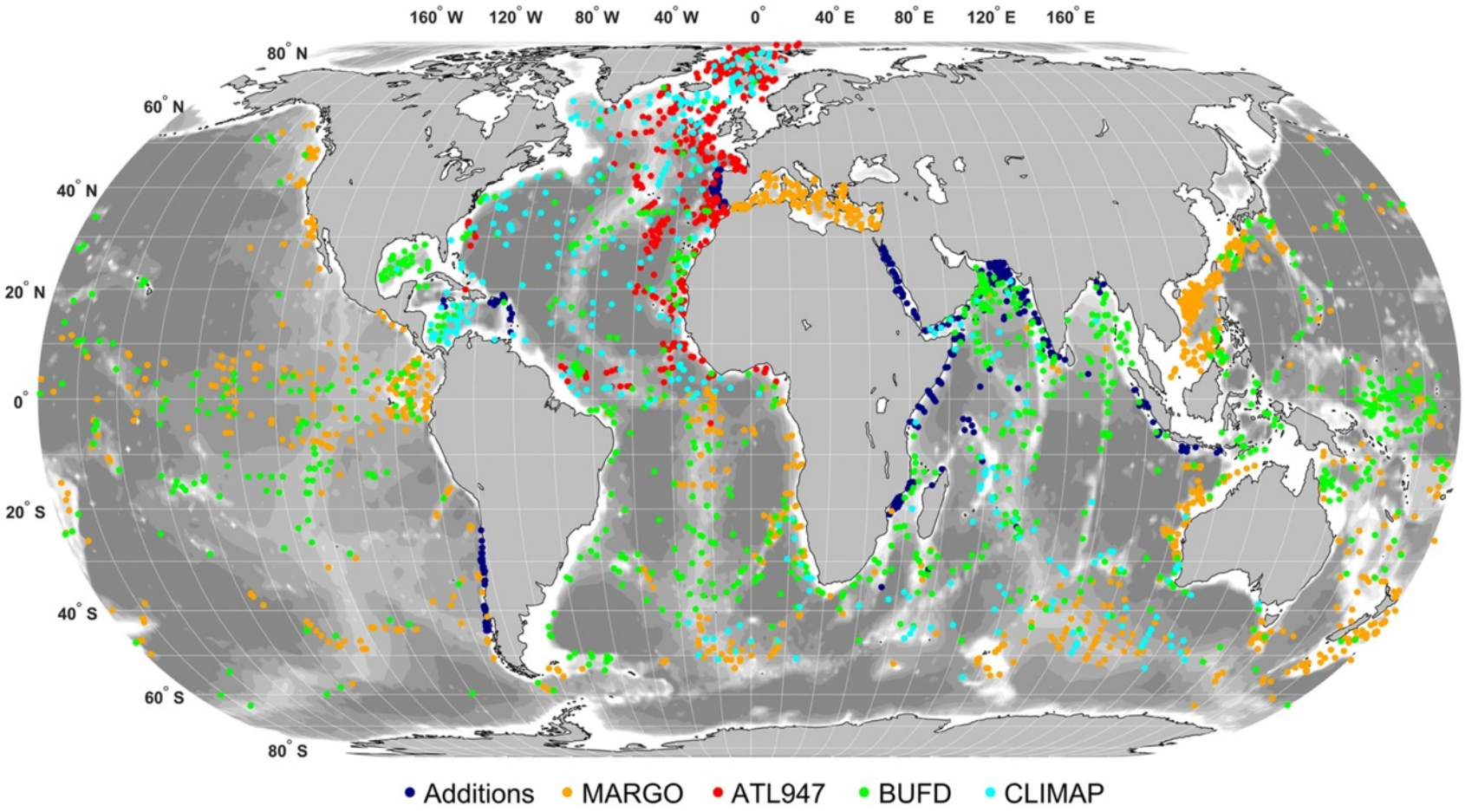

Colours denote the sample source, the first occurrence of a sample in a compilation taking precedence over reuse in later compilations.

THE FORESTS OF THE OCEANS

AURORA
SCIENCE COMMUNICATION

PHOTIC ZONE (first ~ 200 meters deep of the oceans).

Coccolithophores

Are microscopic marine algae that live as far as the sun's rays can reach, in what is known as the **photic zone**

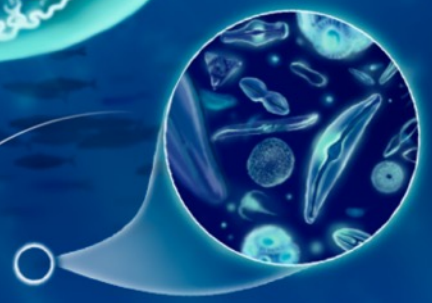

These algae *are part of the diverse marine microscopic world, which is still full of* **mysteries and unknowns.**

During their life cycle, these algae **form various structures** that are composed of the **mineral calcite.**

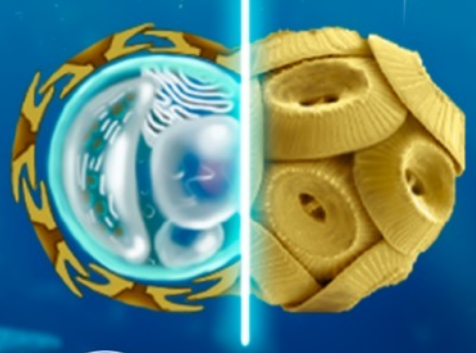

To form their plates, **they need to consume CO2 and solar energy.**

These processes **help** *with the production of* **the oxygen we breathe.**

When coccolithophores **die, their plates fall** and over millions of years **accumulate on the seafloor.**

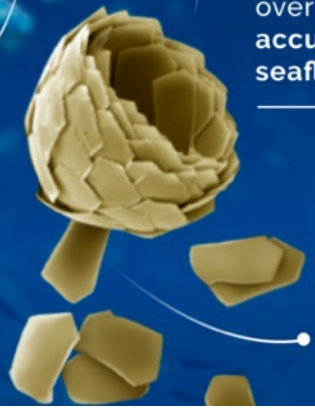

In this way, **they bury CO2** in the deep sea, **helping to reduce global warming on the planet.**

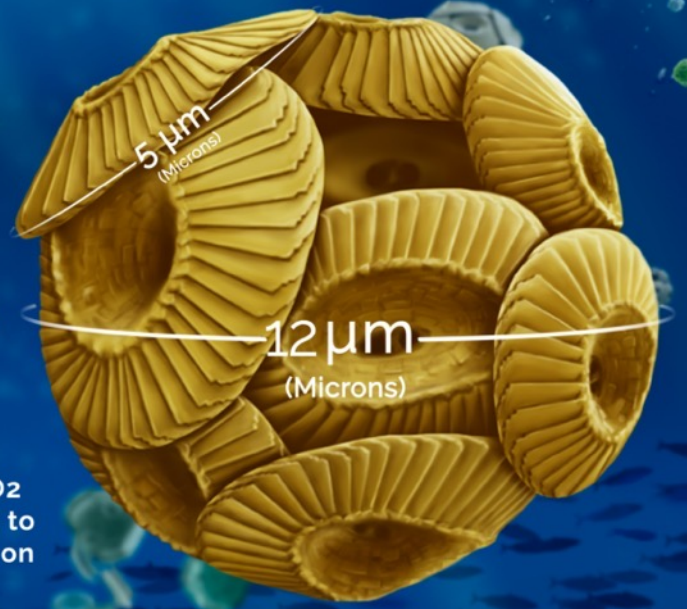

OCEANIC DYNAMICS: THE PRESENT IS THE KEY TO THE PAST

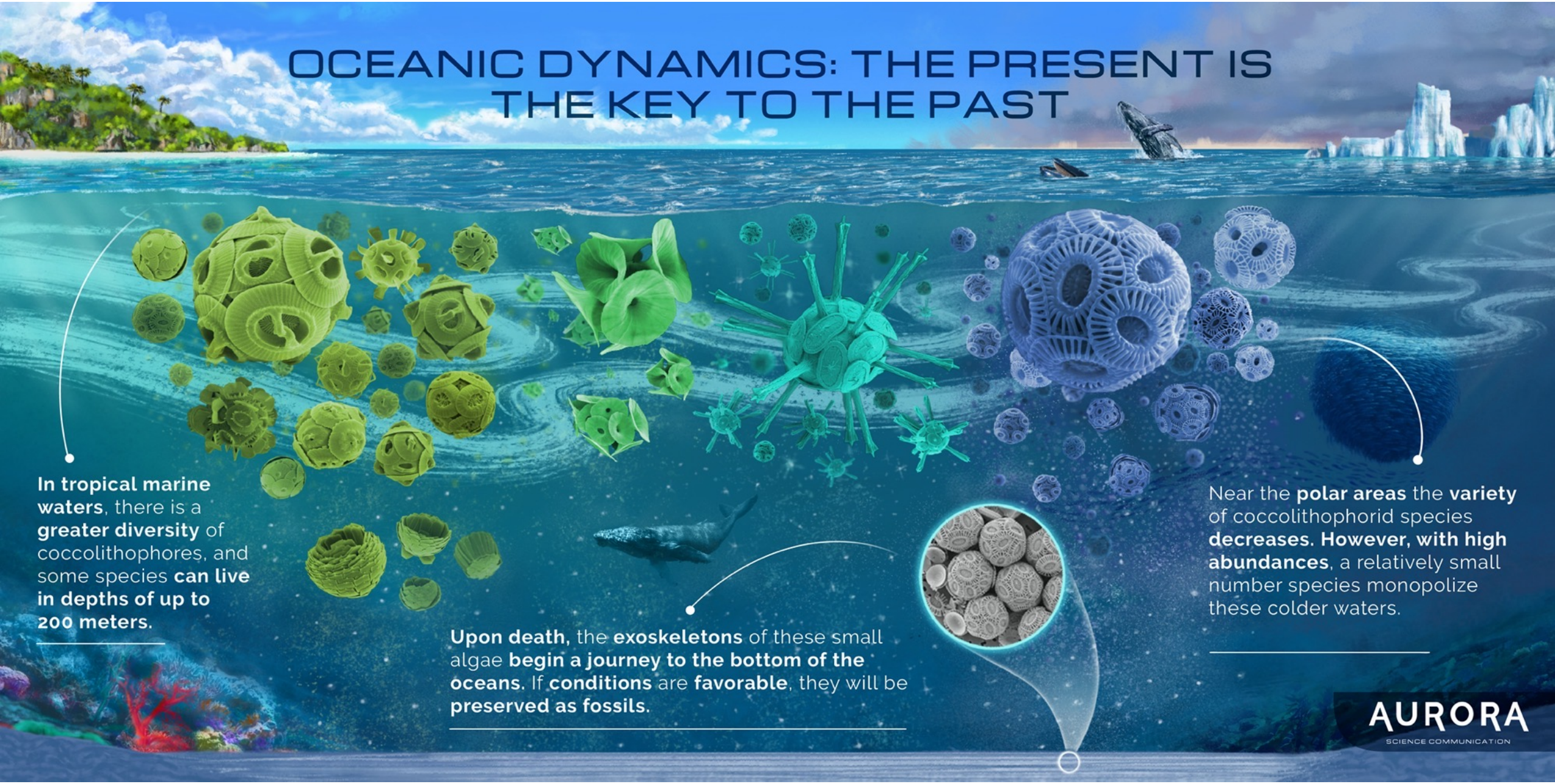

In tropical marine waters, there is a **greater diversity** of coccolithophores, and some species **can live in depths of up to 200 meters.**

Upon death, the **exoskeletons** of these small algae **begin a journey to the bottom of the oceans.** If **conditions** are **favorable**, they will be **preserved as fossils.**

Near the **polar areas** the **variety** of coccolithophorid species **decreases. However, with high abundances**, a relatively small number species monopolize these colder waters.

AURORA
SCIENCE COMMUNICATION

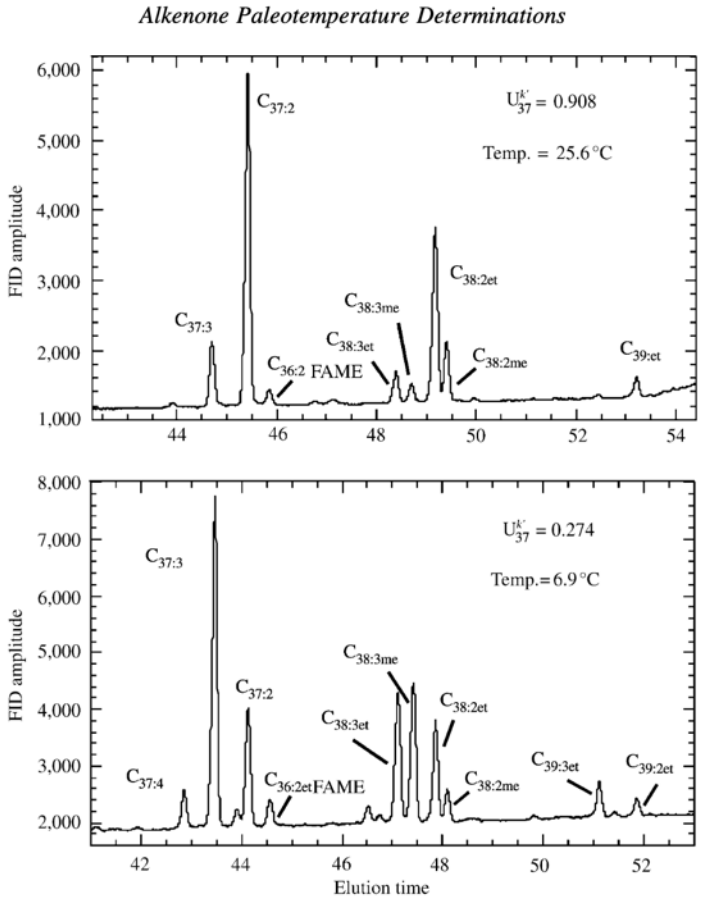

Figure 1 Typical GC-FID chromatograms of alkenone-containing sediment extracts.

$$U_{37}^{K} = \frac{C_{37:2} - C_{37:4}}{C_{37:2} + C_{37:3} + C_{37:4}} \quad (1)$$

$$U_{37}^{K'} = \frac{C_{37:2}}{C_{37:2} + C_{37:3}}. \quad (2)$$

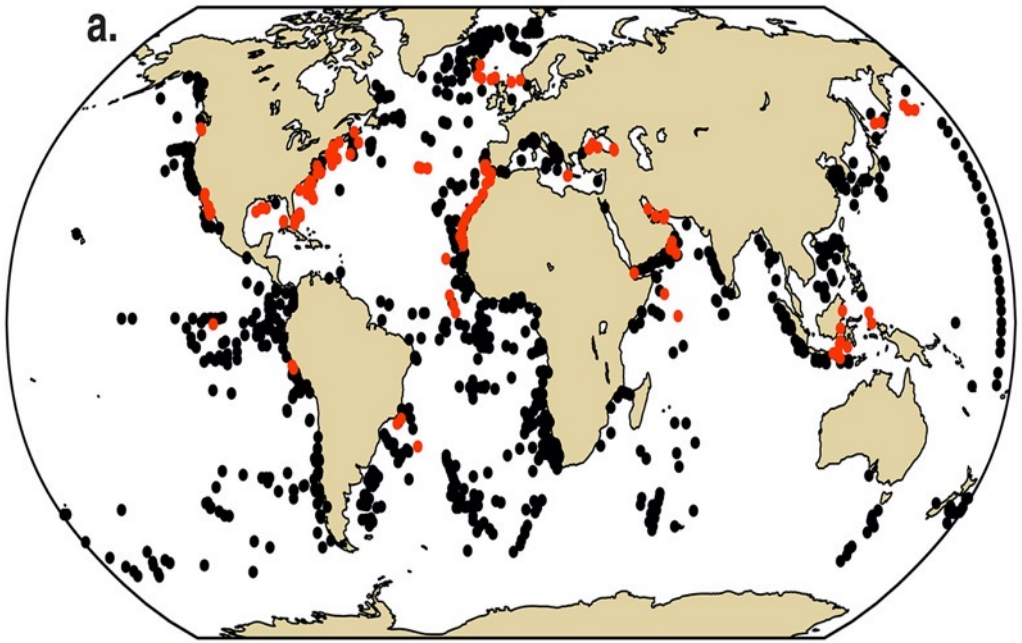

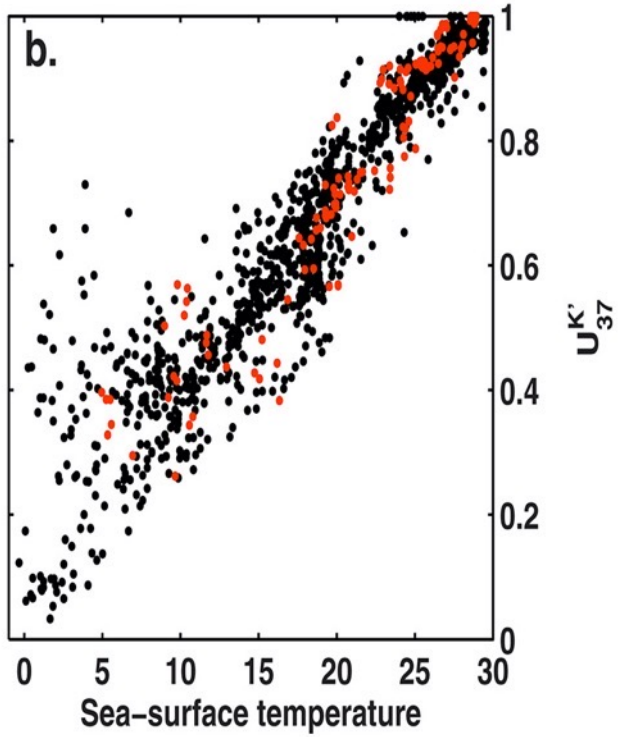

Paleoceanog and Paleoclimatol, Volume: 33, Issue: 3, Pages: 281-301, First published: 06 February 2018, DOI: (10.1002/2017PA003201)

Coccolithophore paleoproductivity and ecology response to deglacial and Holocene changes in the Azores Current System

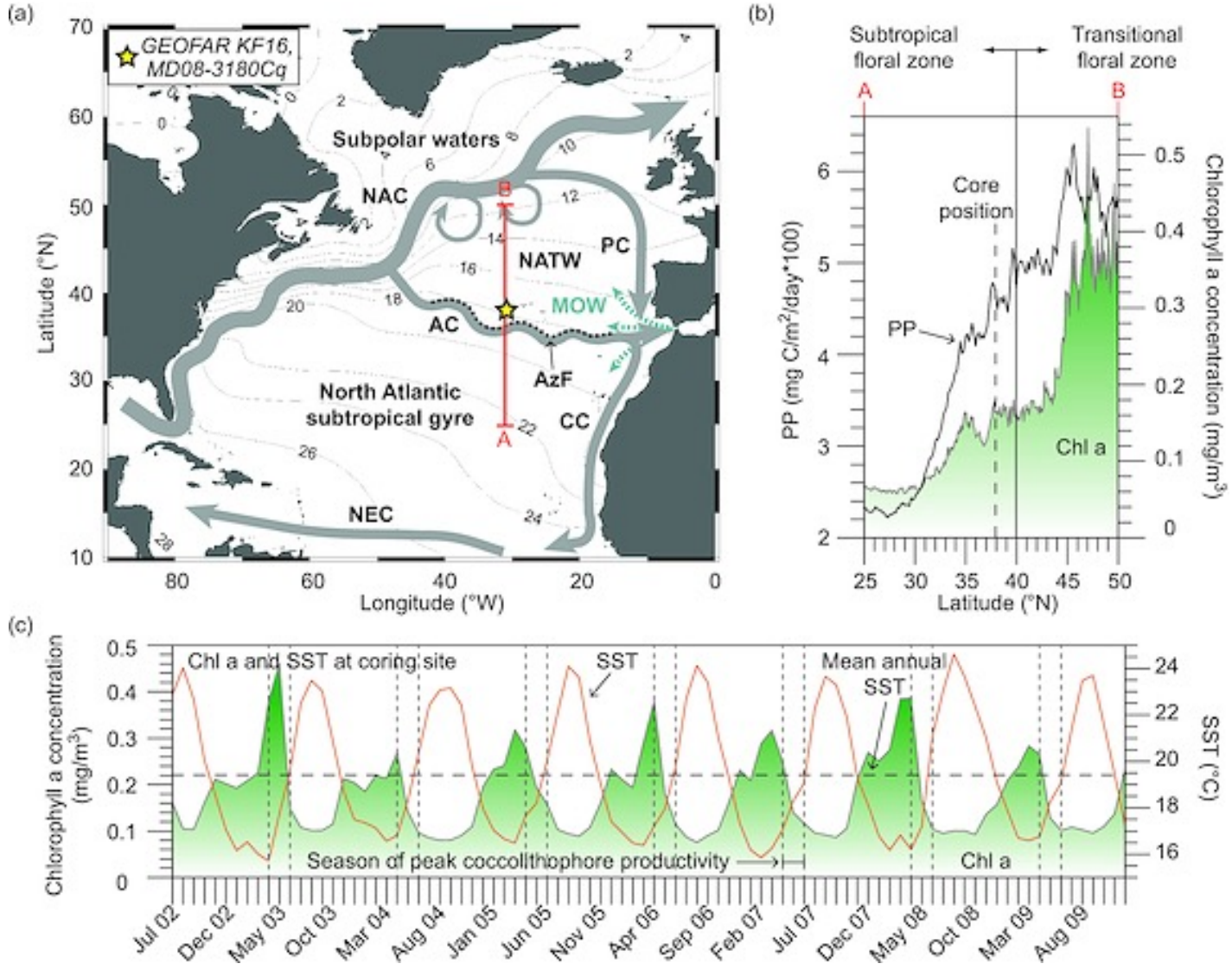

Schwab et al. ; Paleoceanography, Volume: 27, Issue: 3, First published: 08 August 2012, DOI: (10.1029/2012PA002281)

XRF Core Scanner

XRF Core Scanner III (super slit)

XRF Core Scanner II

XRF Core Scanner I

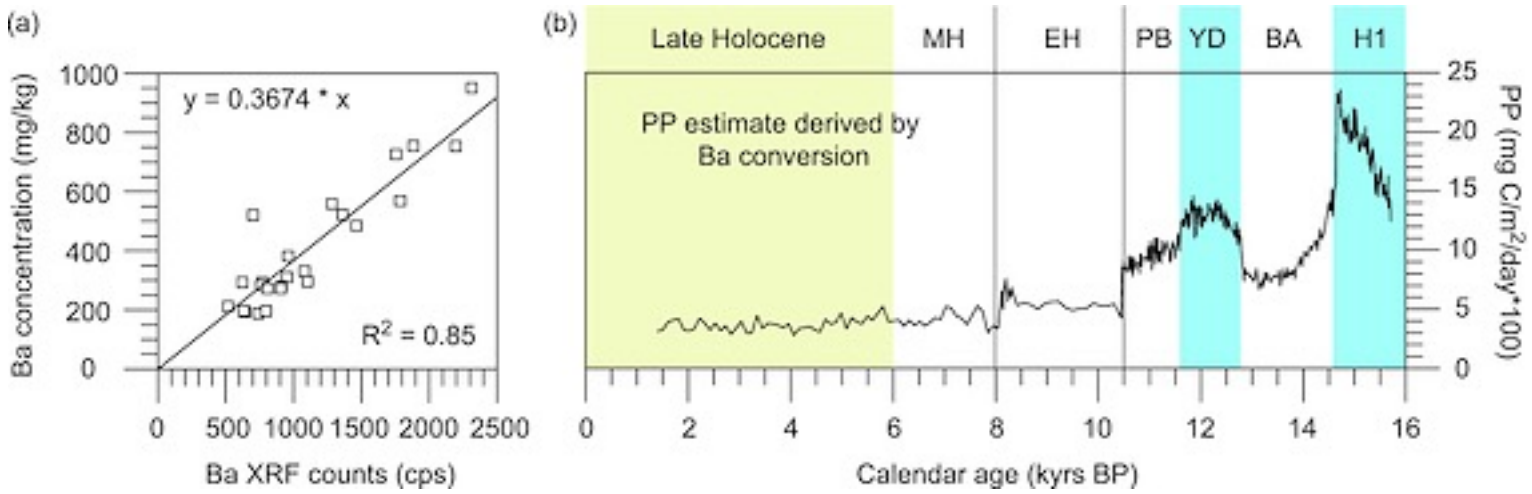

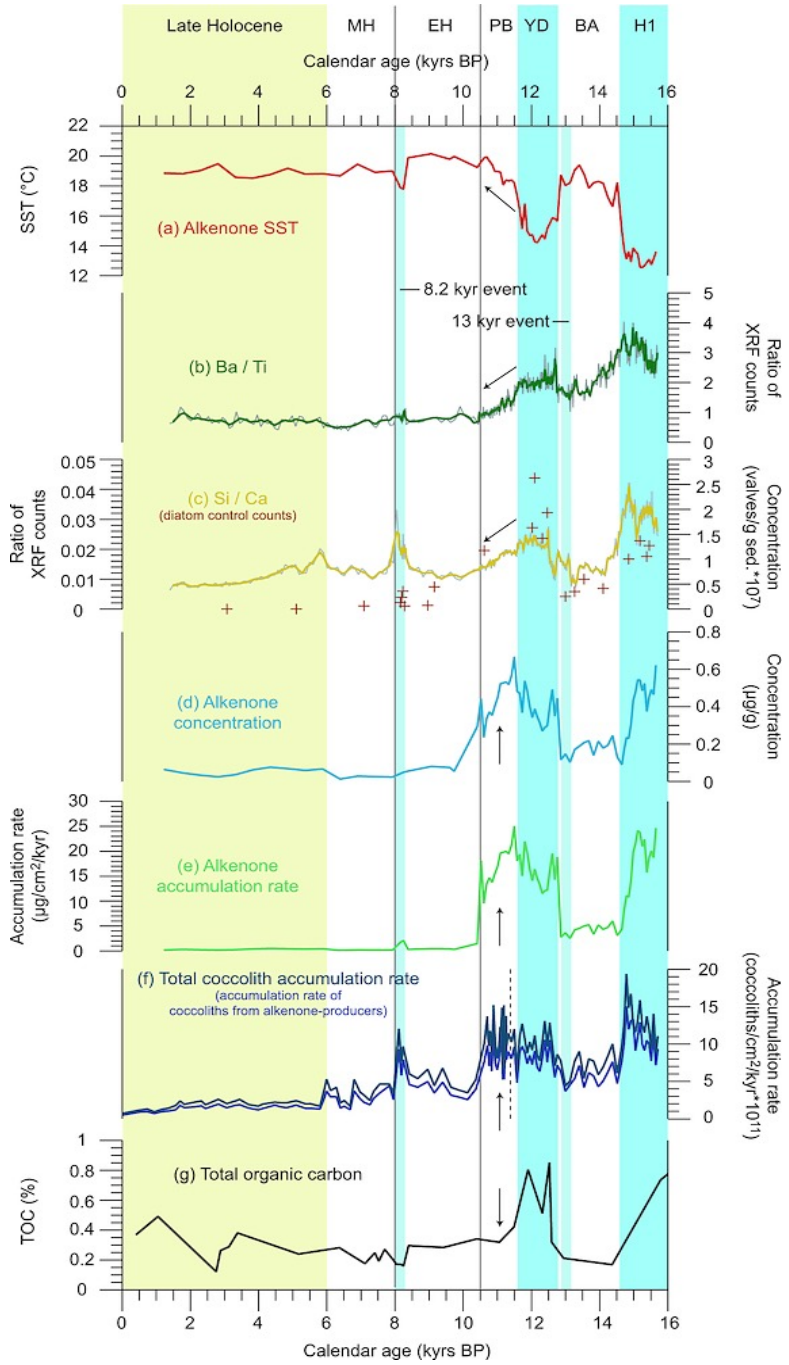

Schwab et al. ; Paleoceanography, Volume: 27, Issue: 3, First published: 08 August 2012, DOI: (10.1029/2012PA002281)

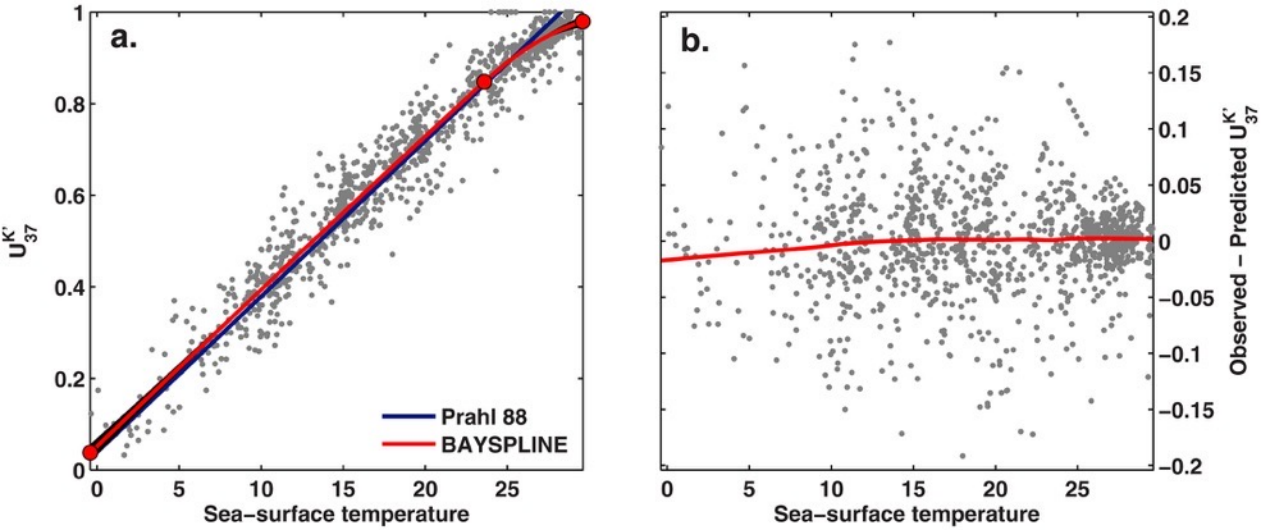

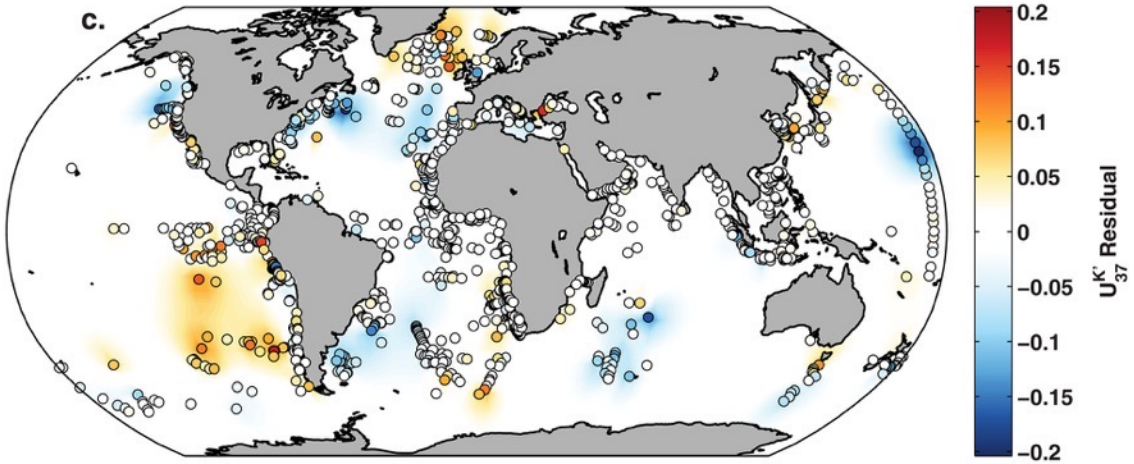

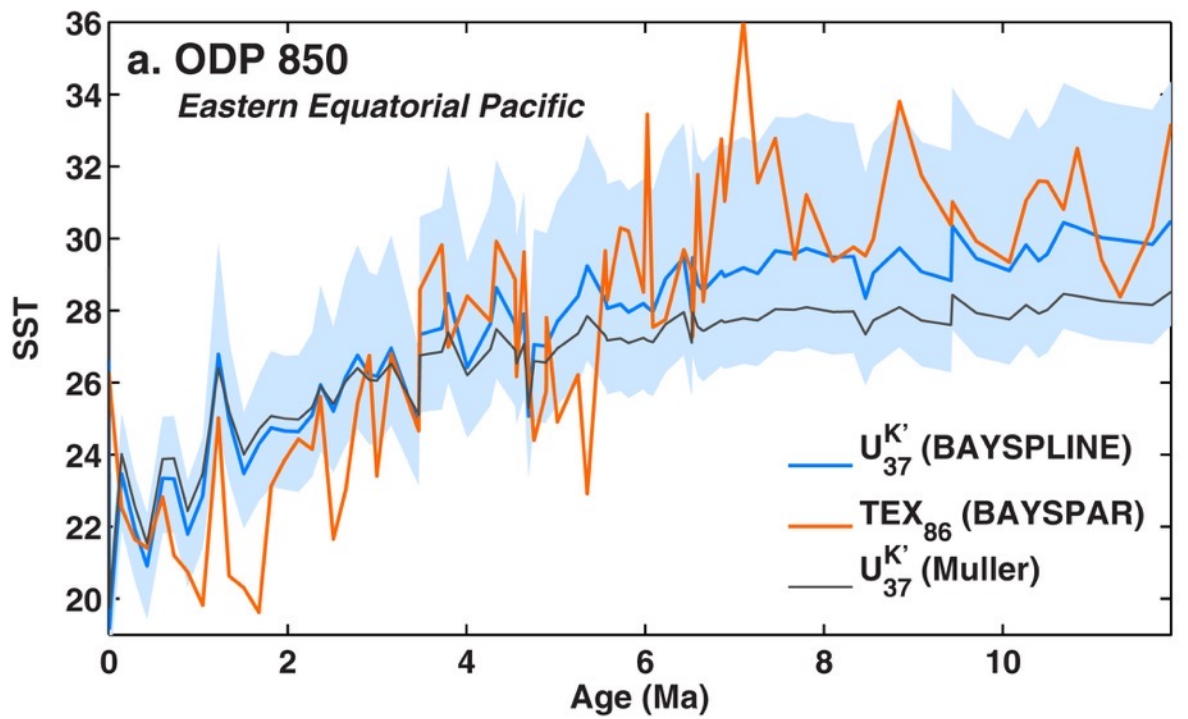

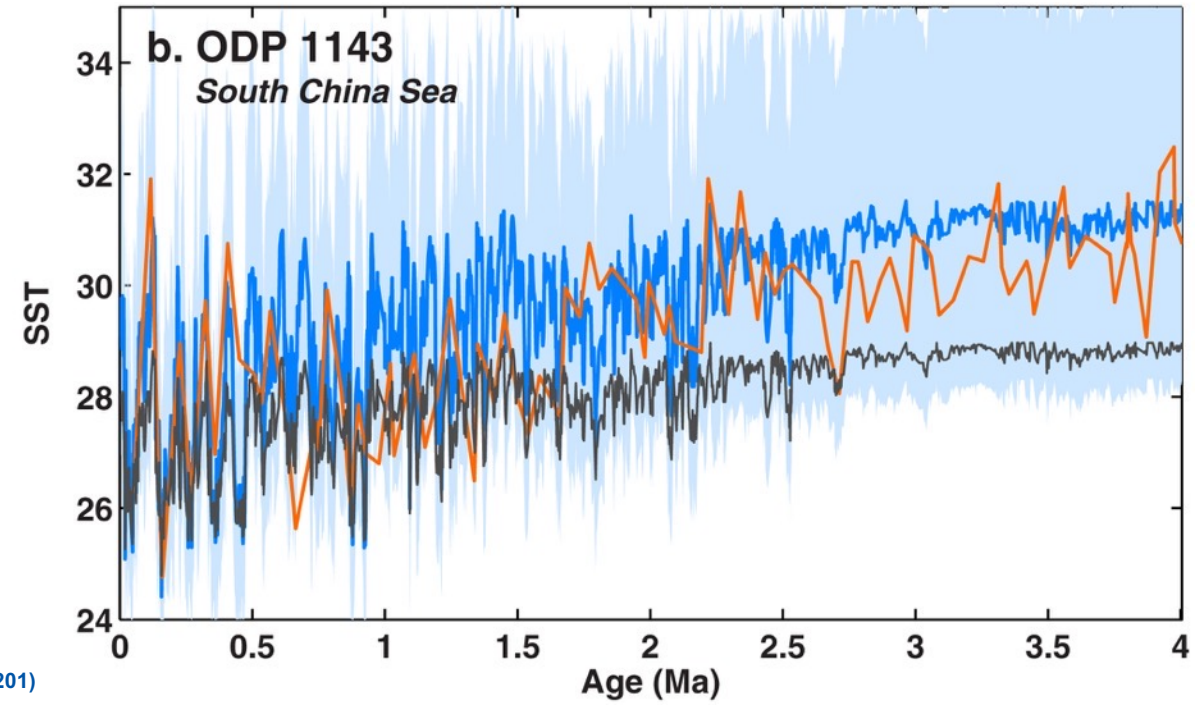

Paleoceanog and Paleoclimatol, Volume: 33, Issue: 3, Pages: 281-301, First published: 06 February 2018, DOI: (10.1002/2017PA003201)

Global and Planetary Change 133 (2015) 49–64

Contents lists available at ScienceDirect

Global and Planetary Change

journal homepage: www.elsevier.com/locate/gloplacha

A reference time scale for Site U1385 (Shackleton Site) on the SW Iberian Margin

D. Hodell [a,*], L. Lourens [b], S. Crowhurst [a], T. Konijnendijk [b], R. Tjallingii [c,1], F. Jiménez-Espejo [d], L. Skinner [a], P.C. Tzedakis [e], Shackleton Site Project Members

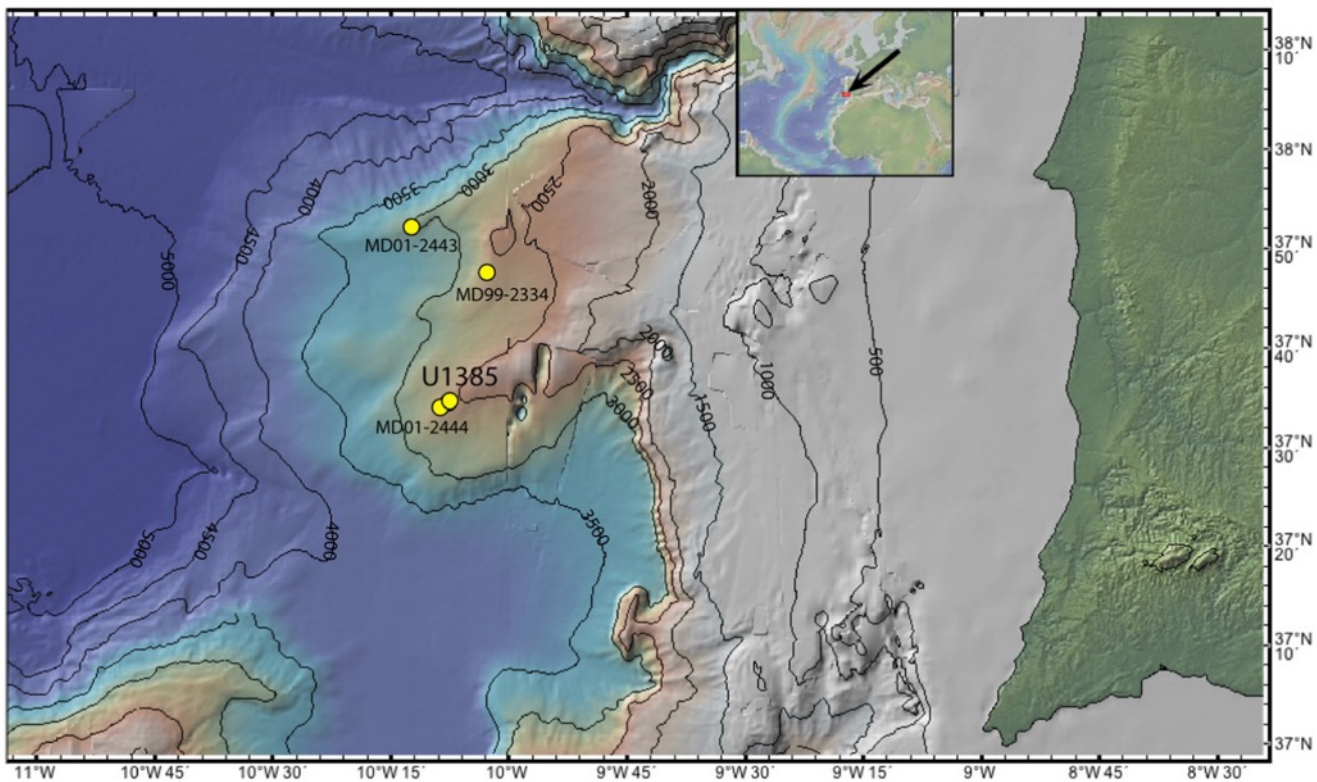

Fig. 1. Location of Site U1385 on the Promonotorio dos Principes de Avis, along the continental slope of the southwestern Iberian margin. Also shown are position of piston cores discussed in the text.

IODP INTERNATIONAL OCEAN DISCOVERY PROGRAM

Exploring the Earth Under the Sea

HOME | ABOUT IODP | PROPOSALS | EXPEDITIONS | RESOURCES | PROGRAM ORGANIZATION | POST-IODP PLANNING

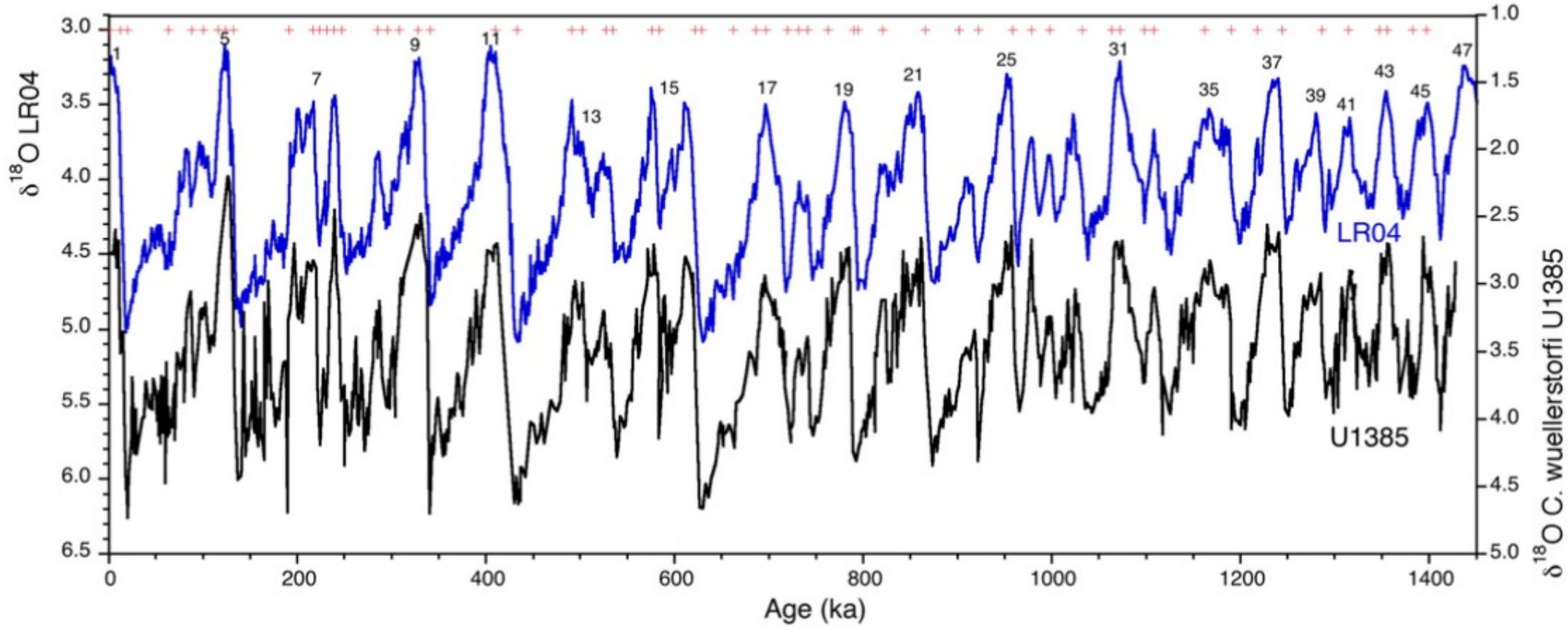

Fig. 6. Correlation of benthic $\delta^{18}O$ at Site U1385 (black) with the LR04 (blue) stack of Lisiecki and Raymo (2005). Red crosses represent the tie points.

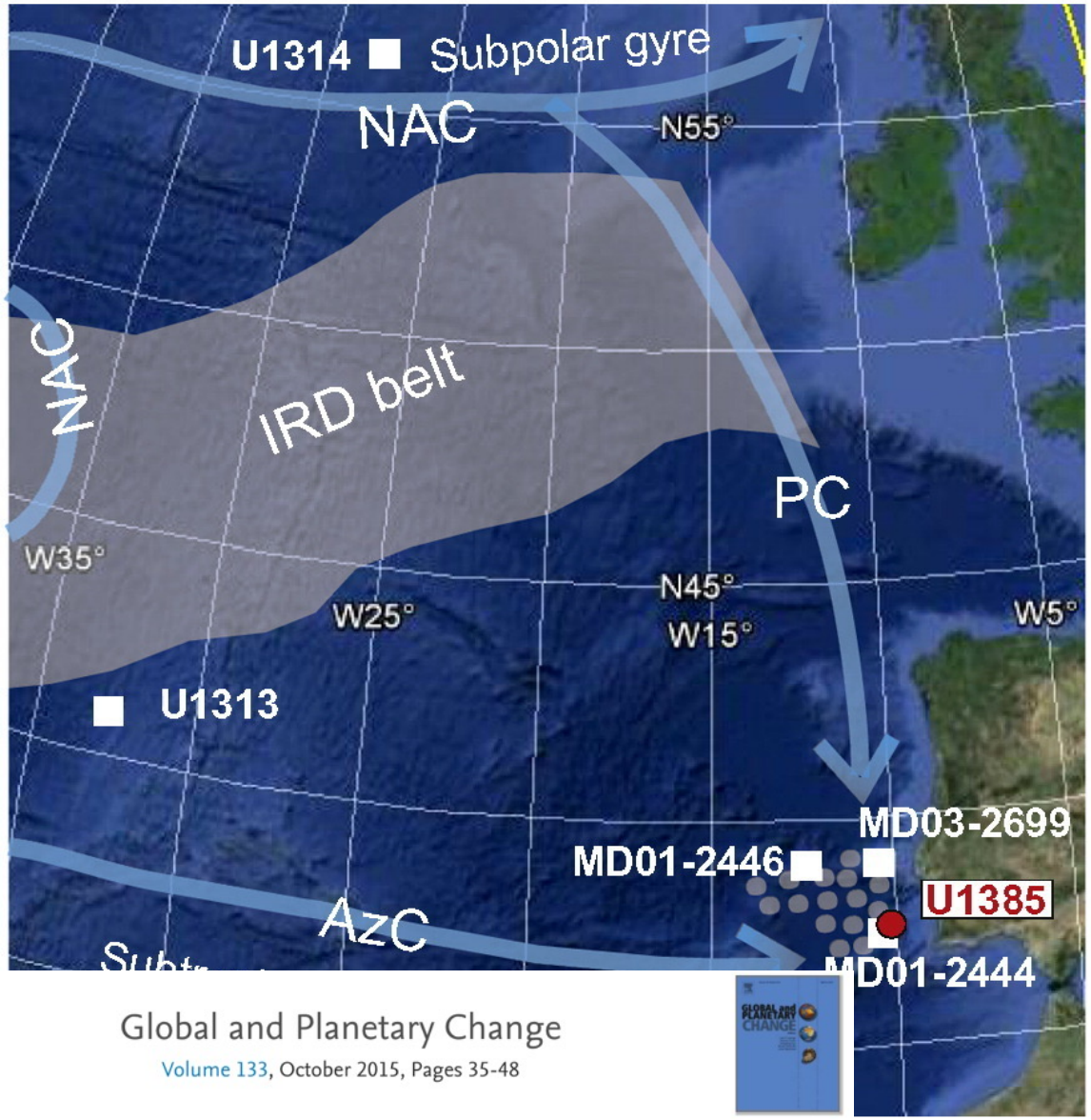

A

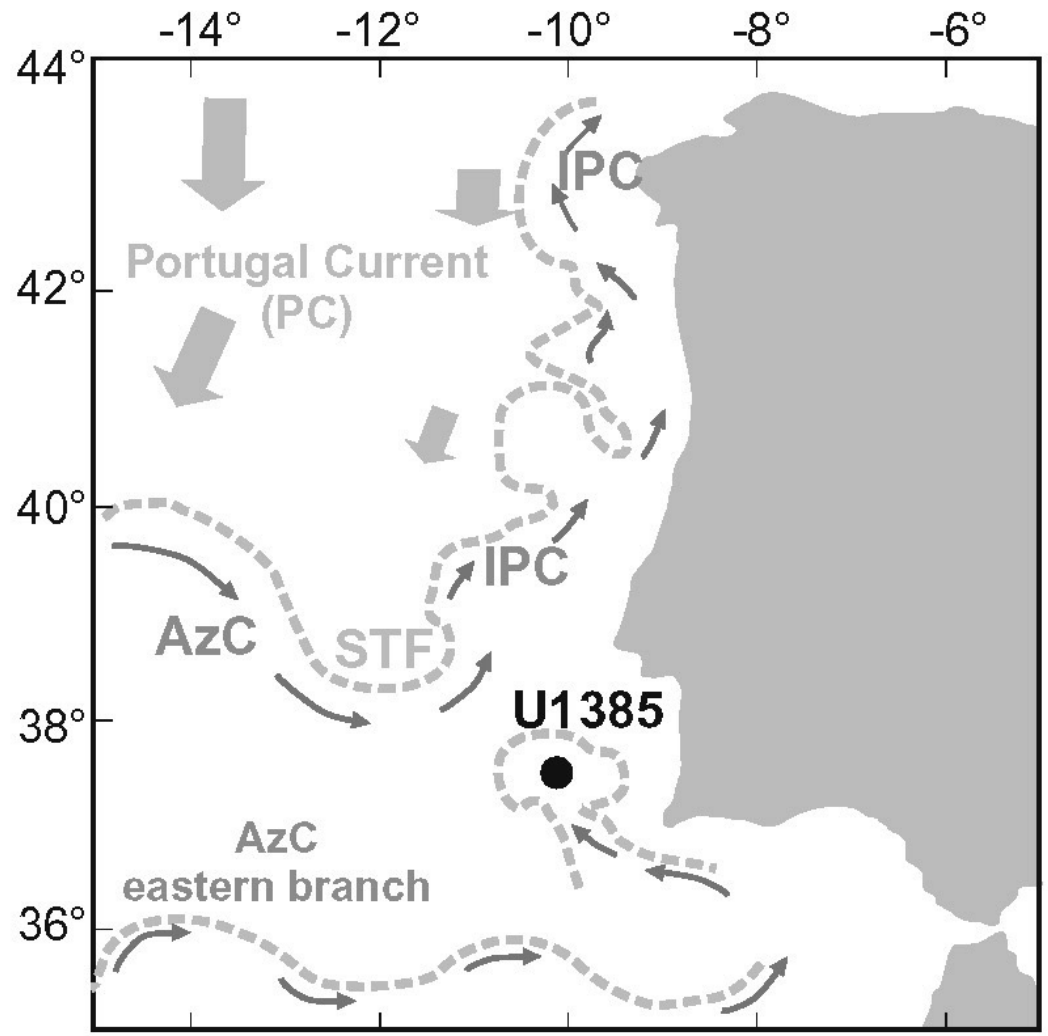

B

Global and Planetary Change
Volume 133, October 2015, Pages 35-48

Coccolithophore variability from the Shackleton
ite (IODP Site U1385) through MIS 16-10

What about the deep ocean ?

The Global Conveyor Belt (and it’s improvement)

Broecker 1987 Rahmstorf 2002 Talley 2013

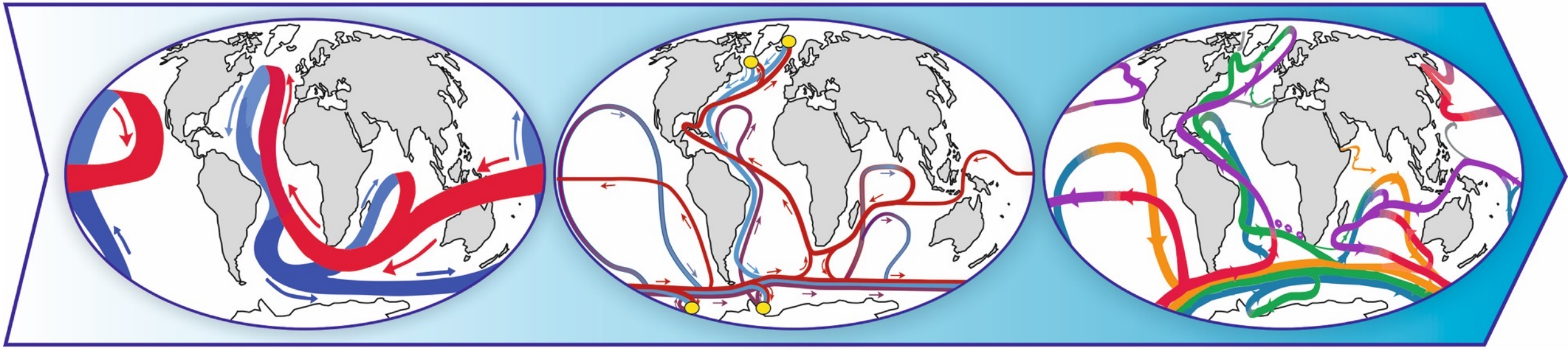

Figure 1: Our understanding of processes and feedbacks between different components of the Earth system has remarkably expanded over the last decades, here illustrated by conceptual visualizations of global ocean circulation over time: from the "Great Ocean Conveyor Belt" (left; Broecker 1987), to more complex ocean circulation dynamics (middle) with different deep water formation sites (yellow dots; Rahmstorf 2002) and (right) to an ocean with different water masses that interact and interfere with each other in a complex manner (Talley 2013). Different colors depict different types of water masses (see aforementioned references).

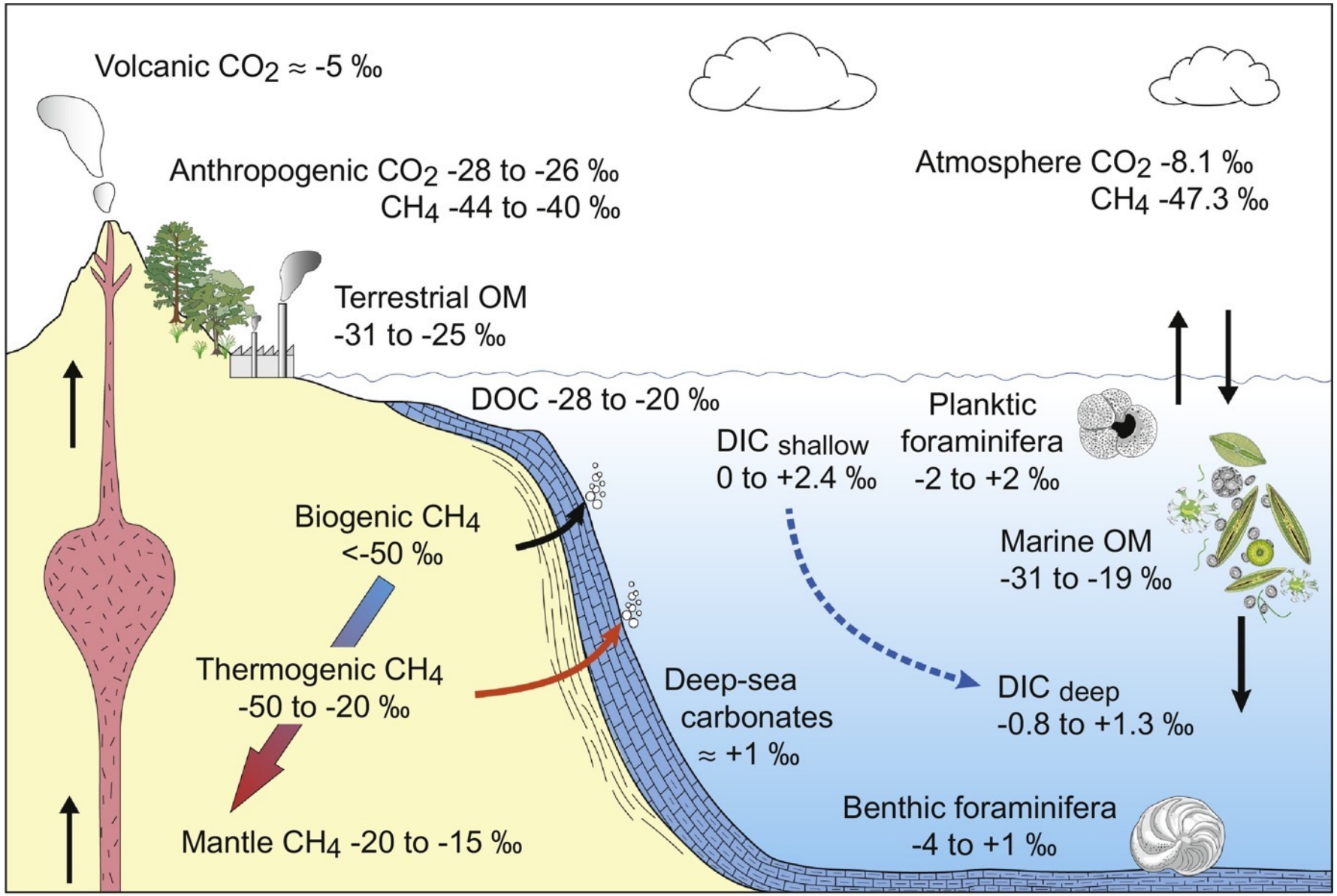

Mackensen& Schmiedl (2019): Stable carbon isotopes in paleoceanography: atmosphere, oceans, and sediments,

Earth-Science Reviews, Volume 197, 2019,

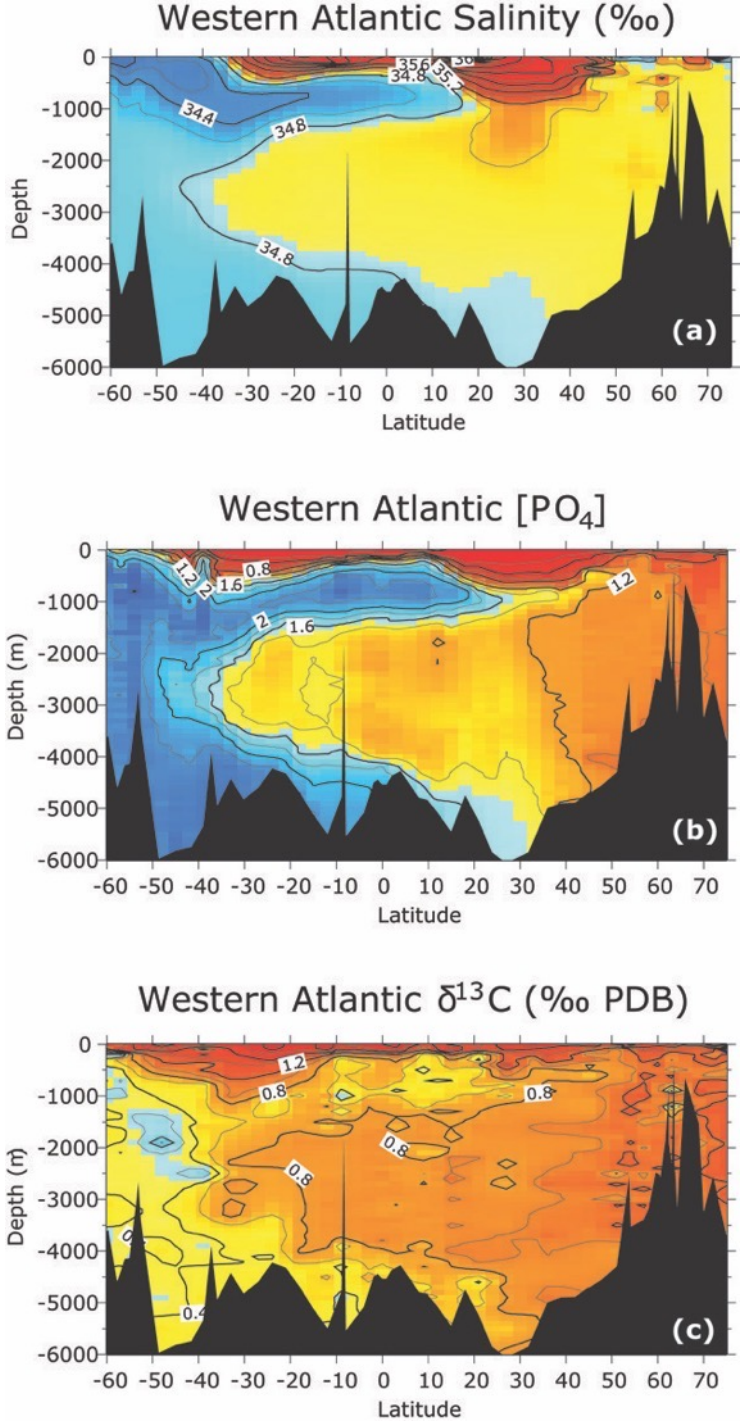

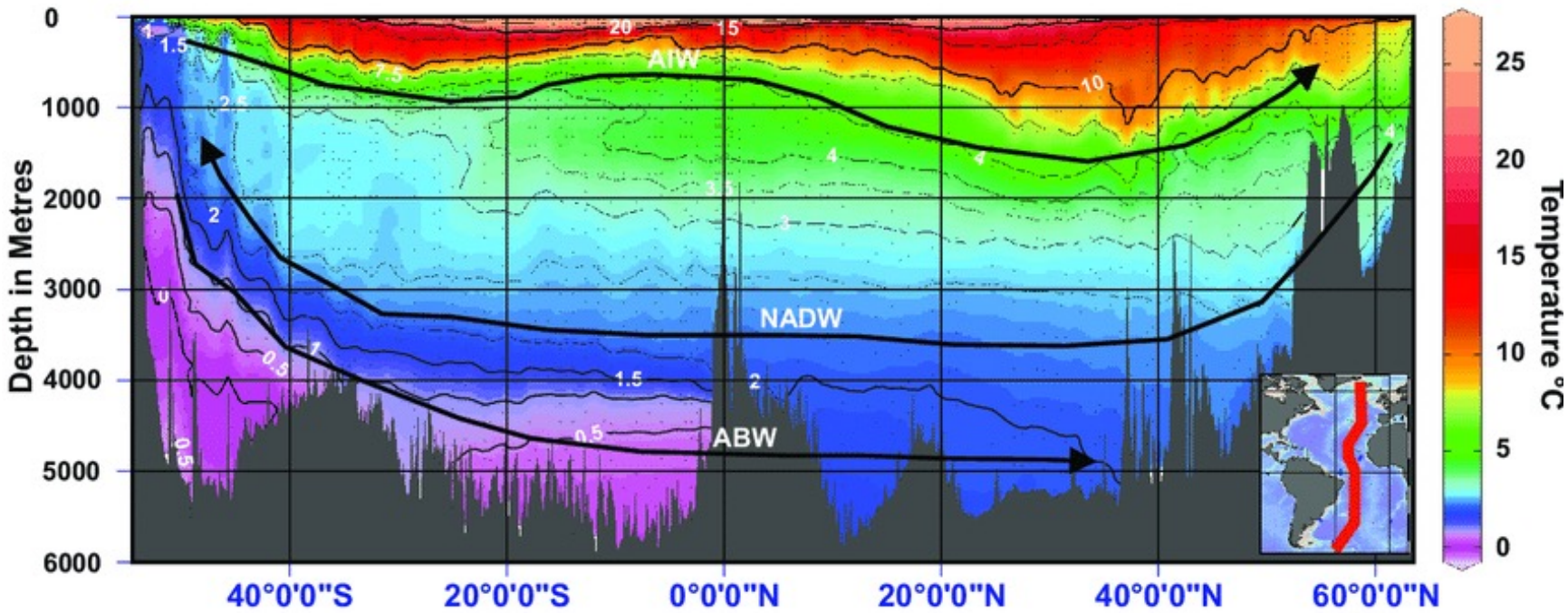

Figure 1: Modern transects from the western Atlantic Ocean.
(a) salinity (Bainbridge 1981), (b) phosphate (Bainbridge 1981), and (c) $\delta^{13}C$ (Kroopnick 1985) where $\delta^{13}C = 1000(^{13}C/^{12}C_{sample}/^{13}C/^{12}C_{standard} - 1)$. NADW, identified by its high salinity, contains more surface water than AABW, and therefore has lower nutrients and higher $\delta^{13}C$, as well as a younger radiocarbon age (Stuiver & Ostlund 1980).

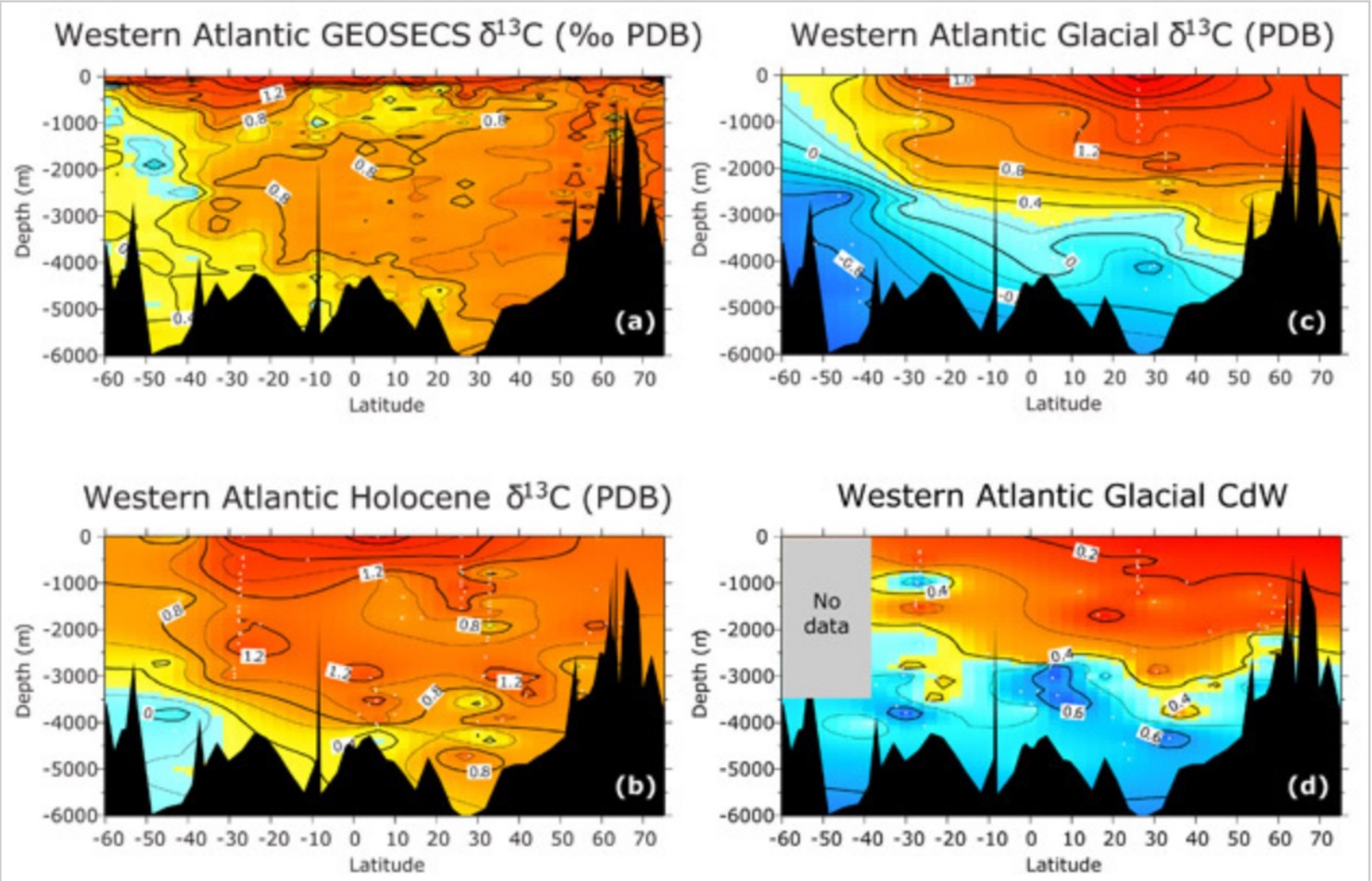

Figure 5: Modern, Holocene, and Glacial western Atlantic transects.
(a) Modern $\delta^{13}C$ (Kroopnick 1985), (b) Holocene, and (c) LGM $\delta^{13}C$ (Curry & Oppo 2005 and Supplementary Information), and (d) LGM CdW (Makou *et al.* 2010, including data compiled by Marchitto & Broecker 2008) transects for the western Atlantic. White dots indicate latitude and depths of cores used to make the glacial transects. The low $\delta^{13}C$ values and high CdW values in the glacial deep North Atlantic mark the penetration of southern ocean waters to the subpolar North Atlantic.

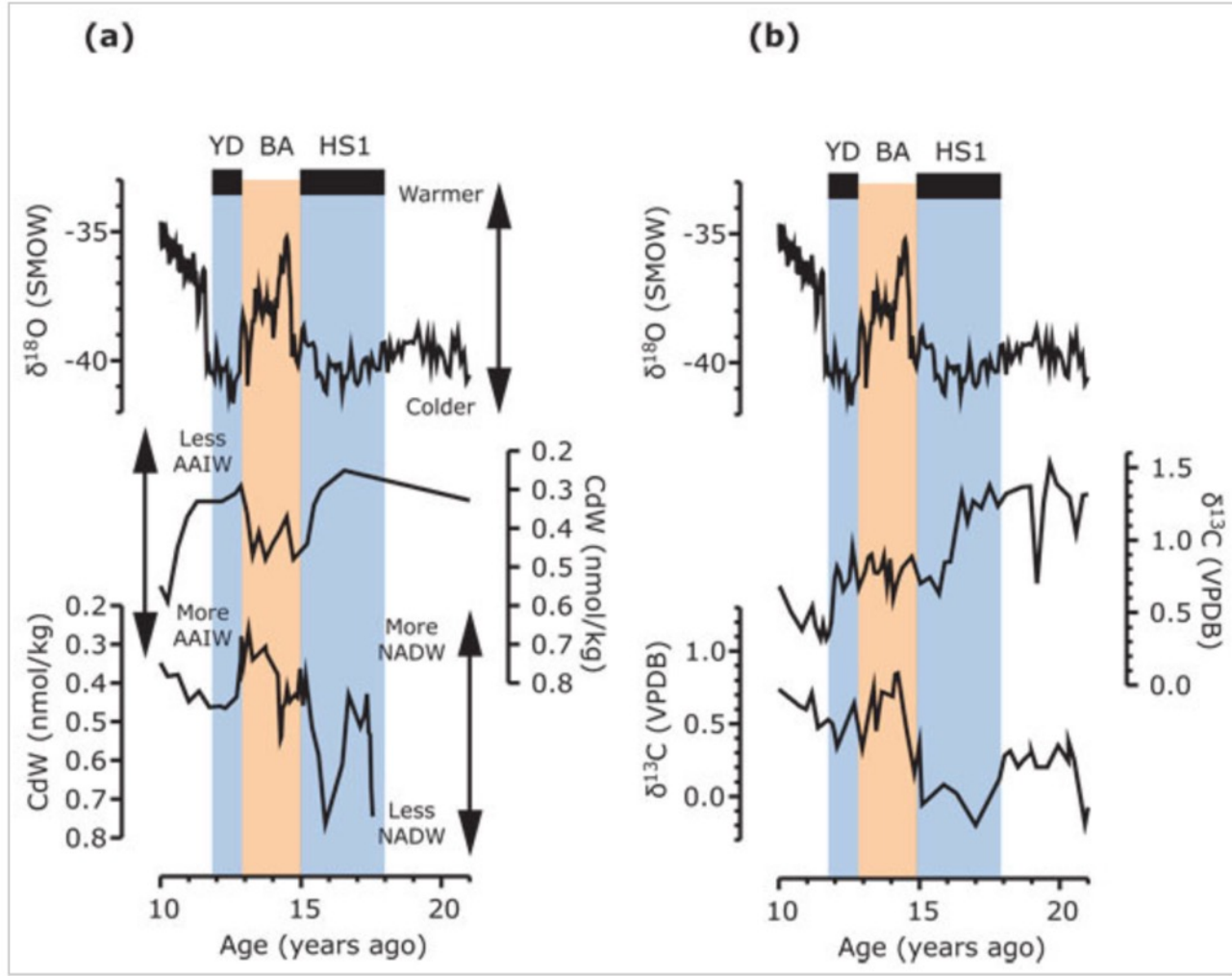

Figure 6: Deglacial Time Series.
(a) top-to-bottom: Greenland Ice Sheet Project (GISP2) $\delta^{18}O$ (Grootes *et al.* 1993), average CdW from Florida Current (24 °N, 83 °W, 751 m; Came *et al.* 2008) and from the deep western North Atlantic (33.7 °N, 57.6 °W, 4450 m, Boyle & Keigwin 1987). (b) top-to-bottom: Greenland Ice Sheet Project (GISP2) $\delta^{18}O$ (Grootes *et al.* 1993), $\delta^{13}C$ from the Florida Current (16.9°N; 16.2°W, 648 m, Lynch-Stieglitz *et al.* 2011), and from the deep eastern North Atlantic (37.8°N, 10.2 °W, 3166m, Skinner & Shackleton 2004). Time scales for the ice core records are from Blunier & Brooks 2001). Generally high CdW and low $\delta^{13}C$ in the deep Atlantic (bottom panels) indicate a relatively small contribution of NADW during the Heinrich Stadial and Younger Dryas. Low CdW values in the shallow North Atlantic suggest reduced northward flow of AAIW at the same time. The Heinrich Stadial (HS1), the Younger Dryas (YD), and the intervening warm period, the Bølling-Allerød (BA) are identified by shading. Note there is some debate about the timing of the Heinrich Stadial.

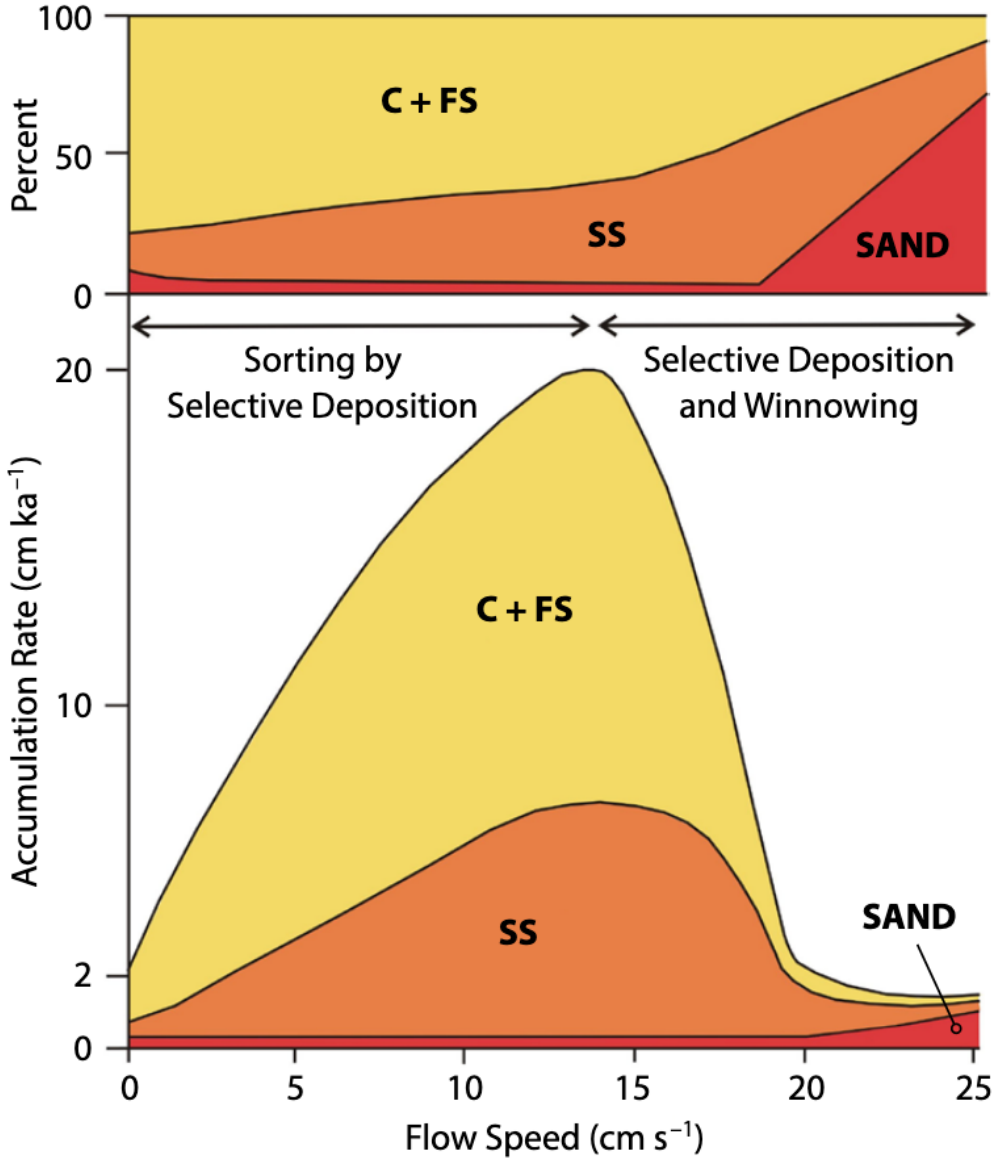

FIGURE 2. Hypothetical variation of accumulation rate and percentage composition of a sediment deposit with increasing current speed advecting sediment to a deposition site. C + FS = clay and fine silt (<10 µm) and SS = sortable silt (10–63 µm) (McCave and Hall, 2006). The "sand" here is a size term that refers to both terrigenous and carbonate—mainly foraminifera—components. At zero speed, a pelagic rate of 2 cm ka^{-1} is assumed. From zero to the peak accumulation rate, the sorting process is all selective deposition. Above that point, arbitrarily put at a flow speed of 13 cm s^{-1}, it is a combination of selective deposition and removal of material with a grain size <63 µm. Erosional winnowing and some sand movement is assumed to occur above a flow speed of 20 cm s^{-1}. The curve is shown as peaking between 10 cm s^{-1} and 15 cm s^{-1}, but this is not at all certain and may well depend on the magnitude-frequency structure of deposition and erosion events. A peak around 10 cm s^{-1} would be entirely feasible, as some velocity with turbidity records suggest the onset of surface erosion above 10–12 cm s^{-1}.

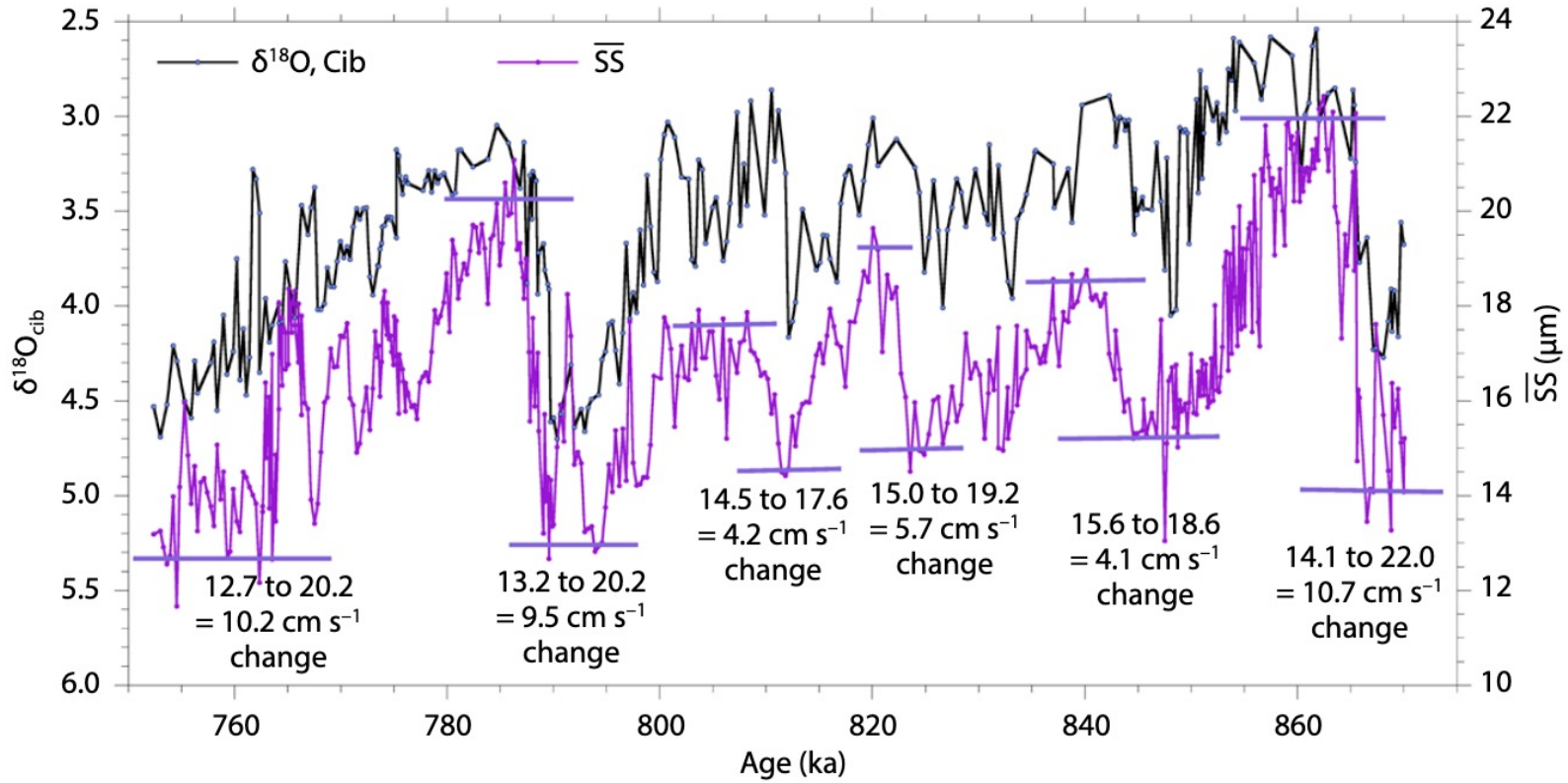

FIGURE 1. This sortable silt record from Gardar Drift south of Iceland under the Iceland-Scotland overflow (Kleiven et al., 2011) spans Marine Isotope Stages 22 to 18 and contains two major glacial-to-interglacial transitions with flow speed changes of ~10 cm s^{-1} and stadial (colder climate)-to-interstadial (warmer climate) shifts of 4–6 cm s^{-1}. (Marine isotope stages are alternating warm and cool periods in Earth history deduced from oxygen isotope ratios of fossil foraminifera shells recovered from deep-sea sediments.) Flow speeds closely track climatic (ice volume) changes indexed by bottom water oxygen isotopic values ($^{18}O/^{16}O$ ratio per mil relative to the VPDB standard [$\delta^{18}O$] of the benthic foraminifera *Cibicidoides wuellerstorfi*). Modern speeds in the region are ~15 cm s^{-1}, so Iceland-Scotland overflow in glacial periods possibly slowed to ~5 cm s^{-1} but did not cease. $\overline{SS}$ = sortable silt mean size.

Broecker 1987 Rahmstorf 2002 Talley 2013

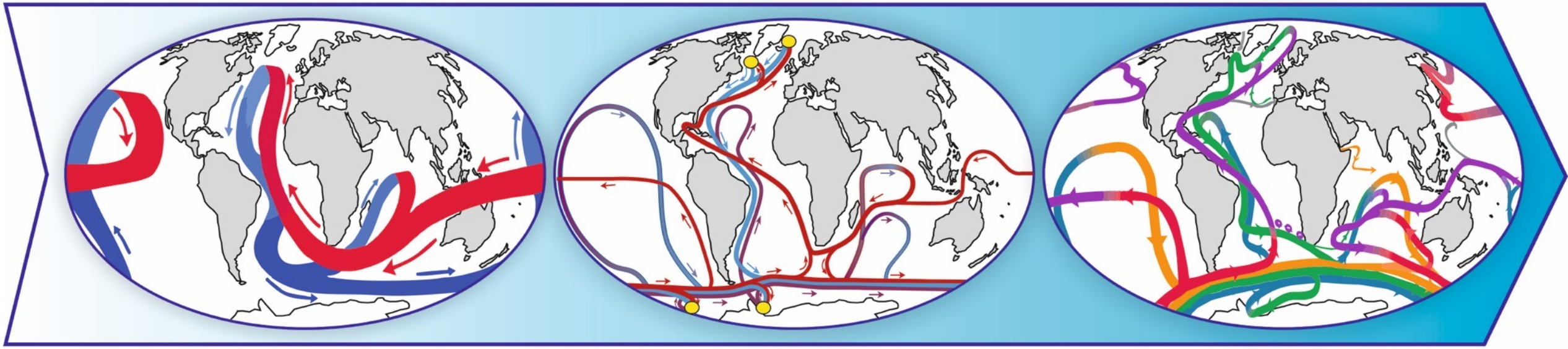

Figure 1: Our understanding of processes and feedbacks between different components of the Earth system has remarkably expanded over the last decades, here illustrated by conceptual visualizations of global ocean circulation over time: from the "Great Ocean Conveyor Belt" (left; Broecker 1987), to more complex ocean circulation dynamics (middle) with different deep water formation sites (yellow dots; Rahmstorf 2002) and (right) to an ocean with different water masses that interact and interfere with each other in a complex manner (Talley 2013). Different colors depict different types of water masses (see aforementioned references).

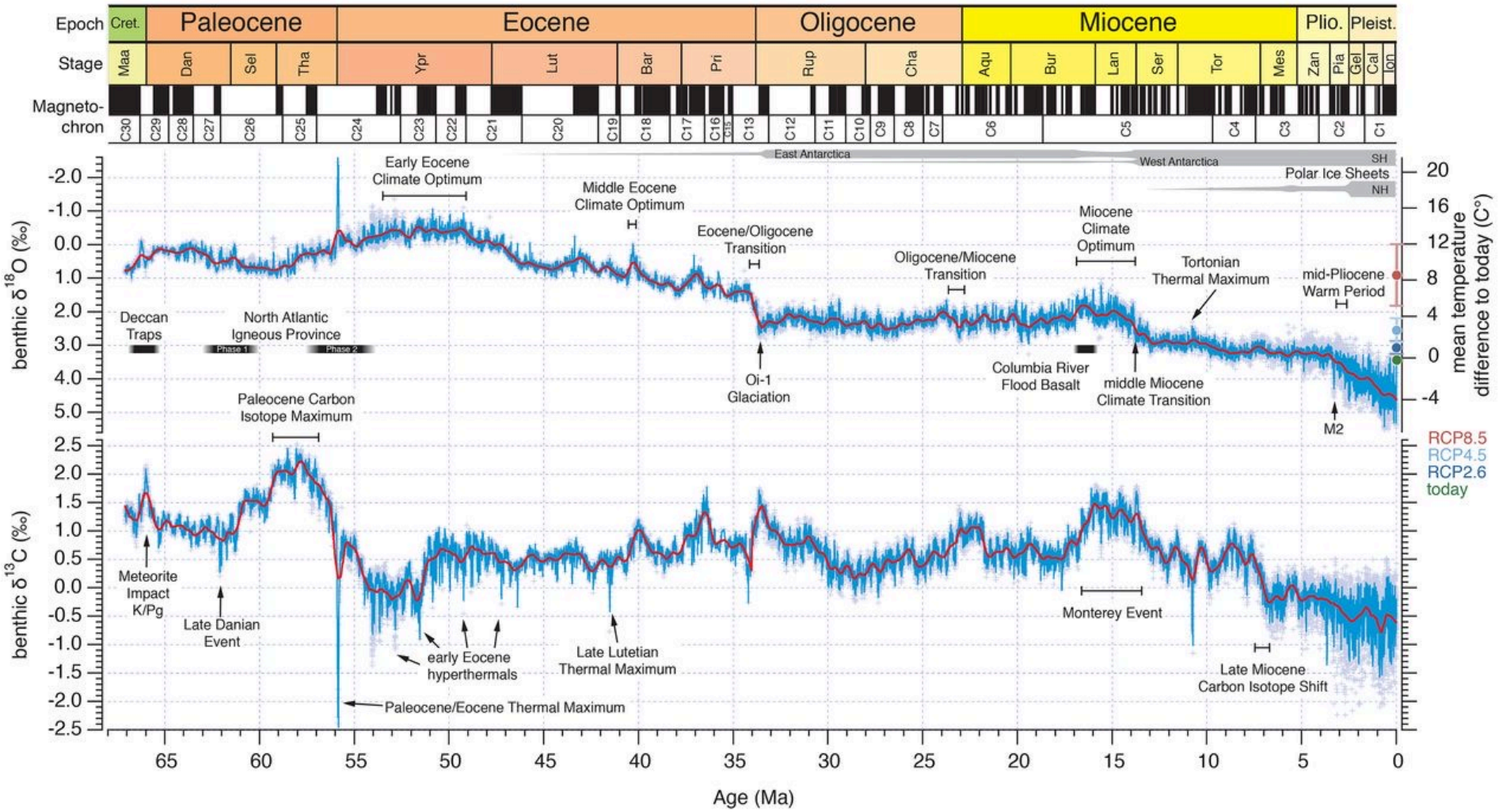

6830 samples

Westerhold, Thomas; Marwan, Norbert; Drury, Anna Joy; Liebrand, Diederik; Agnini, Claudia; Anagnostou, Eleni; Barnet, James S K; Bohaty, Steven M; De Vleeschouwer, David; Florindo, Fabio; Frederichs, Thomas; Hodell, David A; Holbourn, Ann E; Kroon, Dick; Lauretano, Vittoria; Littler, Kate; Lourens, Lucas Joost; Lyle, Mitchell W; Pälike, Heiko; Röhl, Ursula; Tian, Jun; Wilkens, Roy H; Wilson, Paul A; Zachos, James C **(2020):** An astronomically dated record of Earth's climate and its predictability over the last 66 million years. *Science*, **369**, 1383-1387, https://doi.org/10.1126/science.aba6853

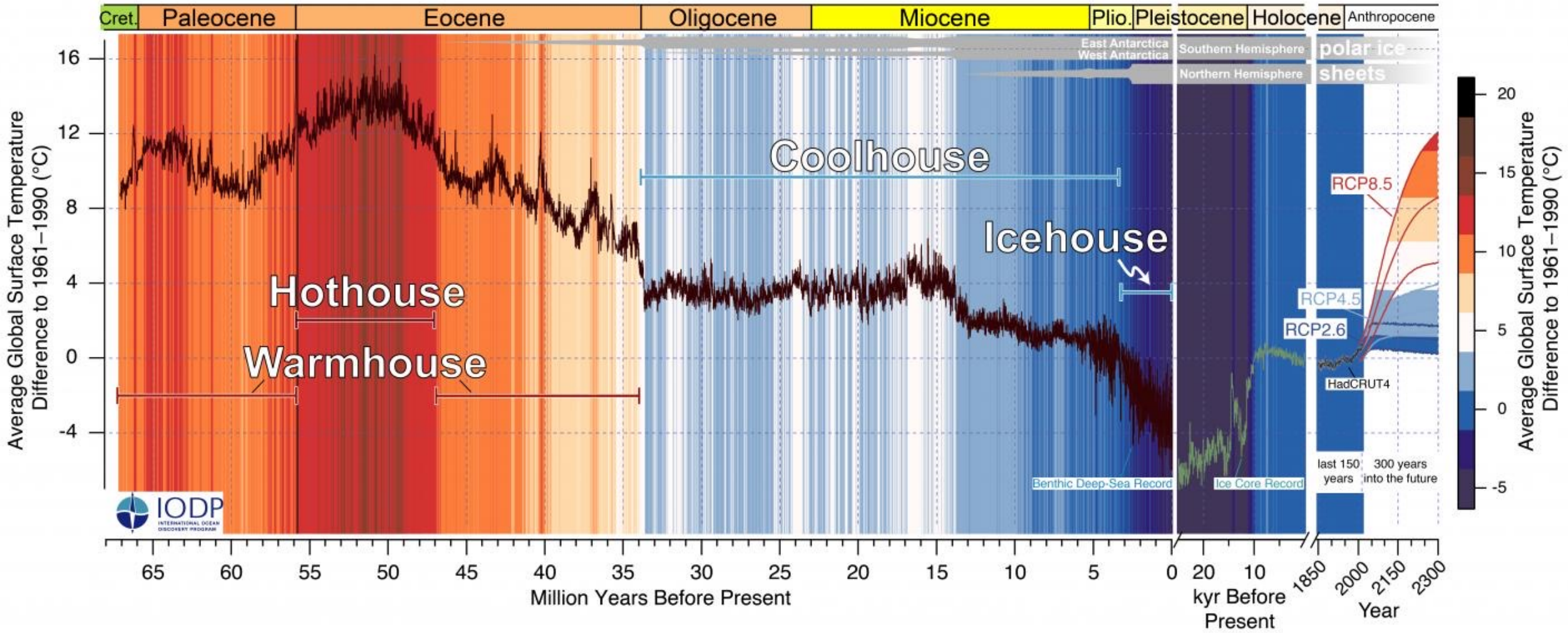
Cret.
Paleocene
Eocene
Oligocene
Miocene
Plio.
Pleistocene
Holocene
Anthropocene
East Antarctica
West Antarctica
Southern Hemisphere
Northern Hemisphere
polar ice sheets
Coolhouse
Icehouse
Hothouse
Warmhouse
RCP8.5
RCP4.5
RCP2.6
HadCRUT4
Benthic Deep-Sea Record
Ice Core Record
last 150 years
300 years into the future
IODP
INTERNATIONAL OCEAN DISCOVERY PROGRAM
Average Global Surface Temperature
Difference to 1961–1990 (°C)
16
12
8
4
0
-4
65
60
55
50
45
40
35
30
25
20
15
10
5
0
Million Years Before Present
20
10
kyr Before Present
1850
2000
2150
2300
Year
20
15
10
5
0
-5
Average Global Surface Temperature
Difference to 1961–1990 (°C)

Northern Red Sea coral reef. *Photo credit: T. Felis, MARUM - Center for Marine Environmental Sciences, University of Bremen*

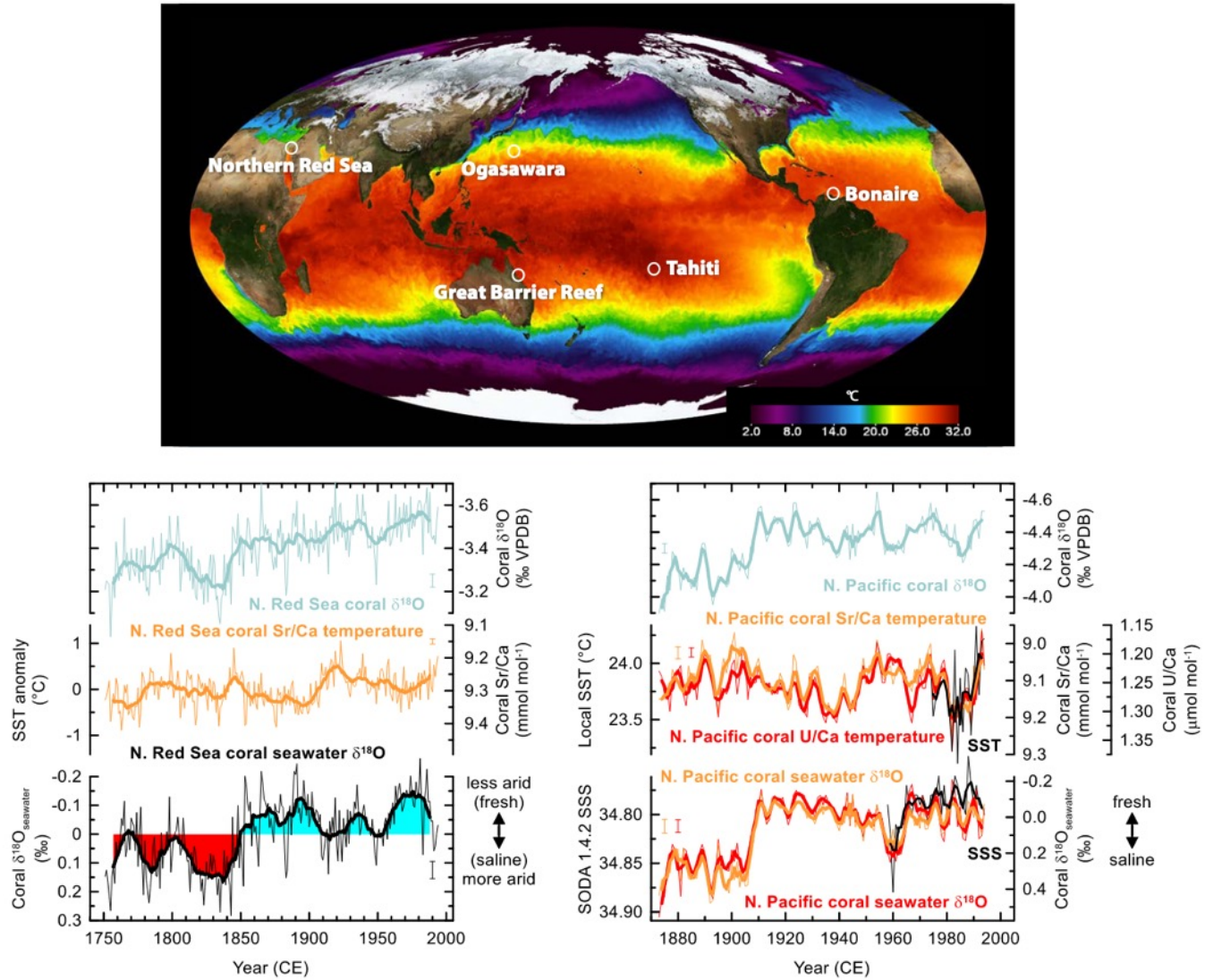

FIGURE 1. (top) Selected tropical and subtropical sites of coral paleoclimate work in the Indo-Pacific and Atlantic Oceans discussed in this paper are indicated on a map showing the multi-scale ultrahigh-resolution (MUR) sea surface temperature (SST) analysis from NASA/Goddard Space Flight Center (downloaded from https://svs.gsfc.nasa.gov/30008). The graphs show annual average proxy records of subtropical sea surface temperature and hydrology during recent centuries derived from bimonthly resolved Sr/Ca (and U/Ca) and $\delta^{18}O$ measurements in modern corals (*Porites* spp.) of (bottom left) the northern Red Sea (Ras Umm Sidd; Felis et al., 2018) and (bottom right) the western North Pacific (Ogasawara; Felis et al., 2009). The corresponding seawater $\delta^{18}O$ reconstructions suggest abrupt shifts toward fresher conditions after 1850 CE and 1905 CE. Bold lines are 13-year (northern Red Sea) and three-year (western North Pacific) running averages. *Modified from Felis et al. (2009) and Felis et al. (2018)*

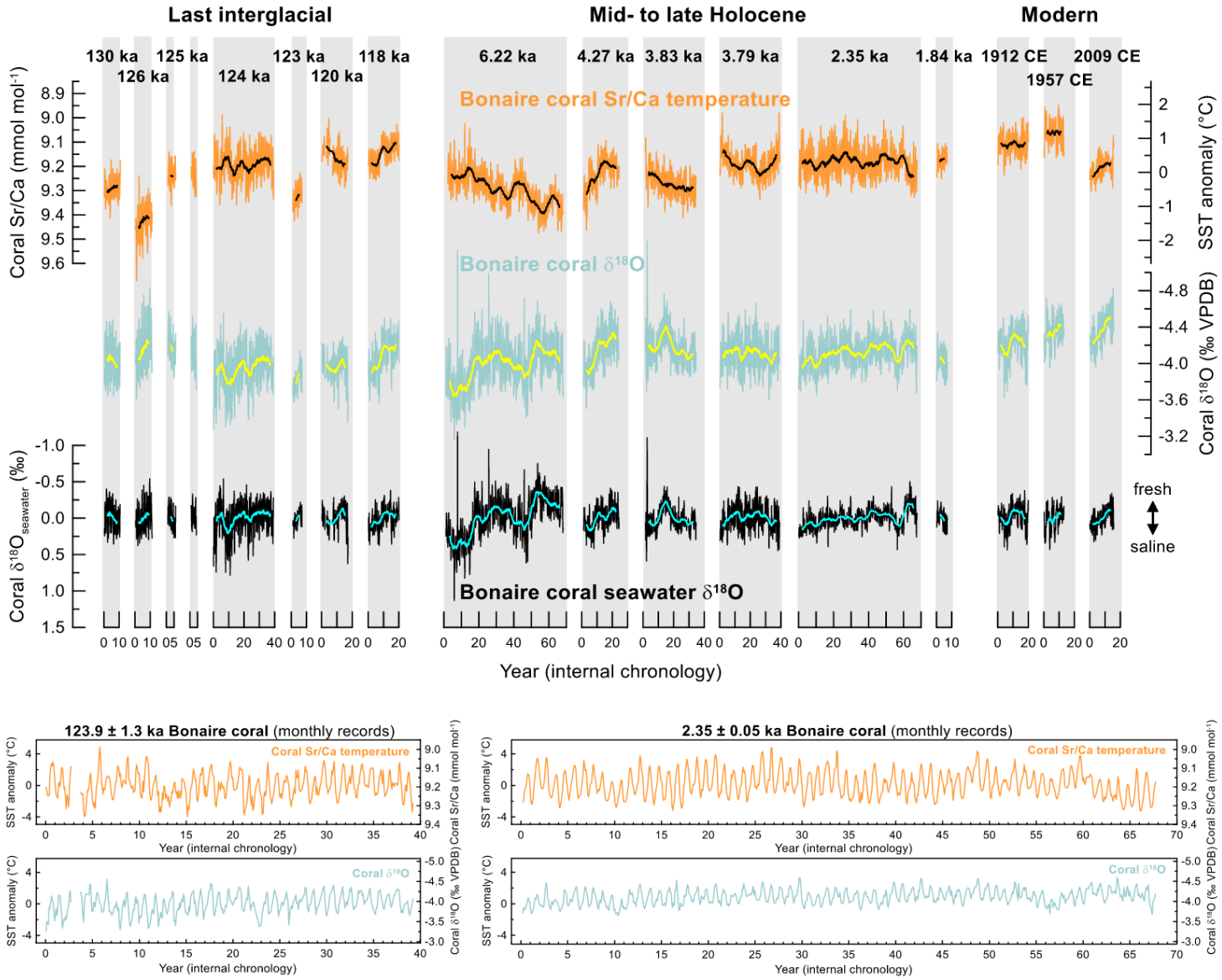

FIGURE 2. (top) Monthly resolved proxy records of tropical Atlantic sea surface temperature (SST) and hydrology for time intervals during the last interglacial (~130,000 to 118,000 years ago) and since the mid-Holocene (~6,000 years ago) derived from Sr/Ca and $\delta^{18}O$ measurements in modern and fossil corals (*Diploria strigosa*) of the southern Caribbean Sea (Bonaire; Giry et al., 2012, 2013; Felis et al., 2015; Brocas et al., 2016, 2018). The corresponding seawater $\delta^{18}O$ reconstructions are shown. Bold lines are 51-month running averages. (bottom) Enlargement of monthly coral Sr/Ca and $\delta^{18}O$ records for time intervals around 124,000 and 2,350 years ago. *Modified from Giry et al. (2012, 2013), Felis et al. (2015), and Brocas et al. (2016, 2018)*